Emission properties of Coordination Complexes: The Impact of Mixed Donors on *f*-Block Elements

By

Ethan Andrew Hiti

A dissertation submitted to the Graduate Faculty of
Auburn University
in partial fulfillment of the
requirements for the Degree of
Doctor of Philosophy

Auburn, Alabama
May 1, 2021

Keywords: actinide, uranyl, lanthanide, salophen, emission spectroscopy

Approved by

German Mills, Chair, Professor, Department of Chemistry and Biochemistry
Anne E. V. Gorden, Co-chair, Associate Professor, Department of Chemistry and Biochemistry at Texas Tech University
Byron H. Farnum, Assistant Professor, Department of Chemistry and Biochemistry
Evangelos Miliordos, James E. Land Assistant Professor, Department of Chemistry and Biochemistry
Ryan Comes, Thomas and Jean Walter Assistant Professor, Physics

Abstract

There is a growing need to understand the fundamental aspects of chemistry concerning *f*-elements. Whether it be through the use of softer donor systems to try and selectively coordinate actinide ions in solution which could be useful in the event of a spill or contamination event, using mixed donor systems to take advantage of the distinct photophysical properties of Ln (III) ions for new emissions agents for biological imaging compounds. The 4*f* or 5*f* orbitals play a pivotal role in their unique chemistry, emission, and optical properties, accessible to these elements. Here, we look at three different aspects of *f-element* chemistry that allow us to look at the nature of the *f*-orbitals while looking at how this affects their emissive properties.

The highly conjugated salimidizine ligand and 3 derivatives are examined for the electronic properties of the ligand and how these can be altered both for selective coordination of metal ions and somewhat tunable emissions. These properties would enable it to be potentially be used in colorimetric or fluorescence sensors for uranyl detection in solution. Examination of these organic frameworks is examined in the presence of copper (II) ions which are considered to be a common "false positive" metal ion due to similar charge to ionic size ratios. Overall, these organic frameworks are able to distinguish via fluorescence intensity the binding of uranyl versus copper. Further details and explanation for this is given through computational modeling of the complexes.

Next, the ability of cyano substituted naphthylsalophens were examined as sensitizers or antennae with Ln (III) ions for 2 photon up-conversion processes. This Schiff base type (-2) ligand forms 3:2 ligand to lanthanide sandwich-type complexes that display characteristic metal centered

emission for Nd (III), Er (III), and Yb (III). Upon excitation at 980 nm, in mixed lanthanide complexes and Er (III) complexes, Er-centered up-conversion emission is observed at 543 nm and 656 nm respectively. This is achieved with power densities as low as 2.18 W cm^{-2}.

Lastly, the naphthylpyrasal ligand in metal complexes was examined. These complexes were characterized through UV-vis spectroscopy, electrochemical analysis, and single crystal X-ray diffraction. This framework shows the ability in solid state to form N-oxide species in the solid state which is not commonly seen with actinides. Three distinct crystallographic species are formed showing a solvent dependance on crystallization solvent mixtures to produce different solid-state morphologies. This species seems to be formed through the presence of peroxides in the crystallization solvents. Through further examination of the solid state, we see that two of these structures produce close to a 5° bend from linearity in the typically linear -yl oxygen bonds

Acknowledgments

I would first and foremost like to thank God for his steadfastness and guidance throughout my entire life as well as giving me the passion for chemistry that has led me to be able to take part in this moment. Without His faithfulness none of this would even be possible.

Secondly, I have to give credit where credit is due, my mom and dad have been so instrumental in this journey. Their constant love, encouragement, and guidance has done more in my life that you will ever be able to comprehend. You both always know when to drop little nuggets of advice or guidance or encouragement at the most pivotal moment to help me push through any adversity that I have faced. Without you and your support in all my endeavors I know that this accomplishment would not have happened. I also want to thank Cobalt, my most wonderful black lab and my best friend. Thank you for always being happy to see me when I come home, even if it is past dinner time, and for always being goofy and a constant source of joy to brighten up my day when thing would seem overwhelming. You truly are the definition of "man's best friend."

Next, I want to thank Dr. Anne Gorden for being my advisor. Thank you for taking a shot with me six years ago when I first picked your lab to work in for my graduate career. Thank you for allowing me the opportunity to do science under your leadership and for all the guidance you gave me along the way. I would also like to thank the rest of my committee: Dr. Jimmy Mills, Dr. Byron Farnum, Dr. Evangelos Miliordos, and Dr. Ryan Comes. Thank you all for your insight and guidance as I have traversed my way through graduate school. Thank you all for your interest and investment in me as a scientist and as a student. Your guidance and dedication have allowed me to get the most out of my time at Auburn.

Another extremely important group that deserves the utmost thanks are my lab mates and friends that I have been able to forge friendships with along the way. Dr. Julie Niklas and Dr. Clay Black, thank you from the bottom of my heart for your many hours of conversation and deliberation involving science and your willingness to answer any question I would throw your way, the regular trips for Friday lunch, and the many game nights to ease the stress of grad school. Dr. Emily Hardy, Dr. Charmain Tutson, Dr. Maya West, and Nick Klann, thank you for helping me get my footing in the lab as I made my transition into the research that I would conduct here at Auburn. Dr. Kara Johnson, Scott Johnson, Jessica Krewall, Josh Krewall, and Alex Bredar, thank you so much for all the get together's with fantastic baked goods and meals as well as mid-week and weekend coffee runs that always allowed me to leave with a full heart and belly!

I also want to thank the undergrads that I have had the privilege of working with over the last three years, J.P. Grundhoefer and Grant Wilkinson. Thank you for your dedication to the projects we were able to work on together and your fervor to dig deeper in the science we were conducting. I hope both of your times in graduate school are as eventful and fulfilling as mine was. I also hope that you get the chances to work with exceptional young scientist as I was able to do with both of you and that you are able to learn as much from them in return as I was ablet to learn from you.

To everyone mentioned and those that were not, I hope the importance of your contribution and investment in me is conveyed throughout the words in this work.

Table of Contents

Abstract ii

Acknowledgments iv

List of Tables viii

List of Figures ix

List of Abbreviations xi

Chapter 1 Introduction 1

Soft Donors for Identification 3

Salen Ligands and *f*-block Coordination 4

Use as Sensors 5

Utilization of Lower Valent Uranium Species 7

Lanthanide Emission 9

References 10

Chapter 2 Salimidizine 24

Introduction 25

Results and Discussion 27

Conclusion 38

Synthesis 40

References 47

Chapter 3 Cyano-Naphthylsalophen 51

Introduction 52

Results and Discussion 55

Conclusion 61

Synthesis 62
References 66
Chapter 4 Naphthylpyrasal 74
Introduction 75
Results and Discussion 77
Conclusion 88
Synthesis 90
References 93
Chapter 5 Future Work and Preliminary Data 100
Conclusions 101
Future Work and Preliminary Findings 103
Modifications to Naphthylsalophen 103
Naphthylpyrasal 107
Synthesis 108
References 118
Appendix 1 B3LYP/cc-pVDZ(-pp) Cartesian Coordinates 120
Appendix 2 Crystallographic Tables 126

List of Tables

Table 3.1 Emission Data of H_2L-CN, and the Nd (III), Yb (III), Er (III) complexes..... 57

Table 3.2 Selected bond lengths from *[Er_2(L-CN)$_3$(H_2O)] and [Er_2(L)$_3$(MeOH)$_3$]*..... 61

Table 5.1 Synthesized Metal Complexes with Substituted Naphthylsalophen Ligands..... 105

List of Figures

Figure 1.1 Examples of salen-U(VI) complexes with All N-donor 4

Figure 1.2 Synthetic scheme of salen ligand “Salqu” 5

Figure 1.3 2,6-bis[1-[(2-hydroxyphenyl)imino]ethyl] pyridine-UO_2 Complex 6

Figure 1.4 Crystal structure of the pyrrophen-UO_2 complex and UV-vis data 7

Figure 1.5 Solid state examples of functionalized UO_2 complexes 8

Figure 1.6 Modified Jablonski Diagram For antenna effect for lanthanide complexes 9

Figure 1.7 Pybox ligand derivative and emission spectra 10

Figure 2.1 Salimidizine Synthetic Scheme 27

Figure 2.2 Salimidizine (L1) titration with Cu^{2+} acetate UV-vis spectra 29

Figure 2.3 DTB-Salimidizine (L2) titration with Cu^{2+} acetate UV-vis spectra 30

Figure 2.4 DTB-Salimidizine (L2) titration with UO_2^{2+} acetate UV-vis spectra 31

Figure 2.5 OMe-Salimidizine (L3) titration with Cu^{2+}& UO_2^{2+} acetate UV-vis spectra 31

Figure 2.6 Fluorescence Spectra of Salimidizine (L1) with Cu^{2+} & UO_2^{2+} titration 32

Figure 2.7 Fluorescence Spectra (L2), (L3), and (L4) with Cu^{2+} & UO_2^{2+} titration 33

Figure 2.8 Projection of crystal data of L1, L2, & UO_2[L1]OAc•DMSO 34

Figure 2.9 Natural transition orbitals of $L_1UO_2^{2+}$(AcO)(W) and L_1Cu^{2+}(AcO) 37

Figure 2.10 Potential energy profiles of $L_1UO_2^{2+}$(AcO)(W) and L_1Cu^{2+}(AcO) 38

Figure 3.1 Energy level diagram and structure of H_2L-CN 53

Figure 3.2 Crystal data projections of previously reported triple decker Ln(III) complexes 54

Figure 3.3 Synthesis of Cyanonaphthylsalophen (H_2L-CN) 56

Figure 3.4 Projection of H_2L-CN and [Er_2(L-CN)$_3$(H_2O)] 56

Figure 3.5 Two-photon UC spectra of [(Y0.76Yb0.16Er0.08)2(L-CN)3(H2O)] 58

Figure 3.6 Two-photon UC spectra of [(Y0.76Yb0.16Er0.08)2(L-CN)3(H2O)] & [Er2(L-CN)3(H2O)] 59
Figure 3.7 Projection of [Er_2(L-CN)$_3$(H_2O)] 60
Figure 3.8 Projection of [Er_2(L)$_3$($MeOH$)$_3$] 60
Figure 4.1 Formation of salens with salicylaldehyde 75
Figure 4.2 Synthetic scheme for Naphthylpyrasal 76
Figure 4.3 Crystal structures with N-Oxide coordination involving Cu(II), Yb(III), & U(IV) .. 77
Figure 4.4 UV-Vis spectra of Naphthylpyrasal and Naphthylpyrasal+UO2+TEA 78
Figure 4.5 Crystal structure Naphthylpyrasal-UO2 from dioxanes/Pentane 80
Figure 4.6 Crystal structure Naphthylpyrasal-UO2 from DCM/Hexane 82
Figure 4.7 Proposed photocatalytic pathway for production of H_2O_2 with uranyl 83
Figure 4.8 UV-Vis spectra of Naphthylpyrasal+UO2+DIPEA and Naphthylpyrasal+UO2+TEMPO 84
Figure 4.9 CV of Naphthylpyrasal ligand and alternate reaction (TEA, DIPEA, TEMPO) conditions 85
Figure 4.10 Crystal structure Naphthylpyrasal-UO2+DIPEA from dioxane/pentane 88
Figure 5.1 Crystal structures of Salimidizine-UO2, [Er_2(L-CN)$_3$(H_2O)], Naphthylpyrasal-UO2-N-oxide 101
Figure 5.2 Functionalized naphthylsalophen ligands 104
Figure 5.3 Sulfonated Naphthylsalophen 107

List of Abbreviations

A	Amps
Å	Angstrom
cm	Centimeter
Cu	Copper
CV	Cyclic Voltammetry
DCM	Dichloromethane
DFT	Density Functional Theory
DIPEA	Di-isopropyl ethylamine
DMF	Dimethylformamide
EDS	Energy Dispersive Spectroscopy
Er	Erbium
ESA	Excited-state Absorption
EtOH	Ethanol
ETU	Energy Transfer Up-conversion
Gd	Gadolinium
L-CN	Cyanonaphthylsalophen ligand
Ln	Lanthanide
MeOH	Methanol
μmol	Micromolar
mmol	Millimole
Nd	Neodymium
nm	Nanometers

NPs	Nanoparticles
RFU	Raw Fluorescence Units
TEA	Triethylamine
TFA	Trifluoroacetic acid
TEMPO	(2,2,6,6-Tetramethylpiperidin-1-yl)oxyl
THF	Tetrahydrofuran
UC	Up Conversion
UO_2	Uranyl
V	Voltage
W	Watts
Yb	Ytterbium
Y	Yttrium

Chapter 1
Introduction

In recent years, a substantial push has been put into studying the 5*f* elements and being able to take advantage of their unique properties.[1] The majority of research in this field centers around the safe use of actinides in commercial nuclear reactors due to our ever-growing need for cleaner energy sources in a highly energy-dependent economy.[2] This coupled with the heightened need to lessen our carbon footprint make this a paramount area of focus. As of December of 2019, there were 96 operational nuclear reactors at 58 nuclear power plants in the U.S. alone,[3] and hence, an increasing need to expand our knowledge of the actinides to maintain them. Although thorium, plutonium and uranium can be used in the nuclear fuel cycle, the most commonly used actinide for this purpose is uranium, and almost 11% of the world's civilian energy generation comes from uranium fueled nuclear reactors.[4] Naturally occurring uranium is made up of ^{238}U (99.275%), ^{235}U (0.720%), and ^{234}U (0.005%); however, the only fissile isotope that could be used in fission reactors is ^{235}U.[5,6] Most reactors aim to keep a controlled fission reaction with "fertile" ^{238}U capturing neutrons from "bred" ^{239}Pu, producing ^{235}U subsequently releasing more neutrons to continue the chain fission reaction.[4,5] Some countries such as France reprocess their spent nuclear fuel rods; however, in the United States, reprocessing is not practiced, instead the fuel rods are either stored on site or at an underground disposal facility.[7]

The global output of nuclear energy comes from 447 operational nuclear power plants in 30 countries, and with 60 new facilities under construction, there is a push for even more renewable energy sources.[8] With this push, the International Atomic Energy Agency (IAEA) has estimated a 42% increase in globally installed nuclear power, and the World Nuclear Association has goals set for 25% of the world's electricity to be provided by nuclear energy by 2050.[8] This shows promise with 28 countries interested in introducing nuclear power and 16 of these building new reactors.[8]

Also, in 2014, the Environmental Protection Agency (EPA) instituted the Clean Air Act in 2014 which is pushing the U.S. to lower their carbon emission output to levels 25% below what they were in 2005.[9] As of 2018, the United states has come to produce about 20% of its electricity from nuclear power but this is still dwarfed by the 70% produced by France.[2] The use of nuclear power is one means to reduce the carbon footprint and decrease the use of fossil fuels, and is thus being pushed for vigorously. Since the United States produces approximately 2,000 metric tons of spent fuel each year,[10] accommodations need to be made for the spent fuel rods being produced, whether through storage or reprocessing.[11,12]

Soft donors for Identification

Many researchers are looking into ways to quickly and efficiently identify and quantify contaminants if a spill were to occur. Since Diamond and collaborators first showed the ability to selectively separate actinides from lanthanides via ion exchange, ways to make this distinction in solution have been examined.[13] Researchers are now looking at using softer donors such as nitrogen or sulfur to bind the metals in a more covalent manner, helping with the design of ligands for better binding and higher selectivity of actinides.[14,15] The Boncella group has looked at imine donors in a 2,2'-bipyridine adduct as a way to coordinate U(IV). They have also investigated using these complexes as substrates that can be used for two electron oxidative addition reactions allowing access to rare bis(imido) uranium (VI) complexes (Figure 1.1 a).[17] Another interesting example of using such softer donors for actinide coordination comes from Karsten Meyer's group. Their efforts to better understand the coordination environment and electronics of the uranyl ion for sequestering purposes has allowed them to use mixed oxygen-nitrogen donors to isolate and characterize uranium (VI) mono-oxo complexes (Figure 1.1 b).[18] Finally, one additional example

of soft donor coordination comes from the Prendergast group. In the hopes of gaining a deeper understanding of the bonding covalency of uranyl using N-donor ligands to coordinate the metal, the ligand they designed utilizes two imidazole N-donors and a pyridine donor to form a rigid tridentate pocket to coordinate uranyl ions (Figure 1.1 c).[19] This ligand has also been used to coordinate lanthanides and other low valent actinides as a way to examine the influence of ligand-metal charge transfer effects and π-π interactions on luminescence.[20–23]

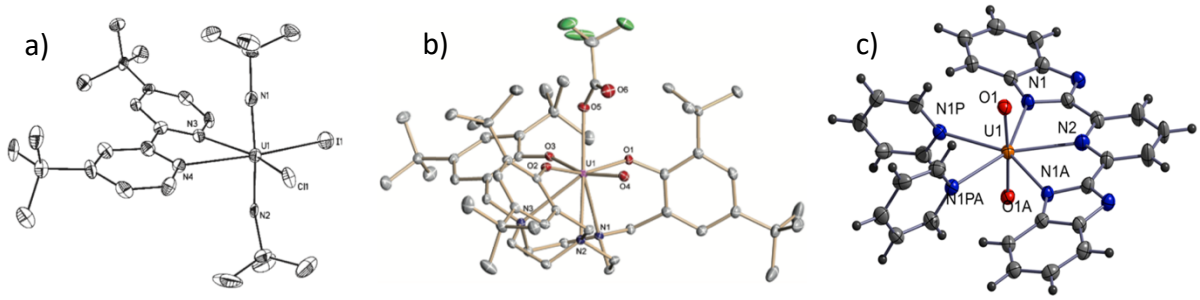

Figure 1.1.Crystal structures of (a) bis(imido) uranium (VI) complexes,[17] (b) uranium (VI) mono-oxo complex,[18] and (c) planar all nitrogen containing U(VI)O_2.[19]

Salen Ligands and *f*-block coordination

Salen type ligands are of interest in selective actinide coordination as imine donor ligands that are straightforward to prepare and manipulate but have been previously characterized in complexes with transition metals in several areas of chemistry. These ligands have shown the ability to form stable complexes with copper (II),[24] manganese (III),[25] and ruthenium (II)[26] for catalysis in organic reactions.[27] Many complexes have also been shown to be effective in asymmetric catalysis such as C-H insertion, cycloadditions, Mannich reactions, and aminations.[28] While this is an established area of research, new interest exist in exploring these ligands for binding *f*-block elements.

Use as Sensors

Salen and salen-type ligands have also been shown to be effective in binding $[UO_2]^{2+}$.[29–31] The name "salen" is derived from the reagents used to form the ligand by way of a condensation reaction, salicylic aldehyde (sal) and ethylene diamine (en), which forms a mixed oxygen and nitrogen tetra-dentate donor pocket (Figure 1.2).[32] The salen mixed donor binding pocket allows for the formation of a wide variety of metal complexes. Previously, the Gorden group has examined salen-type Schiff base ligands for metal complexation as a means of detecting actinide waste products.[32] Due to the extended conjugation of the ligands their UV-Visible spectra experiences detectable alterations upon binding of metal ions.[33] This is potentially one useful way to identify metal contaminants via examining the color/spectral changes produced by the ligand binding the metal ions.[34]

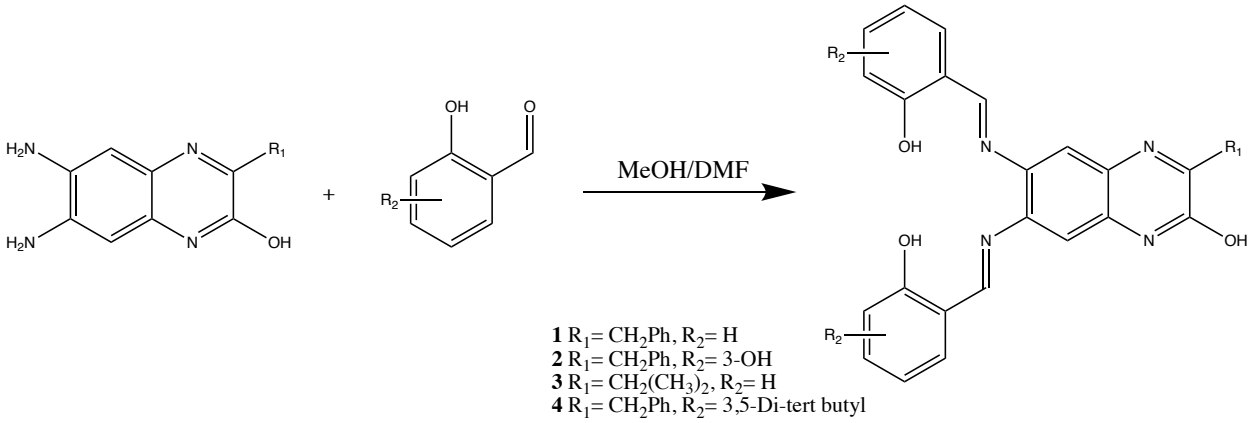

Figure 1.2. Synthetic scheme of salen ligand "Salqu".[35]

The 2-quinoxalinol ligand, "Salqu" (Figure 1.2) was able to show some promise as a chemosensor. Research in this area demonstrated binding of several transition metals as well as uranyl and some selectivity of UO_2^{2+} binding over lanthanides due to its mixed donor binding pocket. However,

binding of Cu^{2+} was competitive with that of UO_2^{2+} due to their similar charge to ionic size ratios.[35] This led to the hypothesis that there might be a way to tune the selectivity of the ligand binding pocket while still retaining the ability to follow changes using UV-Vis spectral or other emission methods. Recent examples in actinide coordination that take advantage of these unique emission methods have come from the Gorden group with ligands which fill up the equatorial plane of the uranyl ion such as pyridine Schiff base donors taking up 5 coordination sites. Occupying these five equatorial sites seems to allow for higher selectivity towards these uranyl metal centers over typical first row transition metals, while showing distinguishable changes via UV-Vis spectra. Also, florescence spectra were recorded in concert with UV-Vis spectra and all metals produced a quenching effect except Zn (II) ions which created a 5-fold increase in fluorescence and a Φ = 1.6.[36]

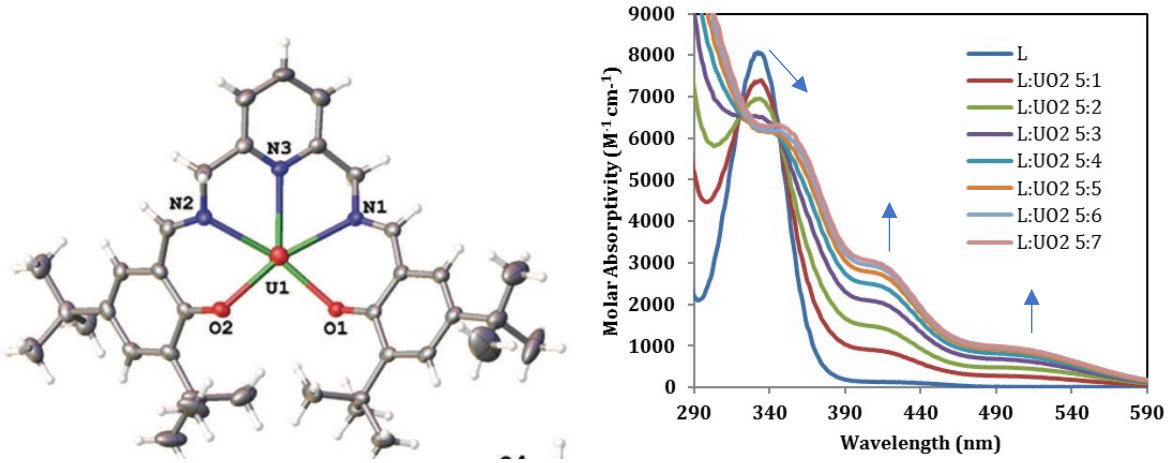

Figure 1.3. 2,6-bis[1-[(2-hydroxyphenyl)imino]ethyl] pyridine-UO_2 Complex(left), UV-Vis titration of 2,6-bis[1-[(2-hydroxyphenyl)imino]ethyl] pyridine with $UO_2(NO_3)_2 \bullet 6H_2O$ in ethanol (Right).[36]

Another example of these selectively coordinating ligand with unique spectral qualities is Dibenzyl 5,5′-((1E,1′E)-(1,2-Phenylene Bis(azanylylidene))bis-(methanylylidene))bis(4-ethyl-3-methyl-1H-pyrrole-2carboxylate)), called pyrrophen.[37] This ligand takes advantage of the salen binding motif while introducing four more coordination sites resulting in a hexadentate binding pocket. The equatorial binding sites for uranyl allow for coordination of the six donor atoms to selectively bind to the metal center in an equidistant fashion. Furthermore, the affinity of this ligand for the uranyl metal center is so pronounced that the presence of U induces displacement of some transition metals from the binding pocket.[37] These observations can be helpful to expand the knowledge required for better understanding of selective sensing of uranyl ions in solution.

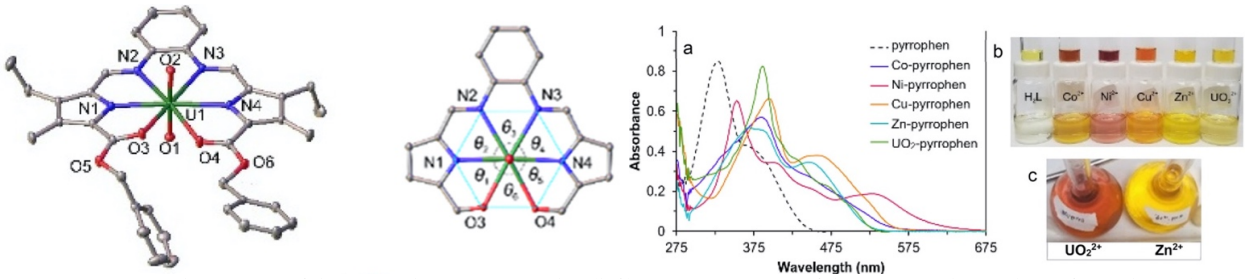

Figure 1.4.Crystal structure of the pyrrophen-UO_2 complex (left), UV-Vis spectra of distinct metal complexes formed in solution as well as colorimetric response to the specific metal ions (right).[37]

Utilization of lower valent Uranium species

A key aspect of *f*-block chemistry is determining a route to access and stabilize lower valent uranium species, specifically that of U(V).[38,39] Accessing this oxidation state of uranium is of interest because U(V) is relevant to nuclear waste remediation and catalysis.[40,41] The difficulty in this endeavor stems from the fact that U(V) is very unstable under environmental conditions, leading to a very short-lived oxidation state due to disproportionation yielding U(IV) and U(VI).[42] To attempt to stabilize these species, there are the extra precautions of working under inert

atmospheres that need to be taken followed by either oxidizing from U (III) [43,44] or U (IV)[45], or reduction of U (VI).[46,47,39]

The path for reduction of $[UO_2]^{2+}$ in recent years seems to be made by functionalization of the -yl oxygens.[40,47–51] These bonds are highly stable and very inert without some sort of electron density transfer to help lengthen these bonds as well as weaken them and increase their reactivity.[6] Work in the Arnold group has shown a suitable route to do this by using their "Pacman" salen containing ligand to help facilitate functionalization of the U-O_{yl} bonds.[52,53] This method takes advantage of using strong donating ligands along the equatorial sites of the uranyl metal center as well as steric and positioning of the terminal oxo group towards an oxophilic lanthanide or transition metal ion to help promote the oxo interactions.

The Hayton group has demonstrated this through using borane mediated reductive silylation of the U-O_{yl} bonds.[54] Here, they elaborate on the use of strong equatorial donors as well as Lewis acid donors to activate the -yl oxygens which allows for functionalization with both a borane and a triphenyl silane coordinated.[54] These are some examples of strategies used to functionalize these chemically "inert" uranyl oxygen bonds.

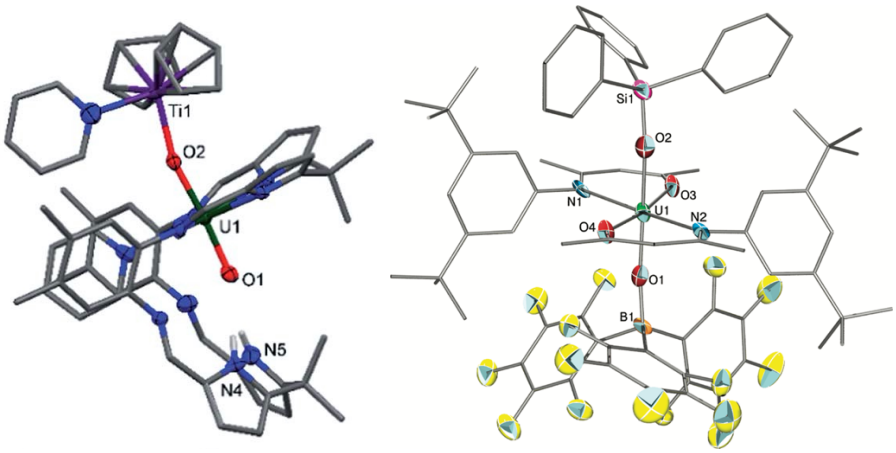

Figure 1.5.(Left) Solid state data from pacman-UO_2 Structure,[53] (Right) Silyl and borane functionalize uranium-oxo bond.[54]

Lanthanide emissions

Lanthanide ion complexes are of interest due to the ability they have to emit specific and well defined spectra as well as having long lived emission lifetimes which arise from *f-f* transitions.[55] Further, they are of particular interest for use in light sources,[56–59] screens and displays,[60–63] and medical imaging technology.[64–67] The antenna effect is utilized in most of these cases as a means to help excite these metal center and achieve these emissive states since direct excitation usually requires high energy lasers.[68] These "antenna" are usually organic frameworks that are easily sensitized. Once light is absorbed a ligand-based singlet excited state is achieved. The electron then progresses through intersystem crossing to afford a triplet excited state. From this sate the excited electron takes place in dipole-dipole or Förster's interactions to finally end up in the emissive *f*-excited state.[68]

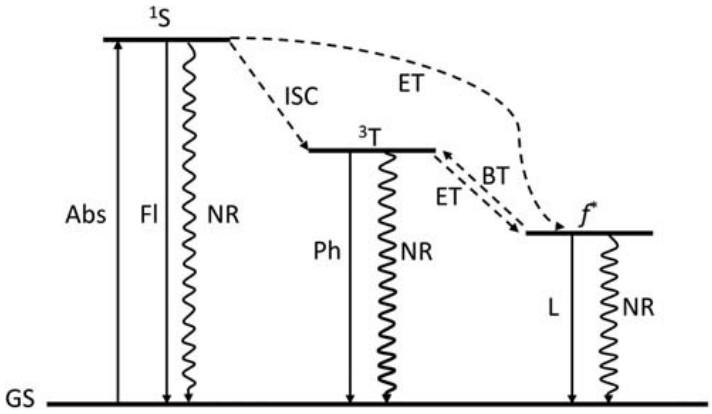

Figure 1.6.Modified Jablonski Diagram demonstrating the antenna effect for lanthanide complexe.[68]

Examples of these systems and how they take advantage of the ligands to sensitize the lanthanide metal centers can be seen throughout the literature. For effective sensitization using organic ligands, the following properties are important: 1) high efficiency at absorbing light, 2) attain intersystem crossing yields near 100%, 3) have triplet energy states that are close to the energy level of the Ln (III) emission but not close enough for energy back transfer, 4) be able to protect the Ln (III) ion form quenching effects due to bound water.[59] The de Bettencourt-Dias group at the University Nevada, Reno has been able follow these criteria through synthesizing and coordination of the ligand Pyridinebis-oxazoline, also known as pybox and its derivitives.[69–73] They have been able to produce high quantum efficiency Tb (III) complexes,[70] as well as rare Tm (III) blue centered and mixed metal polymers.[72]

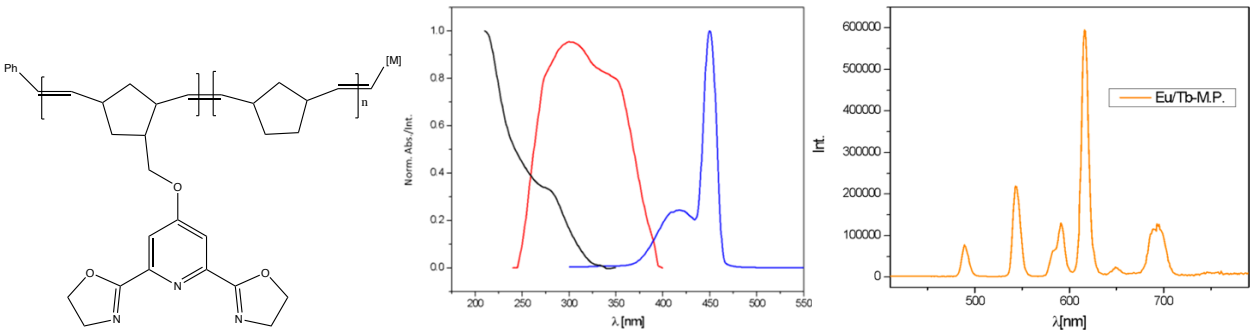

Figure 1.7. (Left)Pybox ligand derivative, (middle)Solid state Absorbance (black line), excitation (red line), and emission (blue line) spectra of Tm (III) complex, (Right)Solid state Eu (III) and Tb (III) mixed metal complex emission spectra.[72]

One area of research of note with these complexes are researched is in photon up conversion. Up conversion is the process by which a photon of lower energy is absorbed, and then electromagnetic radiation of higher energy is emitted.[68,74] To adequately design ligands suitable for sensitizing, three major criteria must be met, they are as follows. First, they must be able to coordinate the target metal which in this case would be the Ln (III) ion. Second, the energy levels

between the ligand and the metal center need to be positioned such that the sensitizers can have uninhibited transfer of the singlet and triplet excitation energy for specific lanthanide ion. Finally, these systems need to be low phonon systems to allow for efficient up conversion processes.[68,72]

Most upconverting species are typically in the form of nanoparticles,[75] fewer examples have been described as discrete molecules for this purpose.[76–78] This transition to discrete molecules can allow for increase in solubility,[79] lowering accumulation in vital organs,[65,80] and increasing biocompatibility.[81,82] Furthermore, finding ways to synthesize these discrete up converting molecules can lead to more efficient and easier ways of tuning emissions for use in vitro or in vivo by altering the Försters distances .[83]

Described in this work are three distinct ligand classes and their metal complexes which were synthesized and characterized: salimidizine (Chapter 2), cyano-naphthylsalophen (Chapter 3), and naphthylpyrasal (Chapter 4). These ligands were examined for their ability to coordinate the f-block metal ions. Chapter 2 explores salimidizine and its derivatives colorimetric and fluorescent sensor for uranyl. The copper (II) ion was also examined since it generally gives false positives for uranyl detection. Chapter 3 covers cyano-naphthylsalophen and its ability to coordinate several Ln (III) ions as well as its usefulness in partaking in two photon up conversion. Chapter 4 examines naphthylpyrasal and its coordination to uranyl. Formation of a unique actinide N-oxide complex is addressed as well as the effect of different N donor molecules on coordination and its solid-state structure. Chapter 5 gives a summary of preliminary work as well as a direction for these projects in the future.

References

(1) Gibson, J. K.; de Jong, W. A. *Experimental and Theoretical Approaches to Actinide Chemistry*; John Wiley & Sons Ltd., 2018. https://doi.org/10.1002/9781119115557.

(2) Schneider, M.; Froggatt, A.; Hazemann, J.; Katsuta, T.; Lovins, A. B.; Ramana, M. V.; von Hirschhausen, C.; Wealer, B.; Stienne, A.; Meinass, F. *The World Nuclear Industry Status Report 2019*; Paris, Budapest, 2019.

(3) Scott, M. *Nuclear Power Outlook*; Annual Energy Outlook 2018; DOE/EIA-0383(2016); U.S. Energy Information Administration: Washington, DC, 2018; p 17.

(4) World Nuclear Association: Uranium and Depleted Uranium. November 2016.

(5) Hála, J.; Navratil, J. D. *Radioactivity, Ionizing Radioation, and Nuclear Energy*, 1st ed.; Konvoj, spol. sr.o. (Ltd.), 2003.

(6) Morss, L. R.; Edelstein, N. M.; Fuger, J.; Katz, J. J. *The Chemistry of the Actinides and Transactinide Elements*, 3rd ed.; Dordrecht: Springer, 2006; Vol. 1.

(7) Kaltsoyannis, N.; Scott, P. *The f Elements*; Oxford University Press, 1999.

(8) *International Status and Prospect for Nuclear Power 2017*; GOV/INF/2017/12-GC(61)/INF/8; International Atomic Energy Agency: Board of Governors General Conference, 2017; p 14.

(9) World Nuclear Association: Nuclear Power in the USA http://www.world-nuclear.org/information-library/country-profiles/countries-t-z/usa-nuclear-power.aspx.

(10) Werner, J. D. *U.S. Spent Nuclear Fuel Storage*; Congressional Report R42513; Congressional Research Service: Washington, DC, 2012.

(11) Hore-Lacy, I. 5 - The “back end” of the nuclar fuel cycle. In *Nuclear Energy in the 21st Century*; Hore-Lacy, I., Ed.; Academic Press: Burlington, 2007; pp 75–92. https://doi.org/10.1016/B978-012373622-2/50008-8.

(12) Hore-Lacy, I. 7 - Environment, health and safety issues. In *Nuclear Energy in the 21st Century*; Hore-Lacy, I., Ed.; Academic Press: Burlington, 2007; pp 111–125. https://doi.org/10.1016/B978-012373622-2/50010-6.

(13) Diamond, R. M.; Street, K.; Seaborg, G. T. An Ion-Exchange Study of Possible Hybridized 5f Bonding in the Actinides1. *J. Am. Chem. Soc.* **1954**, *76* (6), 1461–1469. https://doi.org/10.1021/ja01635a001.

(14) Sessler, J. L.; Melfi, P. J.; Pantos, G. D. Uranium Complexes of Multidentate N-Donor Ligands. *Coord. Chem. Rev.* **2006**, *250* (7-8), 816–843. https://doi.org/10.1016/j.ccr.2005.10.007.

(15) Rosenzweig, M. W.; Scheurer, A.; Lamsfus, C. A.; Heinemann, F. W.; Maron, L.; Andrez, J.; Mazzanti, M.; Meyer, K. Uranium(Iv) Terminal Hydrosulfido and Sulfido Complexes: Insights into the Nature of the Uranium–Sulfur Bond. *Chem. Sci.* **2016**, *7* (9), 5857–5866. https://doi.org/10.1039/C6SC00677A.

(16) Cowie, B. E.; Douair, I.; Maron, L.; Love, J. B.; Arnold, P. L. Selective Oxo Ligand Functionalisation and Substitution Reactivity in an Oxo/Catecholate-Bridged UIV/UIV Pacman Complex. *Chem. Sci.* **2020**, *11* (27), 7144–7157. https://doi.org/10.1039/D0SC02297G.

(17) Spencer, L. P.; Yang, P.; Scott, B. L.; Batista, E. R.; Boncella, J. M. Oxidative Addition to U(V)−U(V) Dimers: Facile Routes to Uranium(VI) Bis(Imido) Complexes. *Inorg. Chem.* **2009**, *48* (24), 11615–11623. https://doi.org/10.1021/ic901581r.

(18) Kosog, B.; La Pierre, H. S.; Heinemann, F. W.; Liddle, S. T.; Meyer, K. Synthesis of Uranium(VI) Terminal Oxo Complexes: Molecular Geometry Driven by the Inverse Trans-Influence. *J. Am. Chem. Soc.* **2012**, *134* (11), 5284–5289. https://doi.org/10.1021/ja211618v.

(19) Copping, R.; Jeon, B.; Pemmaraju, C. D.; Wang, S.; Teat, S. J.; Janousch, M.; Tyliszczak, T.; Canning, A.; Grønbech-Jensen, N.; Prendergast, D.; Shuh, D. K. Toward Equatorial Planarity about Uranyl: Synthesis and Structure of Tridentate Nitrogen-Donor {UO2}2+ Complexes. *Inorg. Chem.* **2014**, *53* (5), 2506–2515. https://doi.org/10.1021/ic4026359.

(20) Piguet, C.; Buenzli, J. C. G.; Bernardinelli, G.; Hopfgartner, G.; Williams, A. F. Self-Assembly and Photophysical Properties of Lanthanide Dinuclear Triple-Helical Complexes. *J. Am. Chem. Soc.* **1993**, *115* (18), 8197–8206. https://doi.org/10.1021/ja00071a032.

(21) Petoud, S.; Bünzli, J.-C. G.; Schenk, K. J.; Piguet, C. Luminescent Properties of Lanthanide Nitrato Complexes with Substituted Bis(Benzimidazolyl)Pyridines. *Inorg. Chem.* **1997**, *36* (7), 1345–1353. https://doi.org/10.1021/ic961305a.

(22) Petoud, S.; Bünzli, J.-C. G.; Glanzman, T.; Piguet, C.; Xiang, Q.; Thummel, R. P. Influence of Charge-Transfer States on the Eu(III) Luminescence in Mononuclear Triple Helical Complexes with Tridentate Aromatic Ligands. *J. Lumin.* **1999**, *82* (1), 69–79. https://doi.org/10.1016/S0022-2313(99)00015-0.

(23) Pemmaraju, C. D.; Copping, R.; Wang, S.; Janousch, M.; Teat, Simon. J.; Tyliszcak, T.; Canning, A.; Shuh, D. K.; Prendergast, D. Bonding and Charge Transfer in Nitrogen-Donor

Uranyl Complexes: Insights from NEXAFS Spectra. *Inorg. Chem.* **2014**, *53* (21), 11415–11425. https://doi.org/10.1021/ic501107a.

(24) Black, C. C.; Gorden, A. E. V. Oxidative Mannich Reactions of Tertiary Amines Using a Cu(II) 2-Quinoxalinol Salen Catalyst. *J. Org. Chem.* **2019**, *84* (15), 9806–9810. https://doi.org/10.1021/acs.joc.9b01409.

(25) Chidara, V. K.; Du, G. An Efficient Catalyst Based on Manganese Salen for Hydrosilylation of Carbonyl Compounds. *Organometallics* **2013**, *32* (18), 5034–5037. https://doi.org/10.1021/om400805v.

(26) Sun, W.; Yu, B.; Kühn, F. E. Ruthenium(II)–Salen Complexes-Catalyzed Olefination of Aldehydes with Ethyl Diazoacetate. *Tetrahedron Lett.* **2006**, *47* (12), 1993–1996. https://doi.org/10.1016/j.tetlet.2006.01.055.

(27) Wu, X.; Hubbard, H. K.; Tate, B. K.; Gorden, A. E. V. One-Pot Metal Templated Synthesis for the Preparation of 2-Quinoxalinol Salen Metal Complexes. *Polyhedron* **2009**, *28* (2), 360–362. https://doi.org/10.1016/j.poly.2008.10.050.

(28) Shaw, S.; White, J. D. Asymmetric Catalysis Using Chiral Salen–Metal Complexes: Recent Advances. *Chem. Rev.* **2019**, *119* (16), 9381–9426. https://doi.org/10.1021/acs.chemrev.9b00074.

(29) Asadi, Z.; Shorkaei, M. R. Synthesis, X-Ray Crystallography, Thermal Studies, Spectroscopic and Electrochemistry Investigations of Uranyl Schiff Base Complexes. *Spectrochim. Acta. A. Mol. Biomol. Spectrosc.* **2013**, *105*, 344–351. https://doi.org/10.1016/j.saa.2012.12.024.

(30) Ghosh, S.; Biswas, S.; Bauzá, A.; Barceló-Oliver, M.; Frontera, A.; Ghosh, A. Use of Metalloligands [CuL] (H2L = Salen Type Di-Schiff Bases) in the Formation of Heterobimetallic

Copper(II)-Uranyl Complexes: Photophysical Investigations, Structural Variations, and Theoretical Calculations. *Inorg. Chem.* **2013**, *52* (13), 7508–7523. https://doi.org/10.1021/ic400422d.

(31) Zhang, Y.; Fanna, D. J.; Shepherd, N. D.; Karatchevtseva, I.; Lu, K.; Kong, L.; Price, J. R. Dioxo-Vanadium(v), Oxo-Rhenium(v) and Dioxo-Uranium(vi) Complexes with a Tridentate Schiff Base Ligand. *RSC Adv.* **2016**, *6* (79), 75045–75053. https://doi.org/10.1039/C6RA12872F.

(32) Gorden, A. E. V.; Wu, X. 2-Quinoxalinol Salen Compounds and Uses Thereof. US2009/0286968A1, November 19, 2009.

(33) Bharara, M. S.; Heflin, K.; Tonks, S.; Strawbridge, K. L.; Gorden, A. E. V. Hydroxy- and Alkoxy-Bridged Dinuclear Uranyl-Schiff Base Complexes: Hydrolysis, Transamination and Extraction Studies. *Dalton Trans.* **2008**, No. 22, 2966–2973. https://doi.org/10.1039/B800469B.

(34) Kaur, B.; Kaur, N.; Kumar, S. Colorimetric Metal Ion Sensors – A Comprehensive Review of the Years 2011–2016. *Coord. Chem. Rev.* **2018**, *358*, 13–69. https://doi.org/10.1016/j.ccr.2017.12.002.

(35) Wu, X.; Bharara, M. S.; Bray, T. H.; Tate, B. K.; Gorden, A. E. V. Synthesis and Characterization of 2-Quinoxalinol Schiff-Base Metal Complexes. *Inorganica Chim. Acta* **2009**, *362* (6), 1847–1854. https://doi.org/10.1016/j.ica.2008.08.037.

(36) Hardy, E. E.; Wyss, K. M.; Eddy, M. A.; Gorden, A. E. V. An Example of Unusual Pyridine Donor Schiff Base Uranyl (UO_2^{2+}) Complexes. *Chem. Commun.* **2017**, *53* (42), 5718–5720. https://doi.org/10.1039/C7CC02747H.

(37) Mayhugh, J. T.; Niklas, J. E.; Forbes, M. G.; Gorden, J. D.; Gorden, A. E. V. Pyrrophens: Pyrrole-Based Hexadentate Ligands Tailor-Made for Uranyl (UO_2^{2+}) Coordination and

Molecular Recognition. *Inorg. Chem.* **2020**, *59* (14), 9560–9568. https://doi.org/10.1021/acs.inorgchem.0c00439.

(38) Selbin, J.; Ortego, J. D. Chemistry of Uranium (V). *Chem. Rev.* **1969**, *69* (5), 657–671. https://doi.org/10.1021/cr60261a004.

(39) Graves, C. R.; Kiplinger, J. L. Pentavalent Uranium Chemistry—Synthetic Pursuit of a Rare Oxidation State. *Chem. Commun.* **2009**, No. 26, 3831–3853. https://doi.org/10.1039/B902969A.

(40) Halter, D. P.; Heinemann, F. W.; Bachmann, J.; Meyer, K. Uranium-Mediated Electrocatalytic Dihydrogen Production from Water. *Nature* **2016**, *530* (7590), 317–321. https://doi.org/10.1038/nature16530.

(41) Fox, A. R.; Bart, S. C.; Meyer, K.; Cummins, C. C. Towards Uranium Catalysts. *Nature* **2008**, *455* (7211), 341–349. https://doi.org/10.1038/nature07372.

(42) Wander, M. C. F.; Shuford, K. L. A Theoretical Study of the Qualitative Reaction Mechanism for the Homogeneous Disproportionation of Pentavalent Uranyl Ions. *Geochim. Cosmochim. Acta* **2012**, *84*, 177–185. https://doi.org/10.1016/j.gca.2012.01.034.

(43) Gardner, B. M.; Kefalidis, C. E.; Lu, E.; Patel, D.; McInnes, E. J. L.; Tuna, F.; Wooles, A. J.; Maron, L.; Liddle, S. T. Evidence for Single Metal Two Electron Oxidative Addition and Reductive Elimination at Uranium. *Nat. Commun.* **2017**, *8* (1), 1898. https://doi.org/10.1038/s41467-017-01363-0.

(44) Settineri, N. S.; Shiau, A. A.; Arnold, J. Two-Electron Oxidation of a Homoleptic U(Iii) Guanidinate Complex by Diphenyldiazomethane. *Chem. Commun.* **2018**, *54* (77), 10913–10916. https://doi.org/10.1039/C8CC06514D.

(45) Graves, C. R.; Scott, B. L.; Morris, D. E.; Kiplinger, J. L. Facile Access to Pentavalent Uranium Organometallics: One-Electron Oxidation of Uranium(IV) Imido Complexes with Copper(I) Salts. *J. Am. Chem. Soc.* **2007**, *129* (39), 11914–11915. https://doi.org/10.1021/ja074889w.

(46) Mizuoka, K.; Kim, S.-Y.; Hasegawa, M.; Hoshi, T.; Uchiyama, G.; Ikeda, Y. Electrochemical and Spectroelectrochemical Studies on UO2(Saloph)L (Saloph = N,N‘-Disalicylidene-o-Phenylenediaminate, L = Dimethyl Sulfoxide or N,N-Dimethylformamide). *Inorg. Chem.* **2003**, *42* (4), 1031–1038. https://doi.org/10.1021/ic0260926.

(47) Hayton, T. W.; Wu, G. Exploring the Effects of Reduction or Lewis Acid Coordination on the U═O Bond of the Uranyl Moiety. *Inorg. Chem.* **2009**, *48* (7), 3065–3072. https://doi.org/10.1021/ic802360y.

(48) Arnold, P. L.; Pécharman, A.-F.; Hollis, E.; Yahia, A.; Maron, L.; Parsons, S.; Love, J. B. Uranyl Oxo Activation and Functionalization by Metal Cation Coordination. *Nat. Chem.* **2010**, *2* (12), 1056–1061. https://doi.org/10.1038/nchem.904.

(49) Pedrick, E. A.; Wu, G.; Hayton, T. W. Reductive Silylation of the Uranyl Ion with Ph3SiOTf. *Inorg. Chem.* **2014**, *53* (23), 12237–12239. https://doi.org/10.1021/ic502267t.

(50) Arnold, P. L.; Pécharman, A.-F.; Lord, R. M.; Jones, G. M.; Hollis, E.; Nichol, G. S.; Maron, L.; Fang, J.; Davin, T.; Love, J. B. Control of Oxo-Group Functionalization and Reduction of the Uranyl Ion. *Inorg. Chem.* **2015**, *54* (7), 3702–3710. https://doi.org/10.1021/acs.inorgchem.5b00420.

(51) Seaman, L. A.; Pedrick, E. A.; Wu, G.; Hayton, T. W. Promoting Oxo Functionalization in the Uranyl Ion by Ligation to Ketimides. *J. Organomet. Chem.* **2018**, *857*, 34–37. https://doi.org/10.1016/j.jorganchem.2017.08.007.

(52) Arnold, P. L.; Hollis, E.; White, F. J.; Magnani, N.; Caciuffo, R.; Love, J. B. Single-Electron Uranyl Reduction by a Rare-Earth Cation. *Angew. Chem. Int. Ed.* **2011**, *50* (4), 887–890. https://doi.org/10.1002/anie.201005511.

(53) Zegke, M.; Zhang, X.; Pidchenko, I.; Hlina, J. A.; Lord, R. M.; Purkis, J.; Nichol, G. S.; Magnani, N.; Schreckenbach, G.; Vitova, T.; Love, J. B.; Arnold, P. L. Differential Uranyl(v) Oxo-Group Bonding between the Uranium and Metal Cations from Groups 1, 2, 4, and 12; a High Energy Resolution X-Ray Absorption, Computational, and Synthetic Study. *Chem. Sci.* **2019**, *10* (42), 9740–9751. https://doi.org/10.1039/C8SC05717F.

(54) Schnaars, D. D.; Wu, G.; Hayton, T. W. Borane-Mediated Silylation of a Metal–Oxo Ligand. *Inorg. Chem.* **2011**, *50* (11), 4695–4697. https://doi.org/10.1021/ic2008649.

(55) de Bettencourt-Dias, A. Lanthanide-Based Emitting Materials in Light-Emitting Diodes. *Dalton Trans.* **2007**, No. 22, 2229–2241. https://doi.org/10.1039/B702341C.

(56) Zhao, Y.-W.; Zhang, F.-Q.; Zhang, X.-M. Single Component Lanthanide Hybrids Based on Metal–Organic Framework for Near-Ultraviolet White Light LED. *ACS Appl. Mater. Interfaces* **2016**, *8* (36), 24123–24130. https://doi.org/10.1021/acsami.6b07724.

(57) Wang, Z.; Wang, Z.; Lin, B.; Hu, X.; Wei, Y.; Zhang, C.; An, B.; Wang, C.; Lin, W. Warm-White-Light-Emitting Diode Based on a Dye-Loaded Metal–Organic Framework for Fast White-Light Communication. *ACS Appl. Mater. Interfaces* **2017**, *9* (40), 35253–35259. https://doi.org/10.1021/acsami.7b11277.

(58) Bao, W.; Yu, X.-Y.; Dong, W.-W.; Zhao, J.; Tian, Z.-F.; Li, D.-S. Novel Composites of Graphitic-Phase Nitrogen Carbon/Lanthanide Coordination Polymers as White Light-Emitting Phosphor. *Z. Für Anorg. Allg. Chem.* **2019**, *645* (22), 1279–1284. https://doi.org/10.1002/zaac.201900245.

(59) Liu, X.; Xu, Y.; Liu, Q.; Zhang, W. 8-Hydroxyquinoline and Eu3+ Incorporated Metal–Organic Framework Nanosystems with Tunable Emissions for White Light and Anticounterfeiting Applications. *ACS Appl. Nano Mater.* **2021**, *4* (1), 313–321. https://doi.org/10.1021/acsanm.0c02671.

(60) Xu, H.; Zhu, R.; Zhao, P.; Huang, W. Monochromic Red-Emitting Nonconjugated Copolymers Containing Double-Carrier-Trapping Phosphine Oxide Eu3+ Segments: Toward Bright and Efficient Electroluminescence. *J. Phys. Chem. C* **2011**, *115* (31), 15627–15638. https://doi.org/10.1021/jp2029714.

(61) Qin, X.; Liu, X.; Huang, W.; Bettinelli, M.; Liu, X. Lanthanide-Activated Phosphors Based on 4f-5d Optical Transitions: Theoretical and Experimental Aspects. *Chem. Rev.* **2017**, *117* (5), 4488–4527. https://doi.org/10.1021/acs.chemrev.6b00691.

(62) SeethaLekshmi, S.; Ramya, A. R.; Reddy, M. L. P.; Varughese, S. Lanthanide Complex-Derived White-Light Emitting Solids: A Survey on Design Strategies. *J. Photochem. Photobiol. C Photochem. Rev.* **2017**, *33*, 109–131. https://doi.org/10.1016/j.jphotochemrev.2017.11.001.

(63) Guo, L.; Zhang, X.; Yang, D.; Liang, H.; Wang, Y. Luminescence Enhancement of Europium(III) Complexes by an Ionic Liquid. *J. Lumin.* **2019**, *215*, 116610. https://doi.org/10.1016/j.jlumin.2019.116610.

(64) Yang, Y.; Wang, P.; Lu, L.; Fan, Y.; Sun, C.; Fan, L.; Xu, C.; El-Toni, A. M.; Alhoshan, M.; Zhang, F. Small-Molecule Lanthanide Complexes Probe for Second Near-Infrared Window Bioimaging. *Anal. Chem.* **2018**, *90* (13), 7946–7952. https://doi.org/10.1021/acs.analchem.8b00603.

(65) Li, D.; He, S.; Wu, Y.; Liu, J.; Liu, Q.; Chang, B.; Zhang, Q.; Xiang, Z.; Yuan, Y.; Jian, C.; Yu, A.; Cheng, Z. Excretable Lanthanide Nanoparticle for Biomedical Imaging and Surgical

Navigation in the Second Near-Infrared Window. *Adv. Sci.* **2019**, *6* (23), 1902042. https://doi.org/10.1002/advs.201902042.

(66) Xu, J.; Gulzar, A.; Yang, P.; Bi, H.; Yang, D.; Gai, S.; He, F.; Lin, J.; Xing, B.; Jin, D. Recent Advances in Near-Infrared Emitting Lanthanide-Doped Nanoconstructs: Mechanism, Design and Application for Bioimaging. *Coord. Chem. Rev.* **2019**, *381*, 104–134. https://doi.org/10.1016/j.ccr.2018.11.014.

(67) Fan, Z.; Jiang, B.; Zhu, Q.; Xiang, S.; Tu, L.; Yang, Y.; Zhao, Q.; Huang, D.; Han, J.; Su, G.; Ge, D.; Hou, Z. Tumor-Specific Endogenous FeII-Activated, MRI-Guided Self-Targeting Gadolinium-Coordinated Theranostic Nanoplatforms for Amplification of ROS and Enhanced Chemodynamic Chemotherapy. *ACS Appl. Mater. Interfaces* **2020**, *12* (13), 14884–14904. https://doi.org/10.1021/acsami.0c00970.

(68) *Luminescence of Lanthanide Ions in Coordination Compounds and Nanomaterials*, 1st ed.; de Bettencourt-Dias, A., Ed.; John Wiley & Sons Ltd.: United Kingdom, 2014.

(69) de Bettencourt-Dias, A.; Viswanathan, S.; Rollett, A. Thiophene-Derivatized Pybox and Its Highly Luminescent Lanthanide Ion Complexes. *J. Am. Chem. Soc.* **2007**, *129* (50), 15436–15437. https://doi.org/10.1021/ja076485+.

(70) de Bettencourt-Dias, A.; Barber, P. S.; Viswanathan, S.; de Lill, D. T.; Rollett, A.; Ling, G.; Altun, S. Para-Derivatized Pybox Ligands As Sensitizers in Highly Luminescent Ln(III) Complexes. *Inorg. Chem.* **2010**, *49* (19), 8848–8861. https://doi.org/10.1021/ic101034y.

(71) De Bettencourt-Dias, A.; Barber, P. S.; Bauer, S. A Water-Soluble Pybox Derivative and Its Highly Luminescent Lanthanide Ion Complexes. *J. Am. Chem. Soc.* **2012**, *134* (16), 6987–6994. https://doi.org/10.1021/ja209572m.

(72) de Bettencourt-Dias, A.; Rossini, J. S. K. Ligand Design for Luminescent Lanthanide-Containing Metallopolymers. *Inorg. Chem.* **2016**, *55* (20), 9954–9963. https://doi.org/10.1021/acs.inorgchem.6b00946.

(73) Johnson, K. R.; Gracia-Nava, M. A.; de Bettencourt-Dias, A. Thiophene-Derivatized Pyridine-Biscarboxamide as a Sensitizer for LnIII Luminescence and 1O2 Generation. *J. Lumin.* **2020**, *224*, 117309. https://doi.org/10.1016/j.jlumin.2020.117309.

(74) Sivakumar, S.; van Veggel, F. C. J. M.; May, P. S. Near-Infrared (NIR) to Red and Green Up-Conversion Emission from Silica Sol−Gel Thin Films Made with La0.45Yb0.50Er0.05F3 Nanoparticles, Hetero-Looping-Enhanced Energy Transfer (Hetero-LEET): A New Up-Conversion Process. *J. Am. Chem. Soc.* **2007**, *129* (3), 620–625. https://doi.org/10.1021/ja065378x.

(75) Lim, E.-K.; Kim, T.; Paik, S.; Haam, S.; Huh, Y.-M.; Lee, K. Nanomaterials for Theranostics: Recent Advances and Future Challenges. *Chem. Rev.* **2015**, *115* (1), 327–394. https://doi.org/10.1021/cr300213b.

(76) Charbonnière, L. J. Bringing Upconversion down to the Molecular Scale. *Dalton Trans.* **2018**, *47* (26), 8566–8570. https://doi.org/10.1039/C7DT04737A.

(77) Monteiro, J. H. S. K.; Hiti, E. A.; Hardy, E. E.; Wilkinson, G. R.; Gorden, J. D.; Gorden, A. E. V.; de Bettencourt-Dias, A. New Up-Conversion Luminescence in Molecular Cyano-Substituted Naphthylsalophen Lanthanide(Iii) Complexes. *Chem. Commun.* **2021**. https://doi.org/10.1039/D0CC08128K.

(78) Nonat, A.; Bahamyirou, S.; Lecointre, A.; Przybilla, F.; Mély, Y.; Platas-Iglesias, C.; Camerel, F.; Jeannin, O.; Charbonnière, L. J. Molecular Upconversion in Water in

Heteropolynuclear Supramolecular Tb/Yb Assemblies. *J. Am. Chem. Soc.* **2019**, *141* (4), 1568–1576. https://doi.org/10.1021/jacs.8b10932.

(79) Cai, Y.; Si, W.; Huang, W.; Chen, P.; Shao, J.; Dong, X. Organic Dye Based Nanoparticles for Cancer Phototheranostics. *Small* **2018**, *14* (25), 1704247. https://doi.org/10.1002/smll.201704247.

(80) Zhao, M.; Li, B.; Wang, P.; Lu, L.; Zhang, Z.; Liu, L.; Wang, S.; Li, D.; Wang, R.; Zhang, F. Supramolecularly Engineered NIR-II and Upconversion Nanoparticles In Vivo Assembly and Disassembly to Improve Bioimaging. *Adv. Mater.* **2018**, *30* (52), 1804982. https://doi.org/10.1002/adma.201804982.

(81) Blanco, E.; Shen, H.; Ferrari, M. Principles of Nanoparticle Design for Overcoming Biological Barriers to Drug Delivery. *Nat. Biotechnol.* **2015**, *33* (9), 941–951. https://doi.org/10.1038/nbt.3330.

(82) Mosquera, J.; García, I.; Liz-Marzán, L. M. Cellular Uptake of Nanoparticles versus Small Molecules: A Matter of Size. *Acc. Chem. Res.* **2018**, *51* (9), 2305–2313. https://doi.org/10.1021/acs.accounts.8b00292.

(83) Brannan, A. C.; Lee, Y. Photophysical Tuning of σ-SiH Copper-Carbazolide Complexes To Give Deep-Blue Emission. *Inorg. Chem.* **2020**, *59* (1), 315–324. https://doi.org/10.1021/acs.inorgchem.9b02409.

Chapter 2
Salimidizine

Introduction

Imidazole and benzimidazole-containing ligands are naturally present in biomolecules and are pertinent to biological and medical applications showing anti-inflammatory and anti-tumor activities.[1,2] Complexes with two such ligands display π-π interactions,[3] while benzimidazole derivatives have been used in polymer enhancing catalysis and as fluorescent probes in sensors to detect Fe (III) and nitric oxide.[4–7] In recent years, imidazole containing d- and f-block metal complexes have been reported in applications organic light-emitting diodes (OLEDs).[8,9] Specific benzimidazole derivatives act as bidentate ligands exhibiting an N-C-C-C-O binding motif (N and O atoms connected with a three-C bridge coordinate to the metal). Such complexes have been reported for transition metals such as copper, nickel, and iron.[10,11] Previous research has demonstrated that ligands can take advantage of soft donors like imine nitrogens such as these in coordination of the actinides.[12,13]

Here, the ligand 2-(1H-imidazo[4,5-b]phenazin-2-yl)phenol (dubbed "salimidizine") represents a class of benzimidazole derivatives with extended conjugation and presents a potential means to investigate coordination by comparing emission properties. This ligand was first synthesized by Amer et. al. in 1999[14], and later spectroscopically characterized in 2011 by Lei and co-workers with various substituents on the terminal benzene ring (X= H, CH_3O, CH_2OH, Br, and Cl).[15] Here, we report crystal structures and fluorescence spectra for this ligand and its coordination complexes with uranyl (UO_2^{2+}) and Cu^{2+}. Uranyl (UO_2^{2+}) and Cu^{2+} were selected because of their similar charge to ionic radius ratios, and their competitive binding behavior in an attempt to characterize clear distinctions between the metal ions. It was observed that upon coordination of uranyl, fluorescence intensity increased, but it was found to decrease dramatically with copper coordination. This is a marked difference - notable in other systems proposed or

characterized with an interest in uranyl detection .[16–19] For example Kim et. al. made use of a diaza-18-crown-6-ether containing ligand with two terminal napthalamide units to increase fluorescence as possible uranyl sensor.[17] In that report, they examined the fluorescence of the ligand when bound to several different group 1 and 2 metals. They observed no change when bound to the group 1 and 2 metals but encountered an extreme decrease in fluorescence when bound to uranyl.

As alternative step in the synthesis to prepare new ligands is possible using 2-(1H-imidazo[4,5-b]phenazine-2-yl)phenol or "salimidizine" and derivatives of this molecule (Figure 2.8). This concept came from trying to extend the conjugation of the backbone with an aim to increase the emission intensity and the extinction coefficient of the metal complexes, while decreasing sample sizes required.[20] Additional benefits include the simplicity of such ligand and that the procedure is very similar to that used preparing the two-armed Salqu-type ligand with either the phenazine backbone or the leucine methyl ester backbone. When the solution is left open to air and heated, the reaction is driven towards the thermodynamically favored imidazole product. Such imidazole containing ligands have been used to coordinate nickel, lead, and iron in a bidentate fashion, and have been used to identify metal ions by inducing either a change in florescence, or UV-vis spectra.[11,21,22] There have also been examples of lanthanide ions being coordinated with bite angles and donor atoms similar to those found in the imidazole ligands, which showed interesting near IR properties.[8,9] The imidazole binding pocket has been previously shown to coordinate actinides and is of interest for selective coordination in terms of detection or isolation of actinides.[12,13] Salimidizine, and three derivatives thereof, were prepared through a condensation reaction between a salicylaldehyde and 2,3-diaminophenazine followed by a subsequent intramolecular cyclization reaction, affording **L1** (salimidizine), **L2** (t-

butylsalimidizine), **L3** (cyanosalimidizine), and **L4** (methoxysalimidizine) in moderate yields (Error! Reference source not found.). To better understand the different ligand-metal interactions with uranyl and Cu (II), quantum chemical calculations were performed to describe the ground and excited electronic states of their complexes with **L1**.

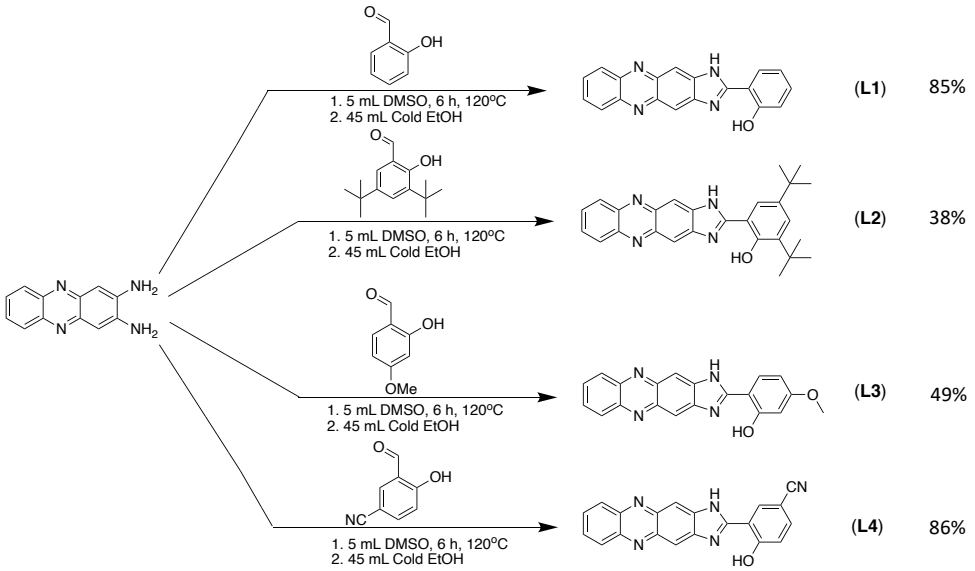

Figure 2.8. Salimidizine synthetic scheme

Results and Discussion

The general synthetic procedure for the salimidizine (**L1**), 3,5-ditertbutyl salimidizine (**L2**), methoxy salimidizine (**L3**), and cyano-salimidizine (**L4**) is as follows: 2,3-diaminophenazine was dissolved in 5 ml of DMSO and stirred at 80°C for 10 minutes to ensure it dissolves completely. Next, the respective salicylaldehyde was added and the mixture was heated to 120°C with stirring for 6 h. The solution reaction was then allowed to cool to room temperature, followed by the addition of 45 ml of chilled EtOH to help the product precipitate out of solution. The solution was allowed to sit at 0°C in a freezer overnight, then filtered and washed with cold

EtOH. The filtered solid was then placed in the vacuum oven overnight hours to dry and to remove any excess solvent.

An experiment to follow coordination using batch titrations was set up to allow for monitoring of the binding of metal to these ligands by UV-Vis spectra. Batch titrations were set up for all samples. Stock solutions of **L1**, **L2**, **L3**, and **L4** were made to 0.001 M solution in 40 mL of dimethylformamide (DMF). Metal stock solutions of both copper (II) acetate and uranyl acetate were made to 0.001 M in 25 mL of deionized H_2O. For each titration experiment, a ligand blank with no metal was made as well as 14 other samples containing 1 equivalent of ligand. Each of these samples, not including the free base, received 0.1 equivalents of metal stock solution; and subsequent aliquots increased the concentration of metal in solution by 0.1 equivalents until 1 equivalent of metal was reached. Further increases of metal occurred in increments of 1 full equivalent until reaching 5 equivalents of metal to ensure that excess metal was present in the sample. Following preparation all samples were aged for 24 hours to allow for complexation to occur, then the UV-vis spectra of each sample was measured. After the first spectra was recorded, 3 μL of 0.1 M trimethylamine (TEA) in DMF was added to the samples to facilitate deprotonation of the ligand. The samples were mixed for 5 minutes and further aged for 1 hour after addition of TEA, followed by collecting their UV-Vis spectra. All samples were 5 mL in volume and contained 10% H_2O.

Titrations with the bare ligand, salimidizine (LI), were conducted with UO_2^{2+} and with Cu^{2+}. In the UV- Vis spectra below, some of the individual spectra were removed for clarity. The UV-vis spectra showed a peak at 439 nm characteristic of the bare ligand and no additional shift were detected after subsequent additions of UO_2^{2+}, even after 5 full equivalents of metal. The only

observed spectral change involved an increase in absorbance with each equivalent of metal added (SI Figure 5). The Cu^{2+} titration showed a much more dramatic shift in the spectra as λmax shifted bathochromically from 416 nm to 455 nm after addition of the first 0.1 equivalent and remains unchanged until a ratio of 1:1 ligand to metal was reached. Between addition of the second equivalent of metal and up to 5 equivalents λ_{max} shifts hypsochromically to 325 nm (Figure 2.9). Although there was no significant shift in the spectra to suggest binding of the uranyl by **L1** under these conditions, we were able to obtain a crystal structure of the **L1** ligand bound to the uranyl.

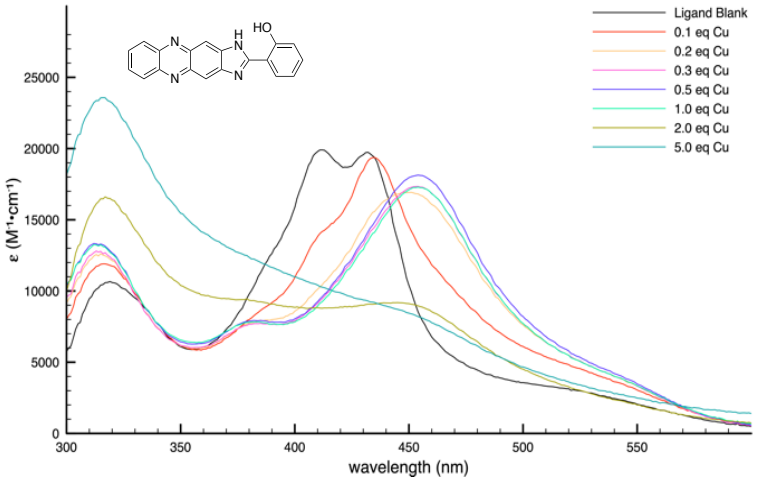

Figure 2.9. Salimidizine (L1) titration with Cu^{2+} acetate

Upon further examination, the UV-Vis data of solutions containing the ditertbutyl-salimidizne ligand were most promising in terms of metal coordination. Addition of base was needed to facilitate coordination, as was made evident from the observed spectral shifts. Ditertbutyl-salimidizne (**L2**) coordination with UO_2^{2+} was characterized by means of batch titration, and the following features were observed: the ligand free base showed a peak centered at 421 nm and after the first 0.1 equivalents of metal were added, a shift to 440 nm was noticed. This change intensified but was not fully defined until 0.3 equivalents were added to the sample (Figure 2.10). This bathochromic shift seemed to demonstrate that a binding event had occurred;

however, the solutions showed no visible colorimetric change as all samples exhibited a similar pale-yellow color.

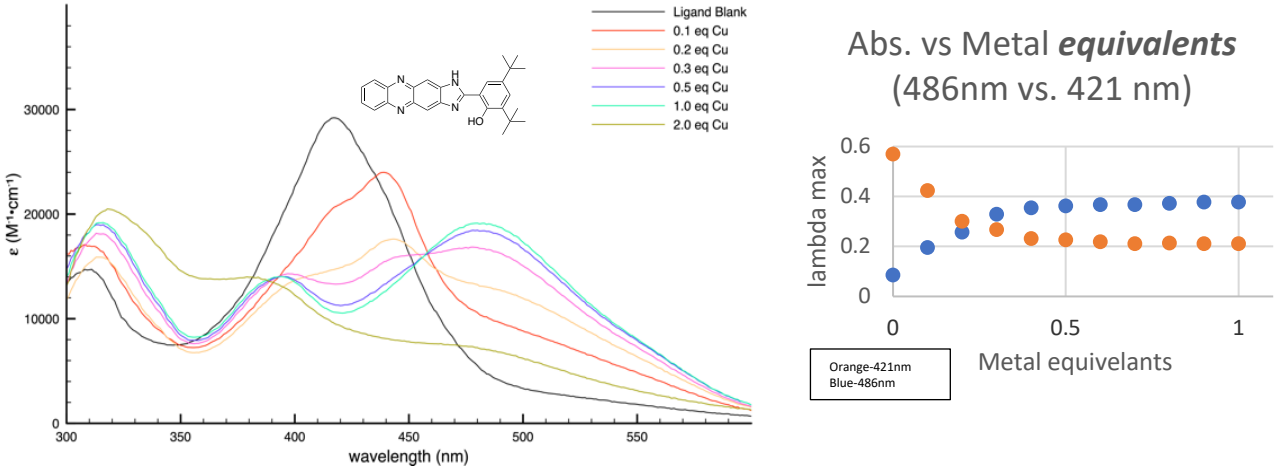

Figure 2.10. Ditertbutyl-salimidizine titration with Cu^{2+} acetate (Left); λ max vs. metal equivalents @ 486nm and 421nm.(right)

This ligand also showed some affinity for Cu^{2+}. The titrations with copper demonstrated significant changes with increases in metal ion concentration. Upon addition of 0.1 to 0.7 equivalents of copper metal the resulting solutions retained a yellow color. From 0.8 to 1.0 equivalents of metal there was a 64 nm bathochromic shift in the spectra, and the solutions turned a rose gold color. From 2.0 to 5.0 equivalents of metal the solutions went back to a yellow color although this was different than the earlier coloration. Further examination of the UV-vis spectra (Figure 2.10 Left) demonstrated that the initial signal of the ligand centered at 421 nm experienced a bathochromic shift when the first 0.1 equivalents of metal was added. Upon addition of 0.4 equivalents the initial signal was completely shifted with a maximum absorptivity now located at 485 nm. Looking at the absorbance vs. equivalents graph (Figure 2.10) it is evident that the shift starts after base and the first 0.1 equivalent of metal solution were added. The addition of base was needed to help with deprotonation of the ligand. The subsequent spectral shifts will either not happen or occur at a very slow rate without base.

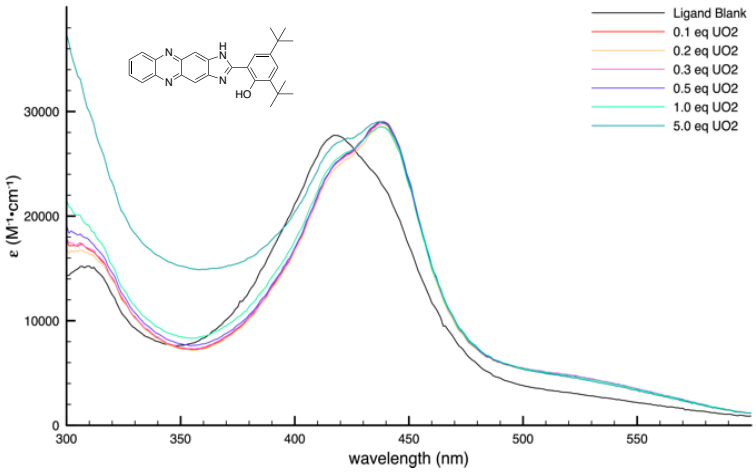

Figure 2.11. Ditertbutyl-salimidizine titration with UO_2^{2+} acetate

Further examination of methoxysalimidizine (**L3**) titrated with Cu^{2+} showed a λ_{max} for the ligand centered at 425 nm (Figure 2.12). After the addition of the first equivalent of metal, it bathochromically shift to its new location at 463 nm. Along with this shift, after 2 full equivalents of metal are added the molar absobtivity in the λ_{max} starts to decrease in intensity. When titrated with UO_2^{2+}, the peak initially had a λ_{max} centered at 425 nm and after the first addition of metal the peak shifts to 441 nm where is remains through the remainder of the titration.

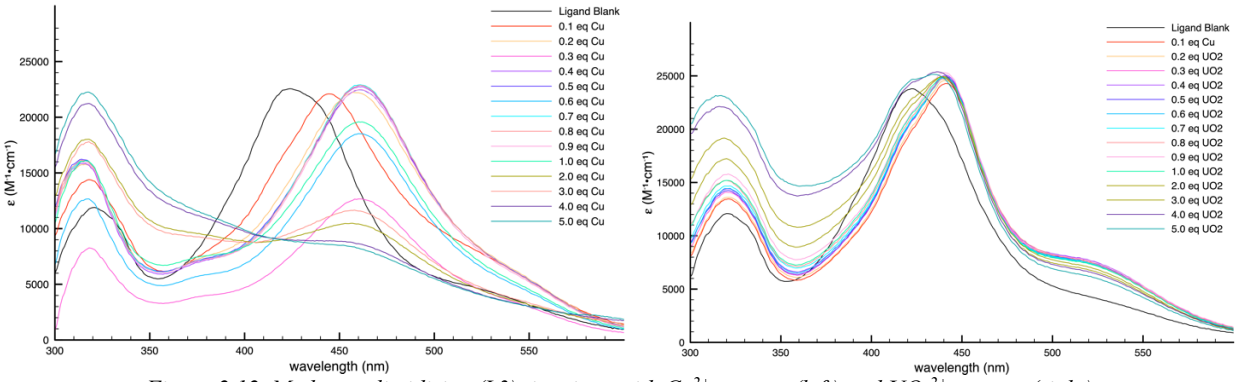

Figure 2.12. Methoxysalimidizine (L3) titrations with Cu^{2+} acetate (left) and UO_2^{2+} acetate (right).

There are a few key details observed in the fluorescence spectra that should be noticed. These titrations were carried out in DMF with 10% H_2O for copper (II) acetate and uranyl acetate similar to that of the batch UV-vis titrations. The bare salimidizine ligand showed some interesting features upon the introduction of metal. For the ligand alone excitation, with excitation at 408 nm, a major peak was produced at 536 nm. After the first addition of Cu^{2+} solution (0.1 equivalents), the emission intensity starts to decrease from 100 Raw Fluorescence Units (RFU) and this continues with each addition of the metal solution to the lowest point at 15 RFU after the addition of 5 equivalents of metal (Figure 2.13 Left).

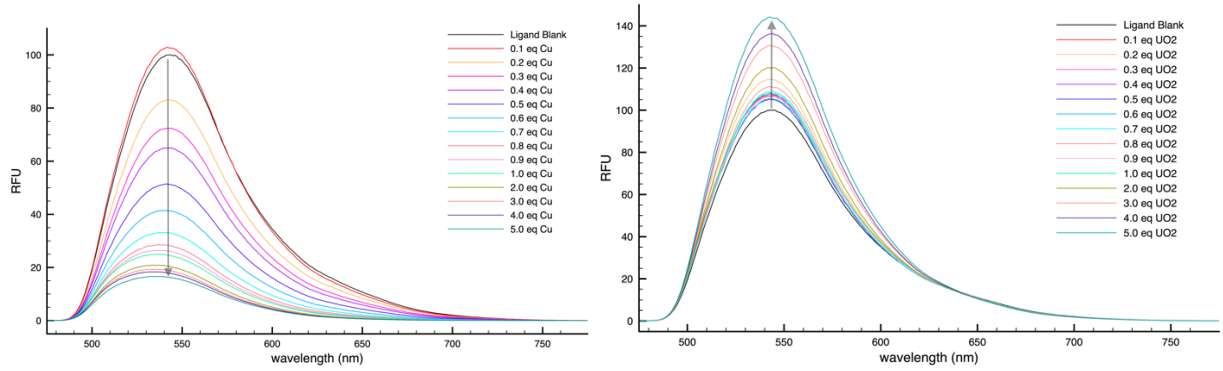

Figure 2.13. Fluorescence spectra of Salimidizine (L1) with Cu^{2+} Acetate (Left) and UO_2^{2+} Acetate (Right) in DMF/ 10% H_2O

More interesting data that can be pulled from the fluorescence spectra comes from the UO_2^{2+} titrations with the salimidizine ligand. In this case the initial peak is centered at 540 nm with an intensity of 100 RFU. Upon addition each aliquot of metal solution, the signal intensified to reach 140 RFU (Figure 2.13 Right). It can also be noted that this trend holds across all the functionalized salimidizines and can be further examined below. Overall, the distinctive change in fluorescence intensity is quite remarkable in comparing the copper and uranyl complexes.

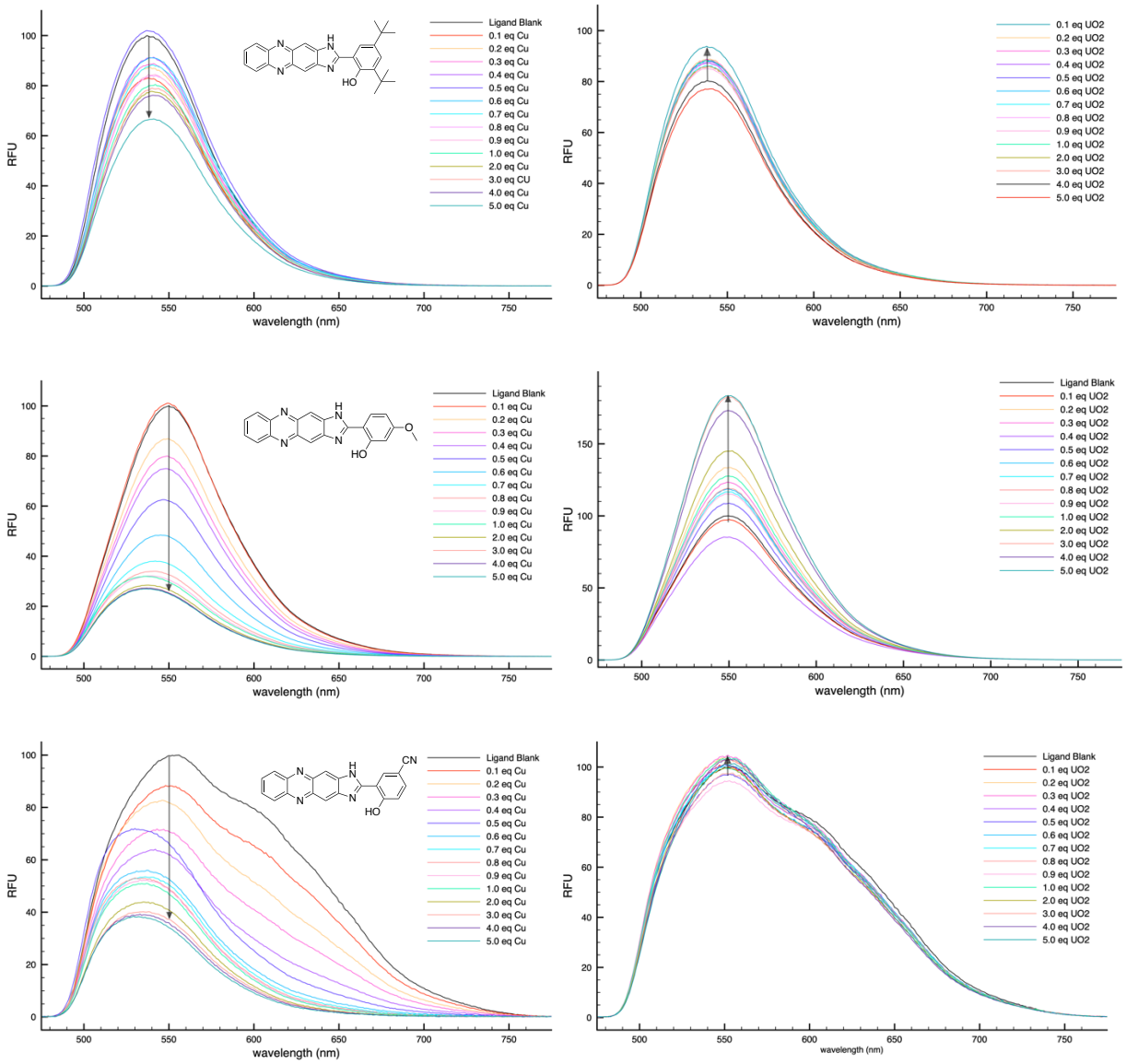

Figure 2.14. Fluorescence spectra of: (L2)-Cu^{2+} Acetate (top L), (L2)-UO_2^{2+} Acetate (top R), (L3)-Cu^{2+} Acetate (mid L), (L3)-UO_2^{2+} Acetate (mid R), (L4)-Cu^{2+} Acetate (bottom L), (L4)-UO_2^{2+} Acetate (bottom R) in DMF/ 10% H_2O.

Analysis of the solid-state structural data collected from X-ray diffraction yielded some interesting findings. Even though there was no significant shift in the spectra to suggest binding of the uranyl by **L1**, we were able to obtain a crystal structure of the **L1** ligand bound to the uranyl. Crystal structures for the 3,5-ditertbutyl salimidizine (**L2**) free ligand, the bare salimidizine (**L1**)

free ligand, and the UO_2[**L1**]OAc•DMSO metal complex were all examined. Crystals of **L1** (*Figure 2.15*a) were grown from layered DMSO and EtOH, crystals of **L2** were grown from slow evaporation of THF (*Figure 2.15*b), and crystals of UO_2[**L1**]OAc•DMSO (*Figure 2.15*c) were grown through slow diffusion of hexanes into a layered solution of free base (**L1**) in DMSO and $UO_2(OAc)_2$ in EtOH.

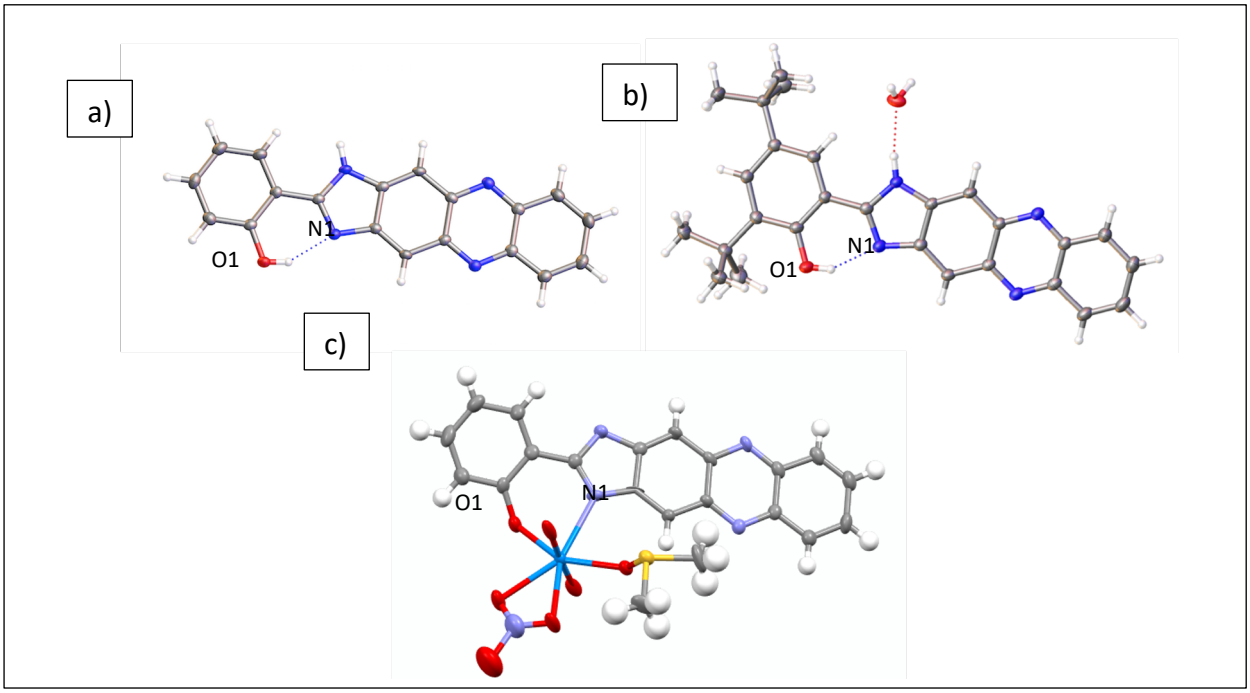

*Figure 2.15. Projection of the asymmetric unit of L1 (a), L2 (b), & UO_2[**L1**](OAc)•DMSO (c). Atoms shown are labelled: H in white, O in red, N in blue, C in grey, S in yellow, U in green.*

Upon examination of the crystal data, the uranium center in UO_2[L1]OAc•DMSO is seven coordinate and adopts a pentagonal bipyramidal geometry. Six oxygen atoms in total and one nitrogen atom occupy these seven sites. The first two coordinating oxygen atoms are terminal oxo groups of the UO_2^{2+} subunit; the three additional oxygen atoms can be accounted for by the coordination of a DMSO solvent molecule and an acetate anion. The remaining oxygen and nitrogen atoms that fill the coordination sphere of the uranium are from the salimidizine ligand. The U-N distance is observed at 2.558(6) Å. The U-O distance is observed at 2.220(6) Å. The O1-

N1 distance in UO_2[**L1**]OAc•DMSO is 2.767(9) Å, which is larger in comparison to the O1-N1 distance of 2.5866(19) Å in **L1**. Upon binding of this bidentate O-N binding site, the O-N distance expands to accommodate the metal. The crystal data shows that a binding event does occur with the bare salimidizine ligand. However, this coupled with the UV-vis data suggests that the process happens at such a slow rate that it is not detectable in the UV-Vis spectra like that of the ditertbutyl-salimidizine with $[UO_2]^{2+}$ and Cu^{2+}.

To explain the opposite activity of the uranyl and copper (II) centers upon complexation, we first optimized the structure of the two complexes with **L1** at their singlet (uranyl) and doublet (copper) ground states. To complete the first coordination sphere of the metals we added an acetate (AcO) and/or a water (W) ligand, constructing totally four complexes: $L_1UO_2^{2+}$(AcO), $L_1UO_2^{2+}$(AcO)(W), L_1Cu^{2+}(AcO), and L_1Cu^{2+}(AcO)(W). The copper and uranyl structures used for the calculations were derived from the crystal structure of UO_2[L1](OAc)•DMSO. Both metals were coordinated by the ligand and an (OAc) counter ion to achieve a neutral species. The water is placed to better reflect the conditions of the spectroscopy experiments and is also needed in the case of the uranyl to fill its fifth coordination site. This enabled us to see the possible effect of the coordination of different solvent molecules. All of our optimized geometries are given in the Appendix 1. Using this geometry, we employed TD-DFT to identify the state with the highest oscillator strength in the region of the absorption frequency used for the experiments (439 nm). The tenth state showed the only non-zero oscillator strength in this region for all cases except $L_1UO_2^{2+}$(AcO)(W), for which it was the eleventh state (always of the same spin as the ground state). The theoretical absorption wavelengths were 415 and 419 nm for the two uranyl complexes,

and 455, 466 nm for the copper ones. These numbers show the little effect of the solvent coordination.

Next, we optimized the geometry of this excited state and we calculated the emission wavelength as the excitation energy of this state at its optimal geometry. It should be mentioned that after optimization, the highest oscillator strength state is the fifth and sixth excited state for the uranyl and copper complexes, respectively. In every case, the excitation corresponds to a ligand-ligand electron transfer. The contours of the natural transition orbitals for the $L_1UO_2^{2+}$(AcO)(W) and L_1Cu^{2+}(AcO) molecules shown in Figure 2.16 are representative for the uranyl and copper systems, respectively. For copper, the electron transition is clearly a ligand-to-ligand transition. For uranyl, the same ligand to ligand transition has substantial involvement of some f-orbital or uranium.

The geometries of the two states differ mainly in the distances of the metal and connected oxygen or nitrogen atoms belonging to L1. Going from the ground to the excited state geometry, U-O distances increase by about 0.2 Å but U-N shorten by 0.04 Å. Likewise, Cu-O distances increase by 0.08 Å for both L_1Cu^{2+}(AcO) and L_1Cu^{2+}(AcO)(W) complexes, but the Cu-N distances are not affected at least within 0.01 Å.

The calculated emission wavelengths of 562 (L_1Cu^{2+}(AcO)), 600 (L_1Cu^{2+}(AcO)(W)), 599 (L_1Cu^{2+}(AcO)), and 607 ($L_1UO_2^{2+}$(AcO)(W)) nm are overestimated relative to the experimental peak maxima, but are in reasonable agreement given the absence of solvent effects and the accuracy of TD-DFT. We then, constructed the potential energy profile of the first ten or eleven electronic states of each complex along

the “reaction” coordinate connecting the minima of the ground and high oscillator strength excited electronic state (Figure 2.17). As in Figure 2.16, the $L_1UO_2^{2+}$(AcO)(W) and L_1Cu^{2+}(AcO) molecules have been selected for Figure 2.17. Comparison of the two potential energy profiles makes clear the reason for the observed fluorescence quenching in the copper case. For uranyl, the initial excitation (left orange arrow) to the non-zero oscillator strength excited state is followed by relaxation to its minimum via a series of conical intersections (upper grey arrow). Radiative decay to ground state (right yellow arrow) generates the recorded fluorescence signal and the system returns to the global minimum of the ground state in a non-radiative manner (lower grey arrow). The same process can in principle occur for copper, but the minimum of the pertinent excited state is shallow. The molecule after a small energy barrier goes to a lower minimum of the same potential energy surface, which has nearly zero oscillator strength and the decay to the ground state happens in a non-radiative manner. Notice that uranyl has also a second minimum in the excited state, which however is higher in energy. The profiles for all four systems (uranyl/copper acetate and/or water) are shown in the Appendix 1. Coordination of water destabilizes the excited state geometry in both cases and enhances the fluorescence quenching in the copper case.

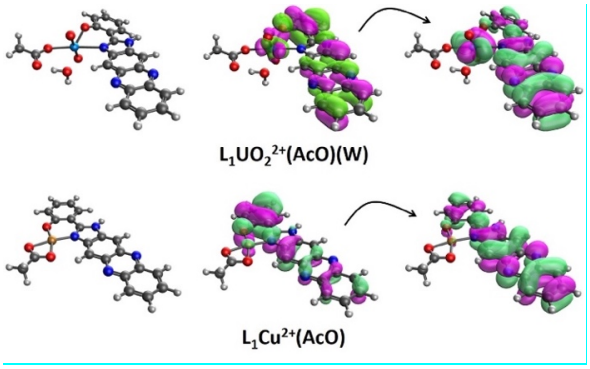

Figure 2.16. Natural transition orbitals corresponding to the excitation from the ground state to the lowest excited state of $L_1UO_2^{2+}$(AcO)(W) and L_1Cu^{2+}(AcO) with non-zero oscillator strength.

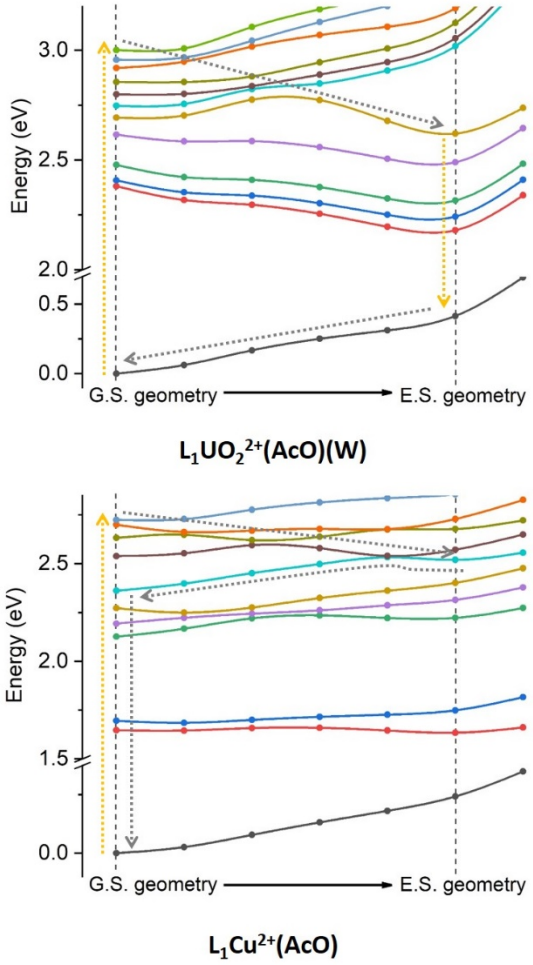

Figure 2.17. Potential energy profiles of the lowest lying electronic states of $L_1UO_2^{2+}$(AcO)(W) and L_1Cu^{2+}(AcO) along the path connecting the geometries of ground state (G.S. geometry) and the excited state (E.S. geometry) with non-zero oscillator strength. Orange and grey arrows indicate radiative and non-radiative transitions.

Conclusion

In conclusion, four derivatives of 2-(1H-imidazo[4,5-b]phenazin-2-yl)phenol, (salimidizine) **L1** and (di t-butylsalimidizine) **L2**, (cyanosalimidizine) **L3**, and (methoxysalimidizine) **L4** have been synthesized. Metal complex UO_2[**L1**](OAc)•DMSO was characterized in the solid state as well as free base of **L1** and **L2**. Ligands **L1**, **L2**, **L3**, and **L4** were characterized using ultraviolet-visible absorption and emission spectroscopies with uranyl and copper. An increase in absorption, in the case of UO_2^{2+} and two new modes

of absorbance were observed in the case of Cu. In the presence of greater than a 1 to 1 ratio of UO_2:1 the emission more than doubled; in contrast, in the presence of any ratio of Cu:1 emission was quenched by at least half. Based on the calculated potential energy profiles we were able to explain these observations. The minimum of the pertinent excited electronic state for copper is shallow and decays readily to a different minimum with zero oscillator strength, and thus the decay to the ground state follows a non-radiative path. This potentially indicates a degree of promise in the foundation of a selective fluorescent indicator for uranyl, as most other examples of these systems selectively quench in the presence of transition metals.

Synthesis

Ligand synthesis

Synthesis of 2-(1H-imidazo[4,5-b]phenazin-2-yl)phenol (Salimidizine, L1). 2,3-Diaminophenazine (0.0006 mol.; 0.1261g) was dissolved in 5 ml of DMSO in a 50 mL round bottom flask and allowed to dissolve. Next, salicylaldehyde (0.0006 mol.;53 µL) was added to the stirring mixture. The reaction was taken up to 120°C and allowed to run for 6 hr. The reaction was then taken off heat and allowed to cool to room temperature, then 45 ml of chilled EtOH was added to the reaction to help the product precipitate out of solution. The solution was allowed to sit at 0ºC overnight then filtered and washed with cold EtOH. The solid was filtered was then placed in the vacuum oven overnight to remove any excess solvent. Yield: 85%. NMR (600MHz, DMF-d7, ppm): 13.84 (s, 1H), 13.17 (s, 1H), 8.32-8.48 (m, 4H), 8.24 (m, 2H), 7.91 (s, 2H), 7.57 (m, 1H), 7.13-7.17 (m, 2H). ESI+ MS m/z (M+ H): Calc: 313.1079; Found: 313.1076.

Synthesis of 2,4-di-tert-butyl-6-(1H-imidazo[4,5-b]phenazin-2-yl)phenol (DTB sutylsalimidizine, L2). 2,3-Diaminophenazine (0.0006 mol.; 0.1261 g) was dissolved in 5 ml of DMSO and allowed to dissolve. Next, 3,5-ditertbutylsalicylaldehyde (0.0005 mol.; 0.1172 g) was added to the stirring mixture. The reaction was taken up to 120°C and allowed to run for 6 hr. The reaction was then taken off heat and allowed to cool to room temperature, 45 ml of chilled EtOH was added to the reaction to help the product precipitate out of solution. The solution was allowed to sit at 0ºC overnight then filtered and washed with cold EtOH. The filtered solid was then placed in the vacuum oven for 16 hours to remove any excess solvent (0.0971g). Yield: 38%. NMR (600MHz, DMF-d7, ppm): δ 1.42 (9H, s), 1.55 (9H, s), 7.63 (1H, s), 7.94-7.95 (2H, m), 8.25-8.60 (5H, m), 14.10(1H, s). ESI+ MS m/z (M+ H): Calc:425.2346; Found: 425.2341.

Synthesis of 2-(1H-imidazo[4,5-b]phenazin-2-yl)-5-methoxyphenol (Methoxysalimidizine, L3). 2,3-Diaminophenazine (0.0006 mol.; 0.1261 g) was dissolved in 5 ml of DMSO in a 50 mL round bottom flask and allowed to dissolve. Next, 2-hydroxy-4-methoxybenzaldehyde (0.0005 mol.;0.0761 g) was added to the stirring mixture. The reaction was taken up to 120°C and allowed to run for 6 hr. The reaction was then taken off heat and allowed to cool to room temperature, then 45 ml of chilled EtOH was added to the reaction to help the product precipitate out of solution. The solution was allowed to sit at 0ºC in a freezer overnight, then filtered and washed with cold EtOH. The filtered solid was then placed in the vacuum oven overnight to remove any excess solvent (0.0847g). Yield: 49%. NMR (600MHz, DMF, ppm): δ 13.47 (s, 1H), 8.33 (s, 2H), 8.21 (s, 3H), 8.02 (s, 1H), 7.88 (s, 2H), 6.72 – 6.68 (m, 2H), 3.92 (m, 3H). ESI- MS m/z(M- H): Calc:341.1044; Found: 341.1182.

Synthesis of 4-hydroxy-3-(1H-imidazo[4,5-b]phenazin-2-yl)benzonitrile (Cyanosalimidizine, L4). 2,3-Diaminophenazine (0.0006 mol.; 0.1261 g) was dissolved in 5 ml of DMSO in a 50 mL round bottom flask and allowed to dissolve. Next, 2-hydroxy-5-cyanobenzaldehyde (0.0005 mol.; 0.0736 g) was added to the stirring mixture. The reaction was taken up to 120°C and allowed to run for 6 hr. The reaction was then taken off heat and allowed to cool to room temperature, then 45 ml of chilled EtOH was added to the reaction to help the product precipitate out of solution. The solution was allowed to sit at 0 ºC in a freezer overnight, then filtered and washed with cold EtOH. The filtered solid was then placed in the vacuum oven overnight hours to remove any excess solvent (0.1467g). Yield: 86%.

NMR (400MHz, DMSO, ppm): δ 7.12 (d, 1H), 7.71-8.10 (m, 3H), 8.19 (d, 2H), 8.41 (s, 2H), 8.64 (s, 1H), 13.65 (s, 2H). ESI+ MS m/z(M+ H): Calc:338.1030; Found: 338.1028.

Synthesis of 2-hydroxy-5-cyanobenzaldehyde. 4-hydroxybenzonitrile (0.020 mol.; 2.38 g) was dissolved in 8 mL of trifluoroacetic acid. Once dissolved, hexamethylenetetraamine (0.040 mol.; 5.61 g) was added to the solution. Gas will evolve upon addition; it was allowed to dissipate. The reaction was heated to 100°C and allow to run for 7 hr. Once taken off heat the reaction was put directly into an ice bath for 5 min. Then it was removed from the ice bath and allow to heat back up to room temperature. Once at room temperature a 10 mL of 50/50 solution of H_2SO_4/H_2O was added to the reaction mixture followed by 60 mL of H_2O. The solution is allowed to stir at room temperature for 30 min. After the 30 min. of mixing a light-yellow solid formed in the solution. The solid was filtered off and the mother liquor was mixed with CH_2Cl_2 for extraction. The organic layer was separated and placed in the refrigerator to allow for recrystallization to allow for recrystallization (0.9080g). Yield: 31%. NMR (400MHz, DMSO, ppm): δ 13.55 (s, 1H), 8.58 (s, 1H), 8.35 (m, 2H), 8.13 (m, 3H), 7.82 (m, 3H), 7.21 (m, 1H). FT-IR (ATR): 1670 cm-1 (νC=O), 2230 cm-1(νC≡N),3207 cm-1 (νR-OH).

Synthesis of Salimidizine (L1)-Cu Complex. (L1) (0.000049 mol.; 0.0153g) was dissolved in 50 mL of THF and was allowed to stir for 20 min at 50ºC to help dissolve the ligand. Next 20 mL of MeOH was added to the reaction mixture followed by anhydrous Cu $(OAc)_2$ (0.000049 mol.; 0.0090 g), followed by triethylamine (0.000098 mol; 20 µL) to assist with deprotonation. The reaction was heated to 66ºC for 48 hours. The reaction was followed by TLC by 3:1 EtOAc: Hex mixture. The reaction mixture was taken off heat and was then taken to dryness under reduced

pressure yielding a brown/black solid the solid was scraped from the round bottom and washed with EtOH and filtered. (0.0213 g). Yield: 96%, Elemental Analysis: calc: C (58.26), H (3.28), N (11.39); found C (58.53), H (3.69), N (11.55).

Synthesis of Salimidizine (L1)-UO_2 Complex. (L1) (0.000049 mol.; 0.0153g) was dissolved in a mixture of 30 mL THF/15 mL MeOH and was allowed to stir for 20 min at 40ºC to help dissolve the ligand. Next uranyl acetate dihydrate (0.000049 mol; 0.021g) was added to the reaction, followed by triethylamine (0.000098 mol; 20 μL) to assist in deprotonation of the ligand. The reaction was heated to 66^0C and allowed to react for 48 hours. The reaction was then taken to dryness under reduced pressure by rotary evaporation to yield a brown/red solid the solid was scraped from the round bottom and washed with EtOH and filtered. (0.0111 g). Yield: 34%, NMR (500 MHz, DMF-d7, ppm): δ 8.49 (s, 1H), 8.39 – 8.28 (m, 5H), 7.92 (s, 1H), 7.66 – 7.47 (m, 3H), 7.16 (d, 3H), 6.97 – 6.65 (m, 2H), 1.40 (s, 3H), Elemental Analysis: calc: C (39.30), H (2.70), N (8.33); found C (38.82), H (3.11), N (8.32).

Synthesis of DTB Salimidizine (L2)-Cu Complex. (L2) (0.000049 mol.; 0.0207g) was dissolved in a mixture of 30 mL THF/15 mL MeOH and was allowed to stir for 20 min at 40ºC to help dissolve the ligand. Next copper (II) acetate (0.000049 mol; 0.009g) was added to the reaction, followed by triethylamine (0.000098 mol; 20 μL) to assist in deprotonation of the ligand. The reaction was heated to 66^0C and allowed to react for 48 hours. The reaction was followed by TLC by 3:1 EtOAc:Hex mixture. The reaction was then taken to dryness under reduced pressure by rotary evaporation to yield a brown/red solid the solid was scraped from the round bottom and washed with EtOH and filtered. (0.0262 g). Yield: 97%, ESI+ MS m/z(M+ H): Calc:547.138,

Found: 548.1805. Elemental Analysis: calc: C (39.30), H (2.70), N (8.33); found C (38.82), H (3.11), N (8.32).

Synthesis of DTB Salimidizine (L2)-UO_2 Complex. (**L2**) (0.000049 mol.; 0.0153g) was dissolved in a mixture of THF/MeOH and was allowed to stir for 20 min at 40^{o}C to help dissolve the ligand. Next uranyl acetate dihydrate (0.000049 mol; 0.021g) was added to the reaction, followed by triethylamine (0.000098 mol; 20 μL) to assist in deprotonation of the ligand. The reaction was heated to 66 ^{0}C and allowed to react for 48 hours. The reaction was followed by TLC by 3:1 EtOAc:Hex mixture. The reaction was then taken to dryness under reduced pressure to yield a brown/red solid the solid was scraped from the round bottom and washed with EtOH and filtered. (0.0235 g). Yield: 62%, NMR (500 MHz, DMF-d7, ppm): δ 8.59 (s, 1H), 8.32 – 8.26 (m. 3H), 7.94 -7.92 (dd, 3H, J=3.3, 3.5), 7.62 (d, 1H, J=2.2), 1.80 (s, 3H), 1.54 (s, 9H), 1.41 (s, 9H). ESI+ MS m/z(M+ Na): Calc:911.305, Found; 911.3776, Elemental Analysis: calc: C (45.20), H (4.19), N (7.27); found C (45.42), H (4.55), N (6.92).

Synthesis of OMe Salimidizine (L3)-Cu Complex. (0.000049 mol.; 0.0175g) was dissolved in a mixture of 12 mL DMF/ 8 mL of H_2O and was allowed to stir for 20 min at 50^{o}C to help dissolve the ligand. Next copper (II) acetate (0.000049 mol.; 0.009g) was added to the reaction, followed by triethylamine (0.000098mol.; 20 μL) to assist in deprotonation of the ligand. The reaction was heated to 100^{0}C and allowed to react for 48 hours. The reaction was followed by TLC by 3:1 EtOAc:Hex mixture. The reaction was then taken to dryness under high vac at 70 ^{o}C to yield a black solid the solid was scraped from the round bottom and washed with EtOH and filtered. (0.0119 g). Yield: 52%, ESI+ MS m/z(M+ H): Calc: 539.063, Found: 539.0908. Elemental Analysis: calc: C (54.83), H (3.76), N (12.08); found C (55.13), H (x3.65), N (12.30).

Synthesis of OMe Salimidizine (L3)-UO_2 Complex. (**L3**) (0.00005mol.; 0.0172g) was dissolved in a mixture of 12 mL DMF/8 mL of H_2O and was allowed to stir for 20 min at 50ºC to help dissolve the ligand. Next uranyl acetate dihydrate (0.00005mol.; 0.021g) was added to the reaction, followed by triethylamine (0.000098 mol; 20 μL) to assist in deprotonation of the ligand. The reaction was heated to 100^0C and allowed to react for 48 hours. The reaction was followed by TLC by 3:1 EtOAc:Hex mixture. The reaction was then taken to dryness under high vac at 70 ºC to yield a brown solid the solid was scraped from the round bottom and washed with EtOH and filtered. (0.0283 g). Yield: 83%, NMR (500 MHz, DMSO, ppm): δ 8.95 (s, 1H), 8.30 – 8.12 (m, 3H), 7.86 (s, 3H), 6.63 (s, 1H), 6.45 (s, 1H), 3.87 (s, 3H). ESI+ MS m/z(M+ H): Calc:842.557 Found:845.3752.

Synthesis of CN Salimidizine (L4)-Cu Complex. (L4) (0.000049 mol.; 0.0164g) was dissolved in a mixture of 12 mL DMF/ 8 mL of H_2O and was allowed to stir for 20 min at 50ºC to help dissolve the ligand. Next copper (II) acetate (0.000049 mol.; 0.009g) was added to the reaction, followed by triethylamine (0.000098 mol; 20 μL) to assist in deprotonation of the ligand. The reaction was heated to 100^0C and allowed to react for 48 hours. The reaction was followed by TLC by 3:1 EtOAc:Hex mixture. The reaction was then taken to dryness under high vac at 70 ºC to yield a black solid the solid was scraped from the round bottom and washed with EtOH and filtered. (0.0210 g). Yield: 93%, ESI+ MS m/z(M+ H): Calc:457.024, Found: 458.100; Elemental Analysis: calc: C (51.51), H (3.73), N (13.65); found C (51.59), H (3.14), N (13.97).

Synthesis of CN Salimidizine (L4)-UO_2 Complex. (**L4**) (0.00005mol.; 0.0164g) was dissolved in a mixture of 12 mL DMF/8 mL of H_2O and was allowed to stir for 20 min at 50°C to help dissolve the ligand. Next uranyl acetate dihydrate (0.00005mol.; 0.021g) was added to the reaction, followed by triethylamine (0.000098mol.; 20 μL) to assist in deprotonation of the ligand. The reaction was heated to 100^{0}C and allowed to react for 48 hours. The reaction was then taken to dryness under high vac at 70 °C to yield a brown solid, the solid was scraped from the round bottom and washed with EtOH and filtered. (0.0283 g). Yield: 83%, NMR (500 MHz, DMF-d7, ppm): δ 10.23 (s, 3H), 8.86 (s, 1H), 8.54 – 8.25 (m, 3H), 7.88 (s, 4H), 3.51(bs, 3H), 1.28 (s, 3H). ESI+ MS m/z(M+ Na): Calc:819.214, Found:819.1835; Elemental Analysis: calc: C (37.62), H (2.68), N (9.97); found C (37.30), H (3.01), N (10.08).

References

(1) Yadav, G.; Ganguly, S. Structure Activity Relationship (SAR) Study of Benzimidazole Scaffold for Different Biological Activities: A Mini-Review. *Eur. J. Med. Chem.* **2015**, *97*, 419–443. https://doi.org/10.1016/j.ejmech.2014.11.053.

(2) Sondhi, S. M.; Singh, J.; Roy, P.; Agrawal, S. K.; Saxena, A. K. Conventional and Microwave-Assisted Synthesis of Imidazole and Guanidine Derivatives and Their Biological Evaluation. *Med. Chem. Res.* **2011**, *20* (7), 887–897. https://doi.org/10.1007/s00044-010-9410-6.

(3) Boudalis, A. K.; Clemente-Juan, J. M.; Dahan, F.; Psycharis, V.; Raptopoulou, C. P.; Donnadieu, B.; Sanakis, Y.; Tuchagues, J.-P. Reversible Core-Interconversion of an Iron(III) Dihydroxo Bridged Complex. *Inorg. Chem.* **2008**, *47* (23), 11314–11323. https://doi.org/10.1021/ic800716r.

(4) Tong, Y.-P.; Zheng, S.-L.; Chen, X.-M. Structures, Photoluminescence and Theoretical Studies of Two ZnII Complexes with Substituted 2-(2-Hydroxyphenyl)Benzimidazoles. *Eur. J. Inorg. Chem.* **2005**, *2005* (18), 3734–3741. https://doi.org/10.1002/ejic.200500174.

(5) Maurya, M. R.; Kumar, M.; Kumar, U. Polymer-Anchored Vanadium(IV), Molybdenum(VI) and Copper(II) Complexes of Bidentate Ligand as Catalyst for the Liquid Phase Oxidation of Organic Substrates. *J. Mol. Catal. Chem.* **2007**, *273* (1), 133–143. https://doi.org/10.1016/j.molcata.2007.03.074.

(6) Ouyang, J.; Hong, H.; Shen, C.; Zhao, Y.; Ouyang, C.; Dong, L.; Zhu, J.; Guo, Z.; Zeng, K.; Chen, J.; Zhang, C.; Zhang, J. A Novel Fluorescent Probe for the Detection of Nitric Oxide in Vitro and in Vivo. *Free Radic. Biol. Med.* **2008**, *45* (10), 1426–1436. https://doi.org/10.1016/j.freeradbiomed.2008.08.016.

(7) Gao, G.; Qu, W.; Shi, B.; Zhang, P.; Lin, Q.; Yao, H.; Yang, W.; Zhang, Y.; Wei, T. A Highly Selective Fluorescent Chemosensor for Iron Ion Based on 1H-Imidazo [4,5-b] Phenazine Derivative. *Spectrochim. Acta. A. Mol. Biomol. Spectrosc.* **2014**, *121*, 514–519. https://doi.org/10.1016/j.saa.2013.11.004.

(8) Katkova, M. A.; Balashova, T. V.; Ilichev, V. A.; Konev, A. N.; Isachenkov, N. A.; Fukin, G. K.; Ketkov, S. Yu.; Bochkarev, M. N. Synthesis, Structures, and Electroluminescent Properties of Scandium N,O-Chelated Complexes toward Near-White Organic Light-Emitting Diodes. *Inorg. Chem.* **2010**, *49* (11), 5094–5100. https://doi.org/10.1021/ic1002429.

(9) Katkova, M. A.; Pushkarev, A. P.; Balashova, T. V.; Konev, A. N.; Fukin, G. K.; Ketkov, S. Yu.; Bochkarev, M. N. Near-Infrared Electroluminescent Lanthanide [Pr(Iii), Nd(Iii), Ho(Iii), Er(Iii), Tm(Iii), and Yb(Iii)] N,O-Chelated Complexes for Organic Light-Emitting Devices. *J. Mater. Chem.* **2011**, *21* (41), 16611–16620. https://doi.org/10.1039/C1JM13023D.

(10) Massacesi, M.; Ponticelli, G. Spectroscopic Studies of Cobalt(II), Nickel(II) and Copper(II) Complexes with N-Ethyl- and N-Propylimidazole. *J. Inorg. Nucl. Chem.* **1974**, *36* (10), 2209–2217. https://doi.org/10.1016/0022-1902(74)80257-5.

(11) Prakash, S. M.; Jayamoorthy, K.; Srinivasan, N.; Dhanalekshmi, K. I. Fluorescence Tuning of 2-(1H-Benzimidazol-2-Yl)Phenol-ESIPT Process. *J. Lumin.* **2016**, *172*, 304–308. https://doi.org/10.1016/j.jlumin.2015.12.009.

(12) Gorden, A. E. V.; DeVore, M. A.; Maynard, B. A. Coordination Chemistry with F-Element Complexes for an Improved Understanding of Factors That Contribute to Extraction Selectivity. *Inorg. Chem.* **2013**, *52* (7), 3445–3458. https://doi.org/10.1021/ic300887p.

(13) DeVore II, M. A.; Kerns, S. A.; Gorden, A. E. V. Characterization of Quinoxolinol Salen Ligands as Selective Ligands for Chemosensors for Uranium. *Eur. J. Inorg. Chem.* **2015**, *2015* (34), 5708–5714. https://doi.org/10.1002/ejic.201501033.

(14) Amer, A. M.; El-Bahnasawi, A. A.; Mahran, M. R. H.; Lapib, M. On the Synthesis of Pyrazino[2,3-b]phenazine and 1H-Imidazo[4,5b] phenazine Derivatives. *Monatshefte Für Chem.* **1999**, *130*, 1217–1225.

(15) Lei, Y. J.; Li, D. Q.; Ouyang, J.; Shi, J. X. Synthesis and Optical Properties of 2-(1H-Imidazo [4,5-] Phenazin-2-Yl) Phenol Derivatives. *Adv. Mater. Res.* **2011**, *311–313*, 1286–1289. https://doi.org/10.4028/www.scientific.net/AMR.311-313.1286.

(16) Sessler, J. L.; Melfi, P. J.; Seidel, D.; Gorden, A. E. V.; Ford, D. K.; Palmer, P. D.; Tait, C. D. Hexaphyrin(1.0.1.0.0.0). A New Colorimetric Actinide Sensor. *Synth. Recept. Sens.* **2004**, *60* (49), 11089–11097. https://doi.org/10.1016/j.tet.2004.08.055.

(17) Kim, M. S.; Tsukahara, T. Studies on Coordination and Fluorescence Behaviors of a Novel Uranyl Ion-Selective Chemosensor Bearing Diaza 18-Crown-6 Ether and Naphthalimide Moieties. *ACS Earth Space Chem.* **2020**, *4* (12), 2270–2280. https://doi.org/10.1021/acsearthspacechem.0c00184.

(18) Halali, V. V.; Balakrishna, R. G. An Expeditious Method for the Ultra-Level Chemosensing of Uranyl Ions. *Anal. Methods* **2020**, *12* (8), 1070–1076. https://doi.org/10.1039/C9AY02715G.

(19) Hu, Q.; Zhang, W.; Yin, Q.; Wang, Y.; Wang, H. A Conjugated Fluorescent Polymer Sensor with Amidoxime and Polyfluorene Entities for Effective Detection of Uranyl Ion in Real Samples. *Spectrochim. Acta. A. Mol. Biomol. Spectrosc.* **2021**, *244*, 118864. https://doi.org/10.1016/j.saa.2020.118864.

(20) Maynard, B. A.; Brooks, J. C.; Hardy, E. E.; Easley, C. J.; Gorden, A. E. V. Synthesis, Structural Characterization, Electronic Spectroscopy, and Microfluidic Detection of Cu+2 and UO2+2 [Di-Tert-Butyl-Salphenazine] Complexes. *Dalton Trans.* **2015**, *44* (10), 4428–4430. https://doi.org/10.1039/C5DT00106D.

(21) Casanova, I.; Duran, M. L.; Viqueira, J.; Sousa-Pedrares, A.; Zani, F.; Real, J. A.; Garcia-Vazquez, J. A. Metal Complexes of a Novel Heterocyclic Benzimidazole Ligand Formed by Rearrangement-Cyclization of the Corresponding Schiff Base. Electrosynthesis, Structural Characterization and Antimicrobial Activity. *Dalton Trans.* **2018**, *47* (12), 4325–4340. https://doi.org/10.1039/C8DT00532J.

(22) Xu, Z.-L.; Li, X.-M.; Wang, Q.-W. Crystal Structure of Poly[(4,5-Imidazoledicarboxylato)Lead(II)], [Pb3(C10H2N4O8)]n. *Z. Für Krist. - New Cryst. Struct.* **2009**, *224* (3), 481–482. https://doi.org/10.1524/ncrs.2009.0209.

Chapter 3
Cyano-naphthylsalophen

Adapted from
J. H. S. K. Monteiro, E. A. Hiti, E. E. Hardy, G. R. Wilkinson, J. D. Gorden, A. E. V. Gorden and A. de Bettencourt-Dias, *Chem. Commun.*, 2021, **57**, 2551-2554 **DOI:** 10.1039/D0CC08128K with permission from the Royal Society of Chemistry.

Introduction

The unique luminescence properties of lanthanide (Ln^{III}) ions make their complexes interesting for a variety of applications.[1–3] These properties include color purity, due to the core nature of the *f* orbitals involved in the emission process, and long luminescence lifetimes, due to the electronic-dipole forbidden nature of the *f-f* transitions, which enable time-delayed emission spectroscopy with increased signal-to-noise ratio.[4–6] The forbidden nature of these transitions makes sensitization of the emission more efficiently achieved through coordinated ligands in a process called the antenna effect.[4–6]

For low energy sensitization, excitation can be achieved through non-linear optical processes, such as two-photon absorption or cumulative effects of multiple first-order absorption phenomena, namely up-conversion (UC). The latter can occur through either excited-state absorption (ESA) or energy transfer up-conversion (ETU) (Figure 3.18a).[7] The presence of spin allowed transitions results in a high absorption cross-section, and long- lived intermediate excited states enable the use of inexpensive and low power continuous-wave lasers to access them.[8] In ETU a sensitizer ion absorbs low-energy photons, followed by energy transfer (ET) to the activator ion, which then emits in a characteristic wavelength. Er^{III} and Yb^{III}-doped nanoparticles (NPs) are among the most efficient UC systems.[9,10] The resonance between the excited states of Yb^{III} ($^4F_{5/2}$, ~10,624 cm^{-1}) and Er^{III} ($^4I_{11/2}$, ~10,346 cm^{-1}) improves the ET rates, and thus contributes to high UC emission intensities. While these NPs find wide application in bioimaging,[11–14] as they can be excited in a region of the spectrum where tissues have low absorption,[15,16] controlling their size, low cell penetrability, undesirable accumulation in the body, and stabilizing the crystalline phase

that yields the highest UC luminesce intensity, such as the β-phase of $NaYF_4$,[17,18] are challenges for their use *in vivo*.[19,20]

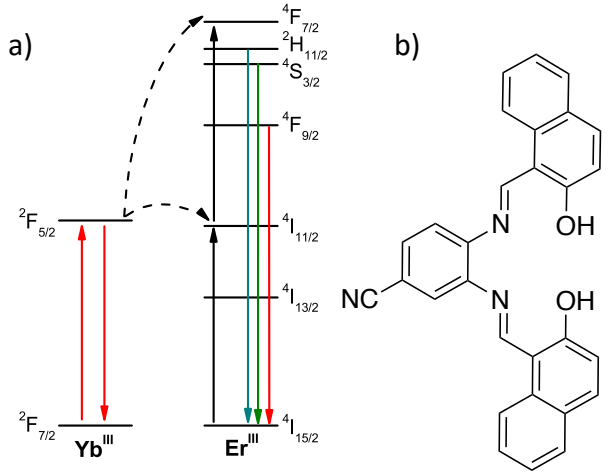

Figure 3.18. a)Energy level diagram illustrating the up-conversion process through ESA (two black up-arrows on Er^{III}) and ETU (dashed arrows, red up-arrow on Yb^{III} followed by top black up-arrow on Er^{III}). b) Structure of H_2L-CN

In contrast, in Ln^{III} complexes toxicity and low cell penetrability are not inherent and emission properties do not depend on the crystalline phase. In addition, judiciously designed ligands allow tuning of solubility, biocompatibility, and photophysics of the complexes, among other properties.[21–23] Salen ligands were chosen for this work due to a broad array of applications and the ability for efficient synthetic approach but also a robust catalogue of metal complexes.[24–27]

UC is important in bioimaging and sensing applications and there is substantial interest in small-molecule probes,[28,29] yet examples using Ln^{III} complexes are less common than those of Ln-$NaYF_4$-based NPs. The lattice on the latter is a low-phonon system, which is necessary for good UC efficiency.[30] Piguet and co-workers pioneered the UC luminescence using Ln^{III} complexes.[31] Charbonnière and co-workers demonstrated UC luminescence in deuterated water in a dimeric Er^{III}

complex, in which this ion is both activator and sensitizer.[32] Hyppännen and co-workers and more recently[33], Piguet and co-workers demonstrated that mononuclear Er^{III} complexes are capable of showing UC luminescence.[34] Many of the known examples have low UC emission intensity despite deuteration of the ligand, or require a transition metal as sensitizer or use metalorganic frameworks to reduce vibrational quenching; others, due to the long distances between the metal ions, require high excitation laser power densities to increase the ET efficiency.[35–39] Thus, the isolation of efficient Ln^{III}-based UC molecules is a current challenge.[40,41]

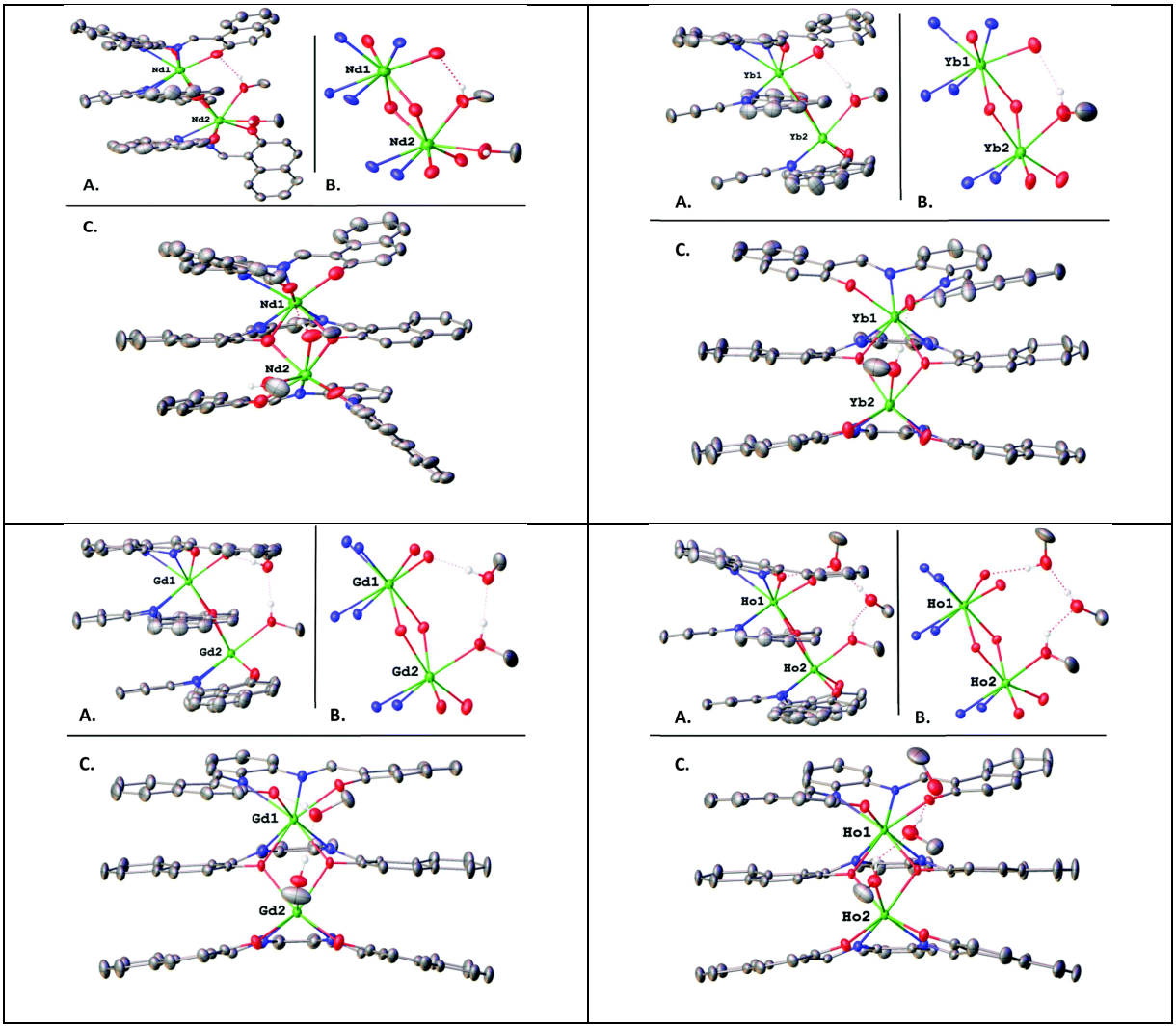

Figure 3.19. previously reported NS-Ln^{III} Complexes. Projection of {Top Left} $[Nd_2(L)_3(H_2O)]$ and its metal binding environment. {Top Right}$[Yb_2(L)_3(H_2O)]$ and its metal binding environment. {Bottom Left}$[Gd_2(L)_3(H_2O)]$ and its metal

binding environment {Bottom Right}}[$Ho_2(L)_3(H_2O)$] and its metal binding environment.[27] Carbon atoms are shown in grey, nitrogen in blue, oxygen in red, and erbium in green.

Recently, Gorden and co-workers showed that naphthylsalophen ligands form Ln^{III} complexes with a rigid sandwich structure in a 2:3 (Ln^{III}:ligand) stoichiometry as seen above in Figure 3.19.[27] These salen type ligands show a broad array of applications and present an efficient synthetic approach but also a robust catalogue of metal complexes. Because the Ln^{III}-Ln^{III} distance in these compounds is in the range 3.768-4.016 Å, well within the range for optimal Förster ET,[7,42] these structures are good candidates for UC luminescence. Therefore, to increase our knowledge of ligand and complex architectures that enable UC properties in Ln^{III}- based molecular systems, we synthesized mixed Er^{III}, Yb^{III} and pure Er^{III} complexes containing a new naphthylsalophen ligand with the cyano-electron-withdrawing group in the backbone. These compounds indeed display UC luminescence, as described below, adding new examples to a small group of molecular Ln^{III} complexes that exhibit this property.

Results and Discussion

The protonated cyano-naphthylsalophen H_2L-CN (Figure 3.18b) is isolated by condensation of 3,4-diaminobenzonitrile with 2-hydroxynaphthaldehyde in EtOH. The Ln^{III} complexes (Gd^{III}, Nd^{III}, Er^{III}, and Yb^{III}) are prepared by addition of the Ln^{III} metal salt, either the chloride or the acetate, in MeOH to the ligand in THF and addition of triethylamine (TEA) to deprotonate the ligand.

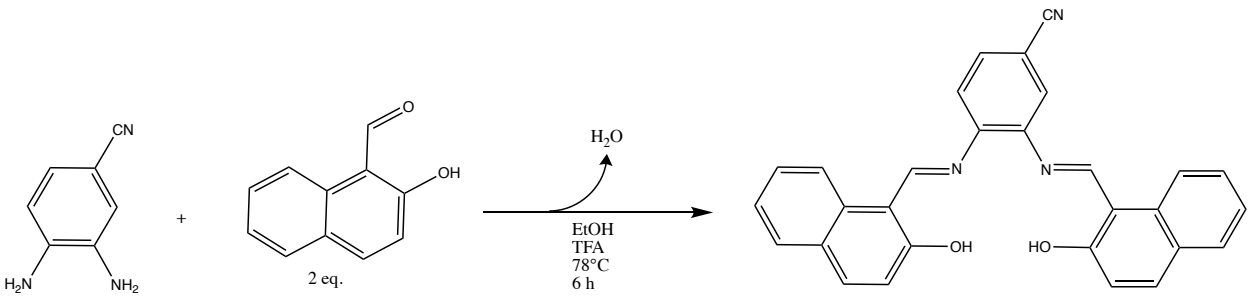

Figure 3.20. Synthesis of CN-Naphthylsalophen

X-ray quality crystals of H_2L-CN indicate that the compound crystalizes in the space group P 21/c (Figure 3.21 left) and does not display interactions with solvent molecules of crystallization. The structure of crystals of $[Er_2(L\text{-}CN)_3(H_2O)]$ (Figure 3.21 middle) shows features similar to previously reported Ln^{III} triple decker complexes.[27] The Er2 metal center is 8-coordinate and the coordination sphere is completed by the ligand, while the Er1 metal center is seven-coordinate, bound to ligand and with its coordination sphere completed by one water molecule (Figure 3.21 right). The distance between both metal centers is 3.816 Å, within the Förster ET range.[7,42]

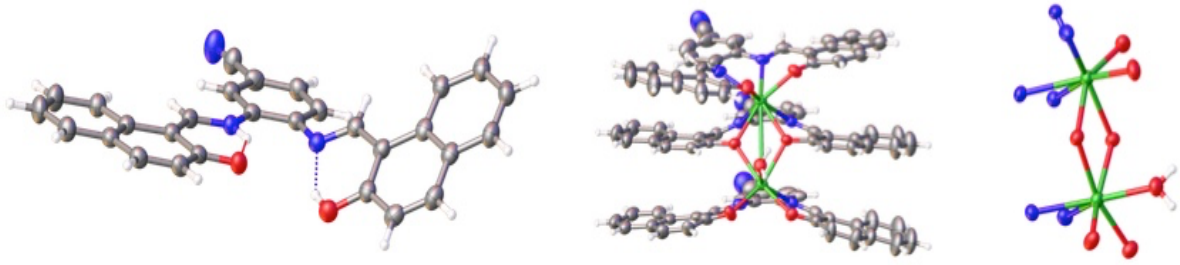

Figure 3.21. {Left} Projection of the front view of L-CN. {Middle} Projection of the front view of $[Er_2(L\text{-}CN)_3(H_2O)]$. {Right} Coordination environments of Er1(bottom) and Er2 (top). Carbon atoms are shown in grey, nitrogen in blue, oxygen in red, and erbium in green.

Deconvolution of the fluorescence and phosphorescence spectra of the Gd^{III} complexes into the vibrational components yields energies at 18,420 and 15,910 cm^{-1} for the excited singlet

and triplet levels, respectively. The triplet energy level is suitably located to sensitize the NIR-emitting Ln^{III} (Nd^{III}, Yb^{III} and Er^{III}). The one-photon solution excitation and emission spectra of Nd^{III}, Yb^{III} and Er^{III} complexes are achieved in dichloromethane. The excitation spectra of the complexes are composed of broad bands, consistent with sensitization of Ln^{III} emission through the ligand. The expected $^4F_{3/2} \rightarrow {}^4I_J$ ($J = 9/2 - 13/2$) transitions are seen in the emission spectrum of the Nd^{III} complex. For the Yb^{III} and Er^{III} complexes the $^2F_{5/2} \rightarrow {}^2F_{7/2}$ and $^4I_{13/2} \rightarrow {}^4I_{15/2}$ transitions, respectively, are observed. The quantum yields of sensitized emission (ϕL^{Ln}) for the Nd^{III} and Yb^{III} complexes are summarized in Table 3.1. They are comparable with reported values for other complexes of these ions.[43–45]

Complexes	*Solvent*	*^1S[a] [cm^{-1}]*	*^3T[a] [cm^{-1}]*	*τ[b] [μs]*	*Φ_L^{Ln} [%]*
[Nd_2(L-CN)$_3$(H_2O)]	*CH_2Cl_2*	*18,420±70*	*15,910±50*	*too weak to quantify*	*0.0054±0.0009*
[Yb_2(L-CN)$_3$(H_2O)]				*1.230±0.027 (81.1)* *6.801±0.197 (18.9)*	*0.154±0.013*
[Er_2(L-CN)$_3$(H_2O)]				*too weak to quantify*	*too weak to quantify*

Table 3.1. Singlet 1S and triplet 3T state energies of the ligands, excited state lifetime τ, and quantum yield Φ_L^{Ln} of sensitized efficiency for the Nd^{III}, Yb^{III} and Er^{III} complexes. λexc = 380 nm and [complex] = 1x10^{-4} M. [a] – Determined at 77 K, using the analogous Gd complexes.[46] [b] – The values in parenthesis indicate the percent contribution of each lifetime.

The emission lifetimes of the Yb^{III} complexes, summarized in Table 3.1, are comparable as well with values reported for this ion.[43,47,48] The excited state decay curves were fitted to a bi-exponential, consistent with the presence of ions in two different coordination environments. We attribute the shortest lifetime to the Yb^{III} site with a coordinated solvent molecule, and the longest one to the Yb^{III} bound only to ligand. We isolated multi-Ln^{III} complexes by adapting the procedure described for the homonuclear complexes synthesis. Er^{III} or Y^{III}, Yb^{III} and Er^{III} were added to the solution of the deprotonated ligand in 2:3 (Ln:L) molar ratio. The [($Y_{0.76}Yb_{0.16}Er_{0.08}$)$_2$(L-

$CN)_3(H_2O)]$ complex can be excited by two low energy photons through an UC process.[7] The resulting spectrum (Figure 3.22) shows Er^{III}-centered transitions in the green ($^2H1_{1/2} \rightarrow {}^4I_{15/2}$ and $^4S_{3/2} \rightarrow {}^4I_{15/2}$) and red ($^4I_{9/2} \rightarrow {}^4I_{15/2}$) upon excitation at 980 nm. The quadratic dependence of the emission intensity (*I*) on the laser power (*P*) (inset of Figure 3.22) confirms the 2-photon nature of the process. By graphing the slopes for the plots of the log(I) versus log(P), we are able to see the linear fits of the transitions at 543 nm ($^4S_{3/2} \rightarrow {}^4I1_{5/2}$) and 655.5 nm ($^4I_{9/2} \rightarrow {}^4I_{15/2}$) which have R^2 values of 0.982 and 0.984 respectively. This linear fit further confirms this process. UC emission is observed for power densities as low as 2.18 W cm^{-2}, which compares favorably with known efficient systems (29 W cm^{-2}).[32,37,34,49] Emission following UC excitation is also observed for $[(Yb_{0.78}Er_{0.22})_2(L\text{-}CN)_3(H_2O)]$ and $[Er_2(L\text{-}CN)_3(H_2O)]$ (Figure 3.23). Although there is an increase of the emission intensity for $[(Yb_{0.78}Er_{0.22})_2(L\text{-}CN)_3(H_2O)]$ as compared with $[(Y_{0.76}Yb_{0.16}Er_{0.08})_2(L\text{-}CN)_3(H_2O)]$, the concentration of Er^{III} is 2.8-fold higher in the former.

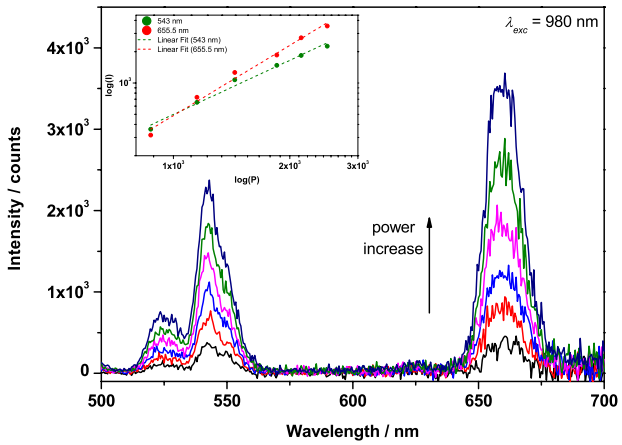

Figure 3.22. Two-photon UC emission spectra of $[(Y_{0.76}Yb_{0.16}Er_{0.08})_2(L\text{-}CN)_3(H_2O)]$ in the solid state using variable laser power. Inset shows plot of the log of the emission intensity I at 543 nm (green dots) or 655.5 nm (red dots) as a function of the log of the laser power P. λexc = 980 nm, P = 0.873 – 2.500 W.

In $[(Yb_{0.78}Er_{0.22})_2(L\text{-}CN)_3(H_2O)]$ and $[Er_2(L\text{-}CN)_3(H_2O)]$ UC emission was observed with power densities as low as 2.18 W cm^{-2} and 6.25 W cm^{-2}, respectively. The UC emission intensity of the latter is lower, due to non-radiative cross-relaxation.[50]

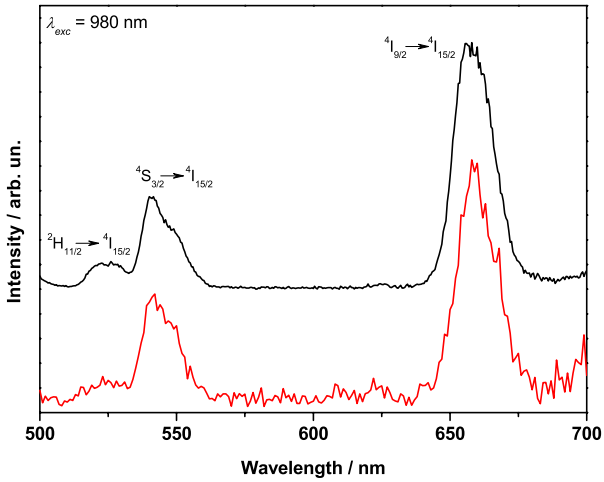

Figure 3.23. Two-photon UC emission spectra of (a) [(Yb0.78Er0.22)2(L-CN)3(H2O)] (black upper trace) and [Er2(L-CN)3(H2O)] (red bottom trace) in the solid state. λ exc = 980 nm, P = 2.5 W.

We were also able to examine the differences in solid state structure by comparing the unsubstituted naphthylsalophen-Er complex with the Cyanonaphthylsalophen complex. This allowed us to shed light on how the electron with drawl of the ligand would affect the packing in the crystal stricture. This could lead way into tuning the Förster distance between these metals and furthermore tuning the emission properties of the complex.[51] To examine our ability fine tune theses distance, yellow/orange plates suitable for X-ray diffraction were grown by slow diffusion of pentane into carbon tetrachloride for the $[Er_2(L\text{-}CN)_3(H_2O)]$ complex, and crystals for $[Er_2(L)_3(MeOH)_3]$ were grown from slow diffusion of MeOH into carbon DCM as well.

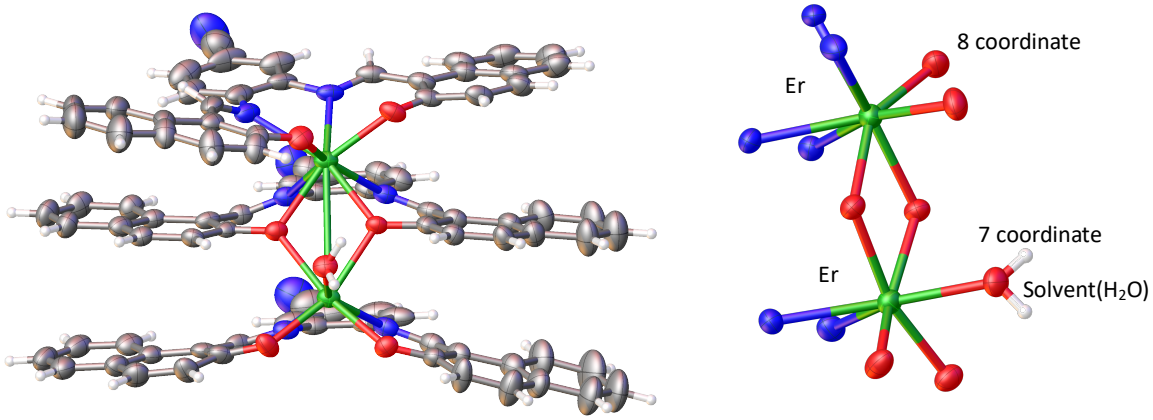

Figure 3.24. Projection of [Er_2(L-CN)$_3$(H_2O)] grown out of 1,4-dioxane/pentane. Carbon atoms are shown in grey, nitrogen in blue, oxygen in red, and erbium in green.

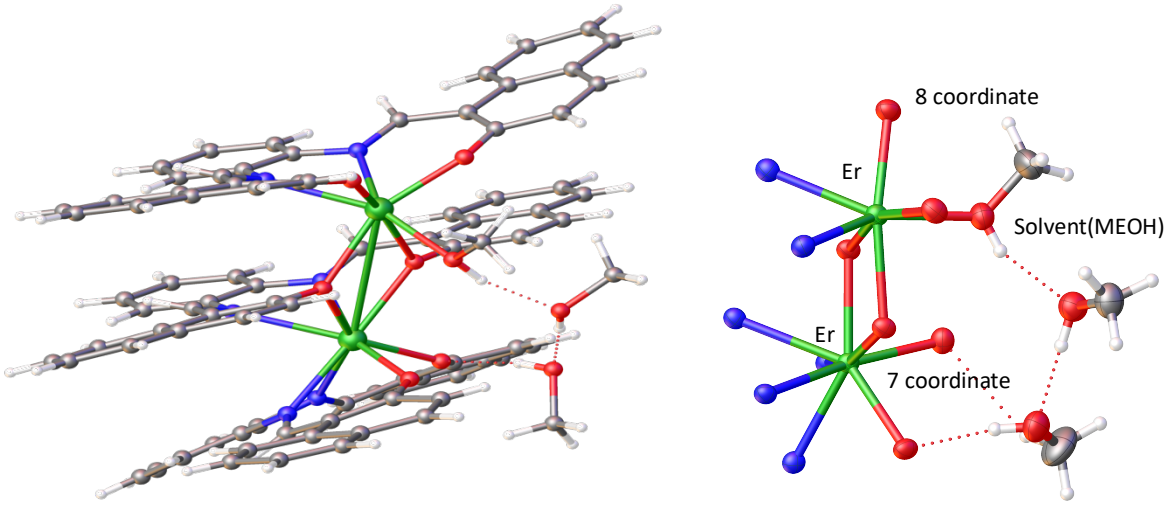

Figure 3.25. Projection of [Er_2(L)$_3$(MeOH)$_3$] Carbon atoms are shown in grey, nitrogen in blue, oxygen in red, and erbium in green.

Looking at Figure 3.7 and Figure 3.8 above pulling specific bond lengths from [Er_2(L-CN)$_3$(H_2O)], we can note that the Er1-Er2 distance is 3.816 (6)Å and in the [Er_2(L)$_3$(MeOH)$_3$] it is 3.830 (2) Å. This length shows the greatest possible deviation with that of 0.014 Å, all other lengths including O-$Er_{Average}$,N-$Er_{Average}$, and the Er-solvent bond lengths are nearly identical (Table 3.2). With this data we can hypothesize that tuning of this distance is achievable with the

addition of electron donating and electron withdrawing substituents on the backbone of the ligand. However, further data will need to be collected on an electron donating complex to further explore and solidify this claim. This will be further explained in chapter five.

Bond lengths	*$[Er_2(L\text{-}CN)_3(H_2O)]$*	*$[Er_2(L)_3(MeOH)_3]$*
$O\text{-}Er_{Average}$	2.273 (4)Å	2.267 (14)Å
$N\text{-}Er_{Average}$	2.468 (5)Å	2.469 (17)Å
$Er_1\text{-}Er_2$	3.816 (6)Å	3.830 (2)Å
$Er_1\text{-}H_2O$	2.379 (4)Å	2.371 (17)Å

Table 3.2. Selected bond lengths from *$[Er_2(L\text{-}CN)_3(H_2O)]$ and $[Er_2(L)_3(MeOH)_3]$*

Conclusion

In conclusion, we isolated three Ln^{III} complexes with a cyano-naphthylsalophen ligand with a 2:3 stoichiometry and sandwich structure. These complexes display efficient one-photon emission Nd^{III}- and Yb^{III}-centered and weak Er^{III}-centered emission. Complexes containing a mixture of Er^{III} and Yb^{III}, or Er^{III}, Yb^{III} and Y^{III} or just Er^{III} also display Er-centered red and green emission upon excitation with a 980 nm laser at low power densities, indicative of UC, making these systems rare examples of upconverting Ln^{III}-based molecules. This work increases our knowledge of molecular complexes of Ln^{III} ions that can be excited at low energy with a low intensity laser and are thus of potential interest for biological imaging applications. We have also shown the ability to alter the Förster distances with altering the electronics of the ligand.

Synthesis

Synthesis of Cyanonaphthylsalophen (L-CN) Aliquots of 3,4-diaminobenzonitrile (0.136 g, 1.02 mmol), TFA (162 μL, 2.11 mmol), and 2-hydroxynaphthaldehyde (0.363 g, 2.11 mmol) were added to 50 mL of EtOH in a 100ml round bottom flask charged with a magnetic stir bar and refluxed for 6 hours. During this time, the solution changed from yellow to orange and an orange precipitate formed. The solution was allowed to cool to room temperature. The resulting solid was filtered and washed with hexanes to yield an orange powder (0.4614 g, 61%). TOF MS (ESI+) m/z (M + H) Calc. 442.1556, Found 442.1568; 1H NMR (400 MHz, DMFd7)δ 7.07 (d, 1H, J = 9.2 Hz), 7.13 (d, 1H, J = 9.1 Hz), 7.42 (dd, 2H, J = 8.4, 7.3 Hz), 7.86 – 7.93(m, 4H), 8.06 (d, 1H, J = 9.6 Hz), 8.12 (d, 1H, J = 8.3 Hz), 8.41 (s, 1H), 8.66 (dd, 2H, J = 12.5,8.5 Hz), 9.87 (s, 1H), 9.96 (s, 1H), 14.97 (s, 2H). FT-IR (ATR): 2224 cm-1(νC≡N),3045 cm-1(νR-OH). Elemental Analysis (calcd. %) for $C_{29}H_{19}N_3O_2$: C, 78.90; H, 4.34; N, 9.52; Found: C, 78.71; H, 4.41; N, 9.67.

Synthesis of $(Er)_2(L\text{-}CN)_3(H_2O)$. The ligand L-CN (0.174 mmol, 0.0768g, 0.0768g) was dissolved in 100 mL of THF in a 250ml round bottom flask and charged with a magnetic stir bar. Er^{III} chloride (0.087 mmol, 0.0332g) was dissolved in MeOH and added to the solution, followed by the addition of triethylamine (TEA) (1.43 mmol, 200 μL). The solution was refluxed for 6 hours. During this time, the color changed from light orange to dark orange. The excess solvent was removed under reduced pressure yielding the solid sample. The solid was recrystallized from a mixture of THF and hexanes, then filtered and washed with ethanol. Yield: 79%. (TOF MS (ESI+) m/z (M + 2H) Calc. 1652.2646, Found 1652.2726.) Elemental Analysis as $C_{87}H_{51}N_9O_6Er_2 \bullet 10H_2O$ Calc'd(%): C, 57.01; H, 3.90; N, 6.88; Found: C, 57.04; H, 4.18; N,6.76.

Synthesis of $(Yb)_2(L\text{-}CN)_3(H_2O)$. The ligand L-CN (0.174 mmol, 0.0768g) was dissolved in 100 mL of THF in a 250ml round bottom flask and charged with a magnetic stir bar. Yb^{III} chloride (0.087 mmol, 0.0337g) was dissolved in MeOH and added to the solution, followed by the addition of triethylamine (TEA) (1.43 mmol, 200 μL). The solution was refluxed for 6 hours. During this time, the color changed from light orange to light yellow. The excess solvent was removed under reduced pressure yielding the solid sample. The solid was recrystallized from a mixture of THF and hexanes, then filtered and washed with ethanol. Yield: 73%. (TOF MS (ESI+) m/z (M + H) Calc. 1665.2767, Found 1665.2777.) Elemental Analysis as C87H51N9O6Yb2•2 H2O Calc'd(%): C, 61.45; H, 3.26; N, 7.41; Found: C, 61.67; H, 3.71; N, 7.67.

Synthesis of $(Nd)_2(L\text{-}CN)_3(H_2O)$. The ligand L-CN (0.174 mmol, 0.0768g) was dissolved in 100 mL of THF in a 250ml round bottom flask and charged with a magnetic stir bar. Nd^{III} chloride (0.087 mmol, 0.0312g) was dissolved in MeOH and added to the solution, followed by the addition of triethylamine (TEA) (1.43 mmol, 200 μL). The solution was refluxed for 6 hours. During this time, the color changed from light orange to dark orange. The excess solvent was removed under reduced pressure yielding the solid sample. The solid was recrystallized from a mixture of THF and hexanes, then filtered and washed with ethanol. Yield: 74%. (TOF MS (ESI+) m/z (M + H) Calc. 1606.9060, Found 1606.2124.)

Synthesis of $(Gd)_2(L\text{-}CN)_3(H_2O)$. The ligand L-CN (0.174 mmol, 0.0768g) was dissolved in 100 mL of THF in a 250ml round bottom flask and charged with a magnetic stir bar. Gd^{III} chloride (0.087 mmol, 0.0323g) was dissolved in MeOH and added to the solution, followed by

the addition of triethylamine (TEA) (200 µL, 1.43 mmol). The solution was refluxed for 6 hours. During this time, the color changed from light orange to dark green. The excess solvent was removed under reduced pressure yielding the solid sample. The solid was recrystallized from a mixture of THF and hexanes, then filtered and washed with ethanol. Yield: 62%. (TOF MS (ESI+) m/z (M + H) Calc. 1633.2444, Found 1634.2382.)

Synthesis of $(Yb_{0.78}Er_{0.22})_2(L\text{-}CN)_3(H_2O)$. The ligand L-CN (0.0603 mmol, 0.0266g) was dissolved in 50 mL of THF in a 100mL round bottom flask and charged with a magnetic stir bar. Yb^{III} chloride (0.0344 mmol, 0.0133g), and Er^{III} chloride (0.0056 mmol, 0.0021g) were dissolved in MeOH and added to the solution, followed by the addition of triethylamine (TEA) (1.43 mmol, 200 µL). The solution was refluxed for 6 hours. During this time, the color changed from light orange to dark orange. The excess solvent was removed under reduced pressure yielding the solid sample. The solid was recrystallized from a mixture of THF and hexanes, then filtered and washed with ethanol. EDS measurements were taken from multiple spots on a sample for statical analysis. Analysis in table below.

CN-Yb*Er	Yb (atomic%)	Er (atomic%)
1	78.04	21.96
2	76.78	23.22
3	80.5	19.5
4	76.66	23.34
5	78.55	21.45
Avg	78.106	21.894
Std Dev	1.563803057	1.563803057

Synthesis of $(Y_{0.76}Yb_{0.16}Er_{0.08})_2(L\text{-}CN)_3(H_2O)$. The ligand L-CN (0. 0.0603 mmol, 0.0266g) was dissolved in 50 mL of THF in a 100mL round bottom flask and charged with a magnetic stir bar. Y^{III} chloride (0.0308mmol, 0.0094g), Yb^{III} chloride (0.0121 mmol, 0.0046g), and Er^{III} chloride (0.0012 mmol, 0.0050g) were dissolved in MeOH and added to the solution, followed by the addition of triethylamine (TEA) (1.43 mmol, 200 μL). The solution was refluxed for 6 hours. During this time, the color changed from light orange to dark orange. The excess solvent was removed under reduced pressure yielding the solid sample. The solid was recrystallized from a mixture of THF and hexanes, then filtered and washed with ethanol. EDS measurements were taken from multiple spots on a sample for statical analysis. Analysis in table below.

CN-Y*Yb*Er	Y (atomic%)	Yb (atomic%)	Er (atomic%)
1	76.64	16.04	7.33
2	75.43	17.45	7.12
3	77.4	14.67	7.94
4	73.86	17.36	8.78
Avg	75.8325	16.38	7.7925
Std Dev	1.545086297	1.309580085	0.744552438

References

(1) BüNzli, J.-C. G. Lanthanide Luminescence for Biomedical Analyses and Imaging. *Chem. Rev.* **2010**, *110* (5), 2729–2755. https://doi.org/10.1021/cr900362e.

(2) Zhao, J.; Gao, J.; Xue, W.; Di, Z.; Xing, H.; Lu, Y.; Li, L. Upconversion Luminescence-Activated DNA Nanodevice for ATP Sensing in Living Cells. *J. Am. Chem. Soc.* **2018**, *140* (2), 578–581. https://doi.org/10.1021/jacs.7b11161.

(3) Hai, J.; Li, T.; Su, J.; Liu, W.; Ju, Y.; Wang, B.; Hou, Y. Reversible Response of Luminescent Terbium(III)-Nanocellulose Hydrogels to Anions for Latent Fingerprint Detection and Encryption. *Angew. Chem. Int. Ed.* **2018**, *57* (23), 6786–6790. https://doi.org/10.1002/anie.201800119.

(4) Bünzli, J.-C. G.; Piguet, C. Taking Advantage of Luminescent Lanthanide Ions. *Chem. Soc. Rev.* **2005**, *34* (12), 1048–1077. https://doi.org/10.1039/B406082M.

(5) *Luminescence of Lanthanide Ions in Coordination Compounds and Nanomaterials*, 1st ed.; de Bettencourt-Dias, A., Ed.; John Wiley & Sons Ltd.: United Kingdom, 2014.

(6) Bünzli, J.-C. G. On the Design of Highly Luminescent Lanthanide Complexes. *Coord. Chem. Rev.* **2015**, *293–294*, 19–47. https://doi.org/10.1016/j.ccr.2014.10.013.

(7) Auzel, F. Upconversion and Anti-Stokes Processes with f and d Ions in Solids. *Chem. Rev.* **2004**, *104* (1), 139–174. https://doi.org/10.1021/cr020357g.

(8) Chen, C.; Wang, F.; Wen, S.; Su, Q. P.; Wu, M. C. L.; Liu, Y.; Wang, B.; Li, D.; Shan, X.; Kianinia, M.; Aharonovich, I.; Toth, M.; Jackson, S. P.; Xi, P.; Jin, D. Multi-Photon near-Infrared Emission Saturation Nanoscopy Using Upconversion Nanoparticles. *Nat. Commun.* **2018**, *9* (1). https://doi.org/10.1038/s41467-018-05842-w.

(9) Zhou, J.; Liu, Q.; Feng, W.; Sun, Y.; Li, F. Upconversion Luminescent Materials: Advances and Applications. *Chem. Rev.* **2015**, *115* (1), 395–465. https://doi.org/10.1021/cr400478f.

(10) Lim, E.-K.; Kim, T.; Paik, S.; Haam, S.; Huh, Y.-M.; Lee, K. Nanomaterials for Theranostics: Recent Advances and Future Challenges. *Chem. Rev.* **2015**, *115* (1), 327–394. https://doi.org/10.1021/cr300213b.

(11) Chen, G.; Qiu, H.; Prasad, P. N.; Chen, X. Upconversion Nanoparticles: Design, Nanochemistry, and Applications in Theranostics. *Chem. Rev.* **2014**, *114* (10), 5161–5214. https://doi.org/10.1021/cr400425h.

(12) Gargas, D. J.; Chan, E. M.; Ostrowski, A. D.; Aloni, S.; Altoe, M. V. P.; Barnard, E. S.; Sanii, B.; Urban, J. J.; Milliron, D. J.; Cohen, B. E.; Schuck, P. J. Engineering Bright Sub-10-Nm Upconverting Nanocrystals for Single-Molecule Imaging. *Nat. Nanotechnol.* **2014**, *9* (4), 300–305. https://doi.org/10.1038/nnano.2014.29.

(13) Wolfbeis, O. S. An Overview of Nanoparticles Commonly Used in Fluorescent Bioimaging. *Chem. Soc. Rev.* **2015**, *44* (14), 4743–4768. https://doi.org/10.1039/c4cs00392f.

(14) Liu, G.; Jiang, F.; Chen, Y.; Yu, C.; Ding, B.; Shao, S.; Jia, M.; Ma, P.; Fu, Z.; Lin, J. Superior Temperature Sensing of Small-Sized Upconversion Nanocrystals for Simultaneous Bioimaging and Enhanced Synergetic Therapy. *Nanomedicine Nanotechnol. Biol. Med.* **2020**, *24*, 102135. https://doi.org/10.1016/j.nano.2019.102135.

(15) Chan, C.-F.; Tsang, M.-K.; Li, H.; Lan, R.; Chadbourne, F. L.; Chan, W.-L.; Law, G.-L.; Cobb, S. L.; Hao, J.; Wong, W.-T.; Wong, K.-L. Bifunctional Up-Converting Lanthanide Nanoparticles for Selective in Vitro Imaging and Inhibition of Cyclin D as Anti-Cancer Agents. *J Mater Chem B* **2014**, *2* (1), 84–91. https://doi.org/10.1039/c3tb21034k.

(16) Jiang, M.; Liu, H.; Zeng, S.; Hao, J. A General In Situ Growth Strategy of Designing Theranostic NaLnF 4 @Cu 2− x S Nanoplatform for In Vivo NIR-II Optical Imaging Beyond 1500 Nm and Photothermal Therapy. *Adv. Ther.* **2019**, *2* (6), 1800153. https://doi.org/10.1002/adtp.201800153.

(17) Zhao, M.; Li, B.; Wang, P.; Lu, L.; Zhang, Z.; Liu, L.; Wang, S.; Li, D.; Wang, R.; Zhang, F. Supramolecularly Engineered NIR-II and Upconversion Nanoparticles In Vivo Assembly and Disassembly to Improve Bioimaging. *Adv. Mater.* **2018**, *30* (52), 1804982. https://doi.org/10.1002/adma.201804982.

(18) Li, D.; He, S.; Wu, Y.; Liu, J.; Liu, Q.; Chang, B.; Zhang, Q.; Xiang, Z.; Yuan, Y.; Jian, C.; Yu, A.; Cheng, Z. Excretable Lanthanide Nanoparticle for Biomedical Imaging and Surgical Navigation in the Second Near-Infrared Window. *Adv. Sci.* **2019**, *6* (23), 1902042. https://doi.org/10.1002/advs.201902042.

(19) Nune, S. K.; Gunda, P.; Thallapally, P. K.; Lin, Y.-Y.; Laird Forrest, M.; Berkland, C. J. Nanoparticles for Biomedical Imaging. *Expert Opin. Drug Deliv.* **2009**, *6* (11), 1175–1194. https://doi.org/10.1517/17425240903229031.

(20) Huang, Y.-W.; Cambre, M.; Lee, H.-J. The Toxicity of Nanoparticles Depends on Multiple Molecular and Physicochemical Mechanisms. *Int. J. Mol. Sci.* **2017**, *18* (12), 2702. https://doi.org/10.3390/ijms18122702.

(21) Wagner, C. L.; Tao, L.; Fettinger, J. C.; Britt, R. D.; Power, P. P. Two-Coordinate, Late First-Row Transition Metal Amido Derivatives of the Bulky Ligand -N(SiPri3)Dipp (Dipp = 2,6-Diisopropylphenyl): Effects of the Ligand on the Stability of Two-Coordinate Copper(II) Complexes. *Inorg. Chem.* **2019**, *58* (13), 8793–8799. https://doi.org/10.1021/acs.inorgchem.9b01159.

(22) Sherstobitova, T.; Maryunina, K.; Tolstikov, S.; Letyagin, G.; Romanenko, G.; Nishihara, S.; Inoue, K. Ligand Structure Effects on Molecular Assembly and Magnetic Properties of Copper(II) Complexes with 3-Pyridyl-Substituted Nitronyl Nitroxide Derivatives. *ACS Omega* **2019**, *4* (17), 17160–17170. https://doi.org/10.1021/acsomega.9b01575.

(23) Brannan, A. C.; Lee, Y. Photophysical Tuning of σ-SiH Copper-Carbazolide Complexes To Give Deep-Blue Emission. *Inorg. Chem.* **2020**, *59* (1), 315–324. https://doi.org/10.1021/acs.inorgchem.9b02409.

(24) Wu, X.; Gorden, A. E. V. An Efficient Method for Solution-Phase Parallel Synthesis of 2-Quinoxalinol Salen Schiff-Base Ligands. *J. Comb. Chem.* **2007**, *9* (4), 601–608. https://doi.org/10.1021/cc070021q.

(25) DiMauro, E. F.; Mamai, A.; Kozlowski, M. C. Synthesis, Characterization, and Metal Complexes of a Salen Ligand Containing a Quinoline Base. *Organometallics* **2003**, *22* (4), 850–855. https://doi.org/10.1021/om0205795.

(26) Niklas, J. E.; Hardy, E. E.; Gorden, A. E. V. Solid-State Structural Elucidation and Electrochemical Analysis of Uranyl Naphthylsalophen. *Chem. Commun.* **2018**, *54* (83), 11693–11696. https://doi.org/10.1039/C8CC05242E.

(27) Hardy, E. E.; Wyss, K. M.; Keller, R. J.; Gorden, J. D.; Gorden, A. E. V. Tunable Ligand Emission of Napthylsalophen Triple-Decker Dinuclear Lanthanide(Iii) Sandwich Complexes. *Dalton Trans.* **2018**, *47* (4), 1337–1346. https://doi.org/10.1039/C7DT03733C.

(28) Kim, H. M.; Cho, B. R. Small-Molecule Two-Photon Probes for Bioimaging Applications. *Chem. Rev.* **2015**, *115* (11), 5014–5055. https://doi.org/10.1021/cr5004425.

(29) Qian, L.; Li, L.; Yao, S. Q. Two-Photon Small Molecule Enzymatic Probes. *Acc. Chem. Res.* **2016**, *49* (4), 626–634. https://doi.org/10.1021/acs.accounts.5b00512.

(30) Liu, G. Advances in the Theoretical Understanding of Photon Upconversion in Rare-Earth Activated Nanophosphors. *Chem. Soc. Rev.* **2015**, *44* (6), 1635–1652. https://doi.org/10.1039/c4cs00187g.

(31) Aboshyan-Sorgho, L.; Besnard, C.; Pattison, P.; Kittilstved, K. R.; Aebischer, A.; Bünzli, J.-C. G.; Hauser, A.; Piguet, C. Near-Infrared→Visible Light Upconversion in a Molecular Trinuclear d-f-d Complex. *Angew. Chem. Int. Ed.* **2011**, *50* (18), 4108–4112. https://doi.org/10.1002/anie.201100095.

(32) Nonat, A.; Chan, C. F.; Liu, T.; Platas-Iglesias, C.; Liu, Z.; Wong, W.-T.; Wong, W.-K.; Wong, K.-L.; Charbonnière, L. J. Room Temperature Molecular up Conversion in Solution. *Nat. Commun.* **2016**, *7*, 11978. https://doi.org/10.1038/ncomms11978.

(33) Hyppänen, I.; Lahtinen, S.; Ääritalo, T.; Mäkelä, J.; Kankare, J.; Soukka, T. Photon Upconversion in a Molecular Lanthanide Complex in Anhydrous Solution at Room Temperature. *ACS Photonics* **2014**, *1* (5), 394–397. https://doi.org/10.1021/ph500047j.

(34) Golesorkhi, B.; Nozary, H.; Guénée, L.; Fürstenberg, A.; Piguet, C. Room-Temperature Linear Light Upconversion in a Mononuclear Erbium Molecular Complex. *Angew. Chem. Int. Ed Engl.* **2018**, *57* (46), 15172–15176. https://doi.org/10.1002/anie.201810022.

(35) Pollnau, M.; Gamelin, D. R.; Lüthi, S. R.; Güdel, H. U.; Hehlen, M. P. Power Dependence of Upconversion Luminescence in Lanthanide and Transition-Metal-Ion Systems. *Phys. Rev. B* **2000**, *61* (5), 3337–3346. https://doi.org/10.1103/PhysRevB.61.3337.

(36) Suffren, Y.; Golesorkhi, B.; Zare, D.; Guénée, L.; Nozary, H.; Eliseeva, S. V.; Petoud, S.; Hauser, A.; Piguet, C. Taming Lanthanide-Centered Upconversion at the Molecular Level. *Inorg. Chem.* **2016**, *55* (20), 9964–9972. https://doi.org/10.1021/acs.inorgchem.6b00700.

(37) Souri, N.; Tian, P.; Platas-Iglesias, C.; Wong, K.-L.; Nonat, A.; Charbonnière, L. J. Upconverted Photosensitization of Tb Visible Emission by NIR Yb Excitation in Discrete Supramolecular Heteropolynuclear Complexes. *J. Am. Chem. Soc.* **2017**, *139* (4), 1456–1459. https://doi.org/10.1021/jacs.6b12940.

(38) Ye, H.; Bogdanov, V.; Liu, S.; Vajandar, S.; Osipowicz, T.; Hernández, I.; Xiong, Q. Bright Photon Upconversion on Composite Organic Lanthanide Molecules through Localized Thermal Radiation. *J. Phys. Chem. Lett.* **2017**, *8* (23), 5695–5699. https://doi.org/10.1021/acs.jpclett.7b02513.

(39) Kalmbach, J.; Wang, C.; You, Y.; Förster, C.; Schubert, H.; Heinze, K.; Resch-Genger, U.; Seitz, M. Near-IR to Near-IR Upconversion Luminescence in Molecular Chromium Ytterbium Salts. *Angew. Chem. Int. Ed.* **2020**, *59* (42), 18804–18808. https://doi.org/10.1002/anie.202007200.

(40) Golesorkhi, B.; Nozary, H.; Fürstenberg, A.; Piguet, C. Erbium Complexes as Pioneers for Implementing Linear Light-Upconversion in Molecules. *Mater. Horiz.* **2020**, *7* (5), 1279–1296. https://doi.org/10.1039/c9mh01899a.

(41) Nonat, A. M.; Charbonnière, L. J. Upconversion of Light with Molecular and Supramolecular Lanthanide Complexes. *Coord. Chem. Rev.* **2020**, *409*, 213192. https://doi.org/10.1016/j.ccr.2020.213192.

(42) Porcher, P.; Caro, P. Crystal Field Parameters for Eu3+ in KY3F10. III. Radiative and Nonradiative Transition Probabilities. *J. Chem. Phys.* **1978**, *68* (9), 4183–4187. https://doi.org/10.1063/1.436280.

(43) Zhang, J.; Petoud, S. Azulene-Moiety-Based Ligand for the Efficient Sensitization of Four Near-Infrared Luminescent Lanthanide Cations: Nd3+, Er3+, Tm3+, and Yb3+. *Chem. - Eur. J.* **2008**, *14* (4), 1264–1272. https://doi.org/10.1002/chem.200701068.

(44) De Bettencourt-Dias, A.; Barber, P. S.; Bauer, S. A Water-Soluble Pybox Derivative and Its Highly Luminescent Lanthanide Ion Complexes. *J. Am. Chem. Soc.* **2012**, *134* (16), 6987–6994. https://doi.org/10.1021/ja209572m.

(45) Wei, H.; Yu, G.; Zhao, Z.; Liu, Z.; Bian, Z.; Huang, C. Constructing Lanthanide [Nd(Iii), Er(Iii) and Yb(Iii)] Complexes Using a Tridentate N,N,O-Ligand for near-Infrared Organic Light-Emitting Diodes. *Dalton Trans.* **2013**, *42* (24), 8951. https://doi.org/10.1039/c3dt50778e.

(46) Crosby, G. A.; Whan, R. E.; Alire, R. M. Intramolecular Energy Transfer in Rare Earth Chelates. Role of the Triplet State. *J. Chem. Phys.* **1961**, *34* (3), 743–748. https://doi.org/10.1063/1.1731670.

(47) Ning, Y.; Liu, Y.-W.; Meng, Y.-S.; Zhang, J.-L. Design of Near-Infrared Luminescent Lanthanide Complexes Sensitive to Environmental Stimulus through Rationally Tuning the Secondary Coordination Sphere. *Inorg. Chem.* **2018**, *57* (3), 1332–1341. https://doi.org/10.1021/acs.inorgchem.7b02750.

(48) Shuvaev, S.; Parker, D. A Near-IR Luminescent Ratiometric Ytterbium PH Probe. *Dalton Trans.* **2019**, *48* (14), 4471–4473. https://doi.org/10.1039/c9dt00411d.

(49) Nonat, A.; Bahamyirou, S.; Lecointre, A.; Przybilla, F.; Mély, Y.; Platas-Iglesias, C.; Camerel, F.; Jeannin, O.; Charbonnière, L. J. Molecular Upconversion in Water in Heteropolynuclear Supramolecular Tb/Yb Assemblies. *J. Am. Chem. Soc.* **2019**, *141* (4), 1568–1576. https://doi.org/10.1021/jacs.8b10932.

(50) Wen, S.; Zhou, J.; Zheng, K.; Bednarkiewicz, A.; Liu, X.; Jin, D. Advances in Highly Doped Upconversion Nanoparticles. *Nat. Commun.* **2018**, *9* (1). https://doi.org/10.1038/s41467-018-04813-5.

(51) Eliseeva, S. V. Luminescence of Lanthanide Ions in Coordination Compounds and Nanomaterials. Edited by Ana de Bettencourt-Dias. *Angew. Chem. Int. Ed.* **2015**, *54* (30), 8598–8598. https://doi.org/10.1002/anie.201504040.

Chapter 4
Naphthylpyrasal

Introduction

Interest in the area of actinide coordination has increased recently due to renewed fervor to understand the reactivity of uranyl and its -yl oxygens.[1,2] With the advancement in scientific technique and experimental capability coupled with the wide range of oxidation states accessible to these elements, 3+, 4+, 5+ and non -yl 6+ oxidation states of uranium are being explored as to gain an even deeper understanding of fundamental *f*-block chemistry.[3–6] Our focus has been centered on the coordination of the UO_2^{2+} cation to try and further understand the unique binding and fundamental chemistry of the *f*-element complexes produced.[7–9] These complexes are of interest to learn more about bonding covalency and their unique chemistry in the hopes of taking what is learned to develop new means of identification and coordination of these metal ions.[10,11] Using salen type ligands has been shown to be a way to increase selectivity towards actinide metals over lanthanide metals in solution due to the softer doners present in the organic framework for the salen type ligand.[9]

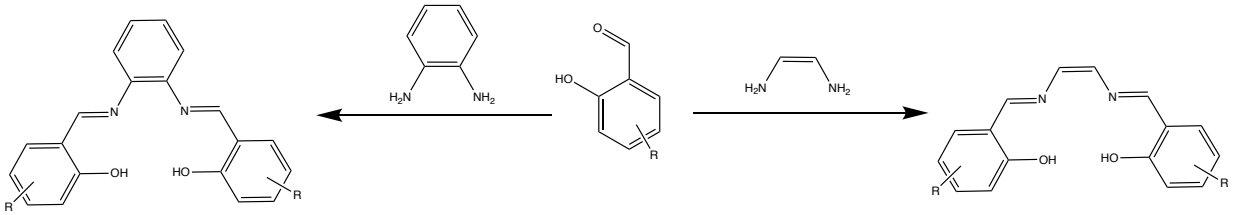

Figure 4.26. Formation of Salens with Salicylaldehydes

Another aspect proven successful in our group that has been examined is the ability to alter the electronics of the salen ligands. We have accomplished this, as seen in the previous chapter, by

incorporating electron donating (EDG) or withdrawing (EWG) substituents to the meta position(s) on the *o*-phenylenediamine backbone.[9] The next logical step of interest was to examine the effects of heterocyclic moieties in the backbone as a way to alter the electronics. This leverages the electron withdrawing nature of the nitrogen in the pyrazine backbone. It was hypothesized that these ligands could provide a route to stabilization of lower valent uranium species. It has been shown by the Bart group at Purdue University that the introduction of heterocycles and conjugated coordinating amines can stabilize radicals on the ligand frame works by which they access lower uranium oxidation states and tune the electronic properties of the metal center as well as functionalize the -yl bonds.[12–15] With this work, direct comparisons will be made between the naphthylsalophen (1,1-((1E,1E)-(1,2-phenylenebis(azanylylidene))bis(methanylylidene))bis(naphthalen-2-ol) ligand and naphthylpyrasal (1,1'-((1E,1'E)-(pyrazine-2,3-diylbis(azaneylylidene))bis(methaneylylidene))bis(naphthalen-2-ol)) ligand to examine the efficacy of this ligand to stabilize a $[UO_2]^+$ species and help understand the effects of changes in the coordination sphere.

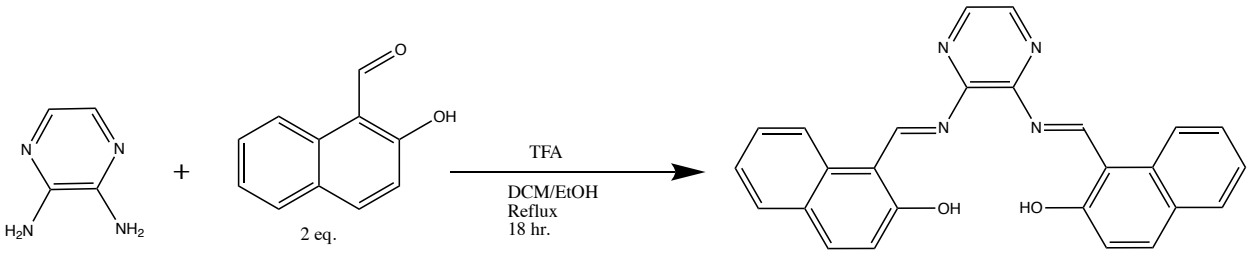

Figure 4.27. Synthetic scheme for naphthylpyrasal

N-Oxide formation is very common in transition metal complexes,[16–22] slightly less common with lanthanides,[23–25] but not common at all in actinide complexes. A brief survey of the literature showed that there were only 3 instances of N-oxide formation with actinides reported.[26–

[28] These N-oxides transition metal complexes have been reported to be used in a variety of way such as catalysis,[29] optics,[30] ion exchange,[31] and magnets.[32] More specifically in heterocyclic N-oxide donors, they can be used as push and pull electron donors and acceptors which allows them to for use in solar cells.[33]

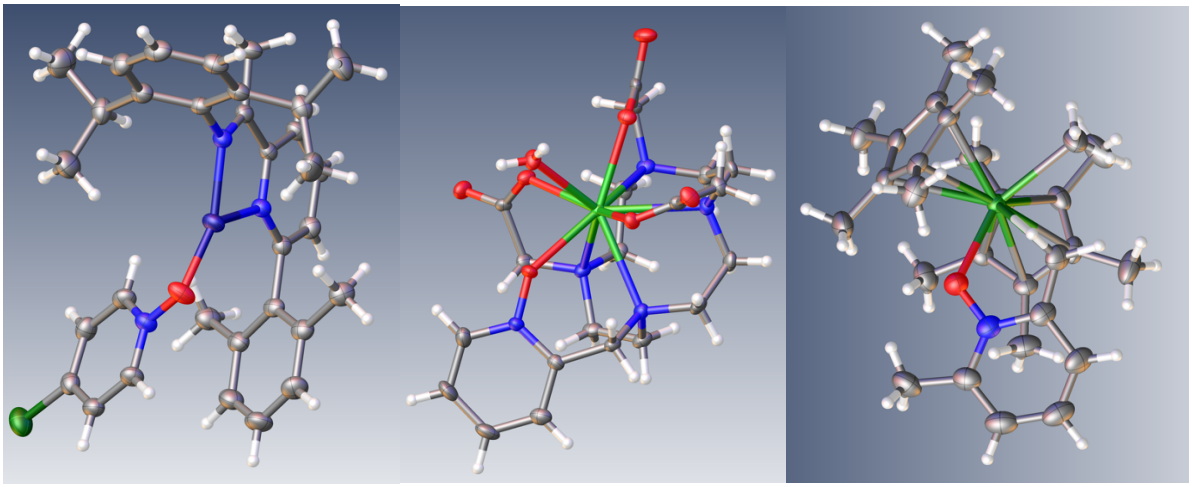

Figure 4.28. Crystal structures with the incorporation of N-Oxide coordination involving Cu(II),[34] Yb(III),[24] U(IV?).[26]

With the assistance of both the heterocyclic backbone of the naphthylpyrasal ligand and the formation of these N-Oxide coordination, we hope to examine the ability of these complexes to make way to future isolation of U (V) species and insight into its unique chemistry. We also hope this will provide additional understanding into the fundamental coordination and *f*-block bonding interactions.

Results and Discussion

The general procedure for the synthesis of the ligand naphthylpyrasal is as follows: 2,3-diaminopyrazine was dissolved in 20 mL DCM and 20 mL EtOH. The addition of 2-hydroxy-1-

naphthaldehyde and 2 molar equivalents of TFA was added, and the reaction is then heated to reflux temperature for 16 hours. A bright orange solid was produced. This solid was filtered from the solution and washed with EtOH.

To set up the complexing reactions, 0.0597 mmol of ligand was dissolved in THF followed by the addition of 2 molar equivalents of trimethylamine. The Et_3N was replaced in subsequent reactions with DIPEA (N,N-Diisopropylethylamine). or TEMPO ((2,2,6,6-Tetramethylpiperidin-1-yl)oxyl) to help with deprotonation of the ligand. Next, 0.0597 mmol of uranyl acetate dissolved in MeOH was added to the reaction mixture, and the reaction weas heated to reflux temperature for 8 hours. Upon addition of the metal salt to the solution, the reaction mixture went from being an orange color to being a deep red color which is characteristic of uranyl complexation in solution. REF To further characterize the properties of the complex, mass spec, NMR, UV-Vis, and crystallization samples were prepared.

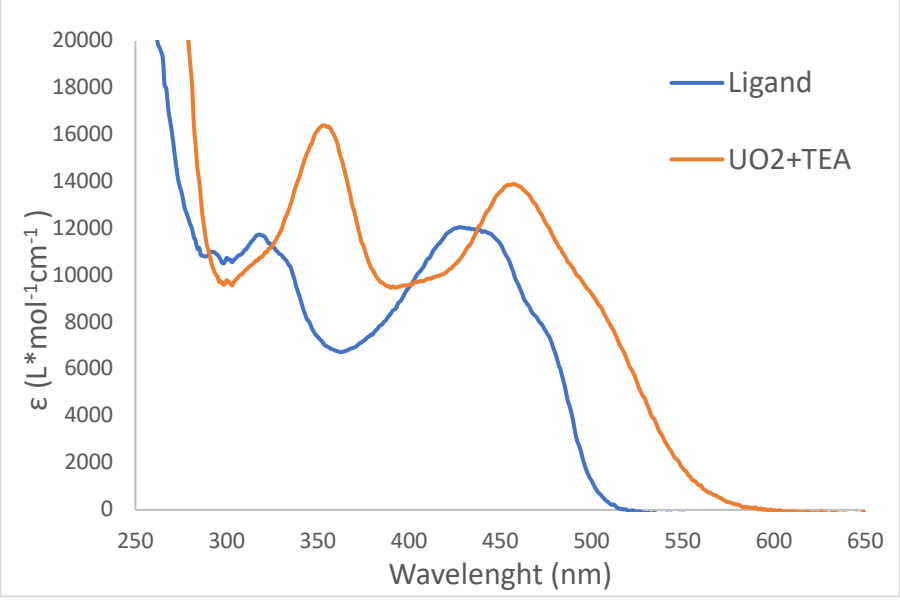

Figure 4.29. UV-Vis spectra of Naphthylpyrasal and Naphthylpyrasal+UO2+TEA

Samples of the free ligand and the ligand with uranyl (UO_2^{2+}) as the acetate salt were prepared for UV-Vis spectroscopy at a concentration of 20 μM in 1,4-dioxane (Figure 4.29). The UV-vis spectra of the ligand is initially centered at 435 nm, but in the sample containing the complex the primary ligand peak shifts bathochromically 25 nm to being centered at 460 nm. In addition, a second feature from the ligand starts at 315 nm and shifts bathochromically to a new position at 355 nm after addition of metal. Both of these features increase in molar absorptivity as well. These features along with the characteristic red color formation in solution suggest successful coordination of uranyl with naphthylpyrasal.

Crystals suitable for x-ray diffraction were grown from two different solvent systems, 1,4-dioxane with slow diffusion of pentane as well as DCM with slow diffusion of hexanes. Crystals grown from the 1,4-dioxane with slow diffusion of pentane yielded deep red crystals, as can be seen in Figure 4.30. This crystal grew in the space group *P 2₁/c.* From this data, the U-O_{phenol} bond lengths average of 2.292 Å and are well within an acceptable range of previously reported bond lengths for U-O bond lengths. The average U-N_{imine} bond lengths of 2.554 Å also fall within expected values.[7] Further examination of the -yl bond lengths shows that the two lengths to be 1.786 Å and 1.779 Å respectively, again typical for such complexes.[7] The -yl oxygens are slightly distorted from linearity at 180° by 4.79°. This deviation seems to arise from possible from small antibonding interactions between the -yl oxygens and the metal center as observed previously in work by Ephritikhine and co-workers.[35] On further examination, it was observed that the naphthyl arms are extremely distorted from planarity. This appears due to the electron withdrawing nature of the pyrazine backbone but more to accommodate the uranyl metal center and the crystal packing.

When compared to the bare naphthylsalophen-uranyl structure,[7] you can see that the naphthyl the arms are very similar to that of the naphthylpyrasal-uranyl complex. Next, we can see the formation of the directly coordinated N-oxide substituent. The U-$O_{N\text{-}oxide}$ Bond length is 2.328 Å. This is slightly shorter than the value previously reported from Pool et. al.; however, that system possessed heterocyclic N donors such as pyridine N-oxides that were not only bound through the N-oxide, but also bound through an carbon adjacent to the uranium metal center through C-H activation.[26]

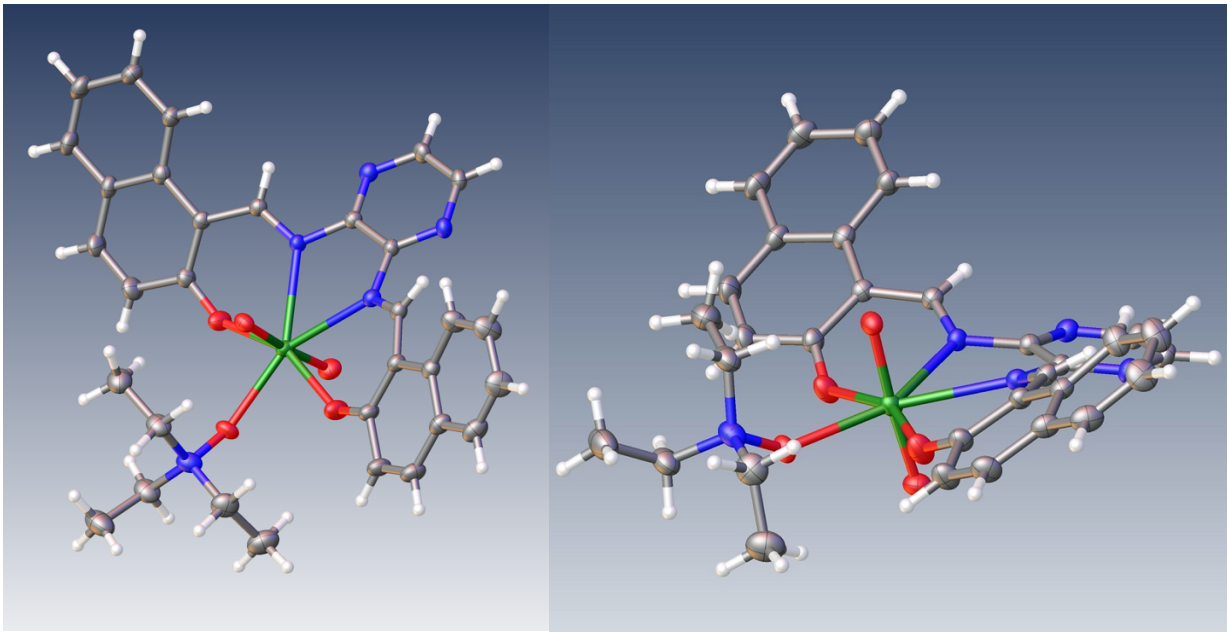

Figure 4.30. Single crystal structural representation of the Naphthylpyrasal- UO_2 crystal structure as grown from 1:1 1,4-dioxane/pentane top view(Left) and side view (Right). Atoms shown are labeled: H in white, O in red, N in blue, C in grey, U in green. Solvent molecules within the unit cell are removed for clarity.

A second crystal suitable for diffraction was grown out of dichloromethane with slow diffusion of hexanes to yield orange/red crystals. The structural diagram can be seen below in Figure 4.31. The crystal was grown in the space group P $2_{1/c}$. The average U-N_{imine} bond length of 2.554 Å is similar in both structures as well as the average U-O_{phenol} bond lengths of 2.289 Å. Again, these are typical

for uranyl complexes of this type.[7] There are several distinct differences that can be observed which when comparing each crystal structure, the first that is of consequence is the removal of the N-oxide that was bound directly to the metal center. In the second structure (Figure 6), the fifth coordination site is filled with an acetate anion left over from the uranyl metal salt that was used in the complexation reaction. The bond length is 2.337 Å, which is similar to that of the U-O bond length in the N-oxide structure, it also falls within the range of similar reported structures.[36] Another feature observed is the presence of the hydrogen bound triethylamine which sits 1.793 Å away from the bound acetate. Looking at the -yl bond length in this structure, the lengths are overall shorter than those observed in the N-oxide containing structure, at 1.768 Å and 1.762 Å, respectively. There is also less distortion in the linearity of these -yl oxygens from the previous structure. The -yl (O-U-O) angle in this structure sits slightly distorted at 177.1°. Although it does not possess an N-oxide substituent in this case, the triethylamine unit still shows up as part of the asymmetric unit in the crystal structure. Also similar to the previous structure, the naphthyl arms are significantly rotated from planarity due to the electron withdrawing nature of the pyrazine unit as well as ruffling to accommodate the uranyl metal center as is comparable to other salophen type structures.[7]

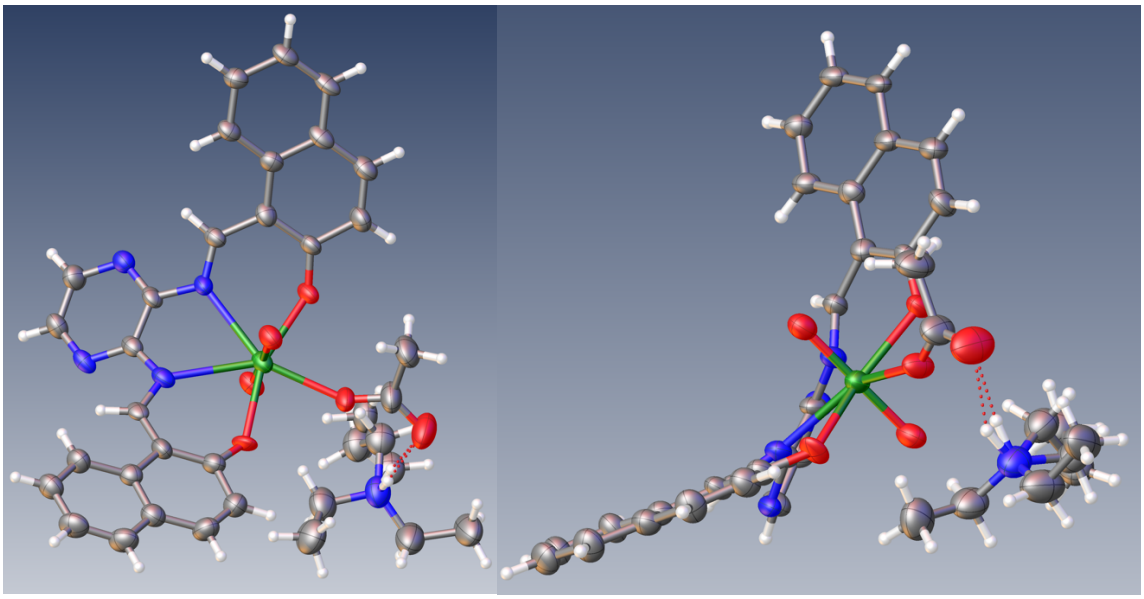

Figure 4.31. Naphthylpyrasal- UO_2 crystal structure grown from DCM/Hexane. Atoms shown are labeled: H in white, O in red, N in blue, C in grey, U in green.

In order to better understand how these N-Oxides and the N-Oxide complexes were being formed, it was tested if they form with the addition of different nitrogen in lieu of adding triethylamine as base. Before experiments with alternate N donors, where the oxygen was coming from to form the nitrogen-oxygen bond in the N-oxide was explored. Initially, it was plausible that the N-oxide was produced from wet 1,4-dioxanes used for the experiment, but this product formed even with dioxanes dried with molecular sieves. Detailed investigation into the characteristics of 1,4-dioxane revealed a better reason for this process. In a paper by Panwar and coworkers, these N-oxides were formed with tertiary amines in the presence of H_2O_2.[37] As an ether, the solvent 1,4-dioxane is a peroxide forming substance. From this, it is possible trace peroxides formed in of the 1,4-dioxane during the crystallization (not protected from light) that facilitated the formation of the coordinated N-oxide. Furthermore, both the Cahill group and Forbes group have demonstrated the ability to produce in situ peroxides from photoexcitation of the uranyl ion.[38,39] They hypothesized the conditions required for these phenomena to occur. There must be O_2 or H_2O present, sunlight or

ambient lab light. The mechanism proposed for this phenomena is: 1) excitation of U (VI), 2) followed by hydrogen abstraction from intermediate organic radical , 3) reduction of O_2 to form U (V), 4) subsequent production of the oxidized product with formation of H_2O_2, 5) thereby regenerating U(VI), and 6) finally formation of the uranyl-peroxo species and hydrogen.[38]

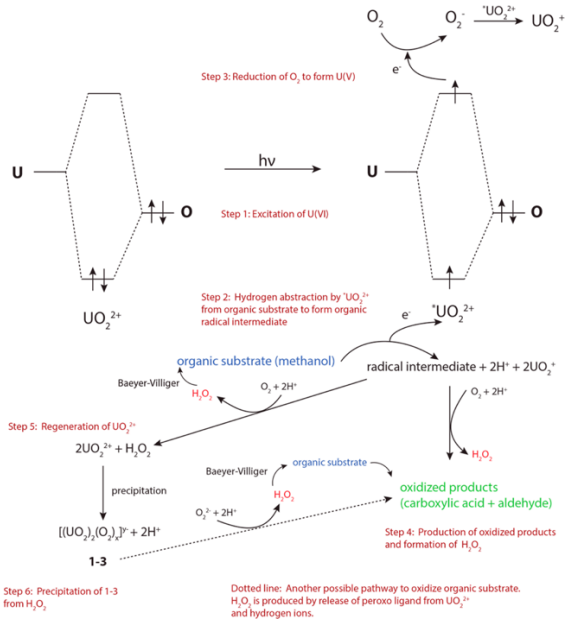

Figure 4.32. Proposed photocatalytic pathway for production of H_2O_2 with uranyl and incorporation into Uranyl compound.[38]

From these proposed mechanisms, it follows that in the formation of our N-oxide species a similar path as detailed previously above. However, due to steric hinderance from the ligands naphthyl arms, there is no opportunity to bind side on. Instead, the oxygen species only binds end on, allowing it to then further react with a free hydrogen left as a byproduct in solution. From here, a similar process as described by Strukul and coworkers where the presence of the peroxide and the metal center lead to oxidation of the tertiary amine of TEA to form the N-oxide.[40] This N-oxide is then bound to the uranium metal center. Thus, two plausible sources of the formation of the N-oxide species in the crystal data are clear. Further calculations will be used to support this mechanism.

In subsequent experiments, TEMPO and DIPEA were added as the nitrogen donors in the experiments with all the same conditions of the previously described experimental procedure. The UV-Vis spectra of both the reaction with TEMPO and the reaction with DIPEA, as we can see below in Figure 4.33, have very similar spectra to the original reaction with TEA. The initial ligand peak has peaks centered at 315 nm and 435 nm. Also, similar to that of the TEA reaction, once the metal complex is made the ligand peak at 315 shifts bathochromically to 355 nm and the peak at 435 nm to shifts bathochromically to 460 nm. Both of these also increase in molar absobtivity with addition of metal as well.

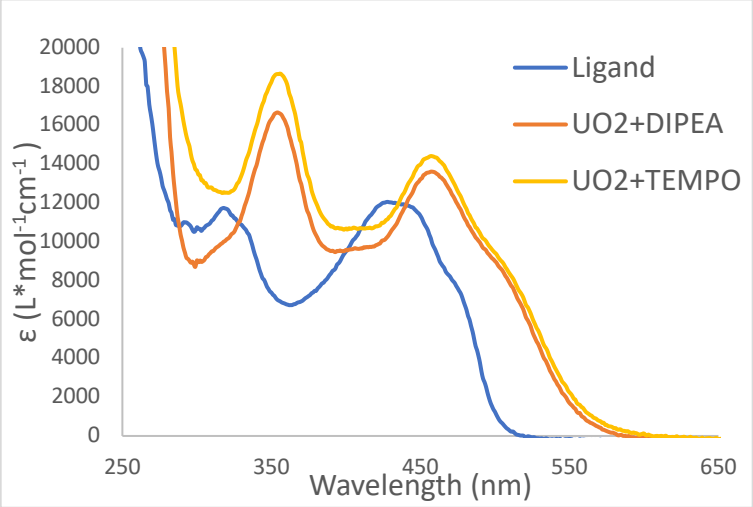

Figure 4.33. UV-Vis spectra of Naphthylpyrasal and Naphthylpyrasal+UO2+TEMPO and Naphthylpyrasal+UO2+DIPEA

The complexes were also characterized electrochemically be means of cyclic voltammetry. All samples were made to be 500 μM concentration $TBAPF_6$ was used as the supporting electrolyte in DCM. DCM was chosen to help with poor aqueous solubility of the ligand. All reported values are referenced to the Fc^+/Fc couple. In Figure 4.34 below, the ligand shows two oxidation events at

0.25 V and 0.55 V and a reduction event at -2.00 V that is broad and not well defined. When we slow down the scan rate from 100 mV s^{-1} to 50 mV s^{-1}, we can see these features become more pronounced. The oxidation peaks at 0.25 V and 0.55V show more definition and seem to be the reverse features of the peaks at -2.45 V and -2.74 V. These feature becomes more defined and line up with previously reported salen processes of a 2 electron reductions of the ligand which were stated to be quasi-reversible.[7,41] With electrochemical characterization of the ligand done, we moved on to examine the complex and how the addition of TEA, DIPEA, and TEMPO would affect these compounds both chemically and in coordination environment.

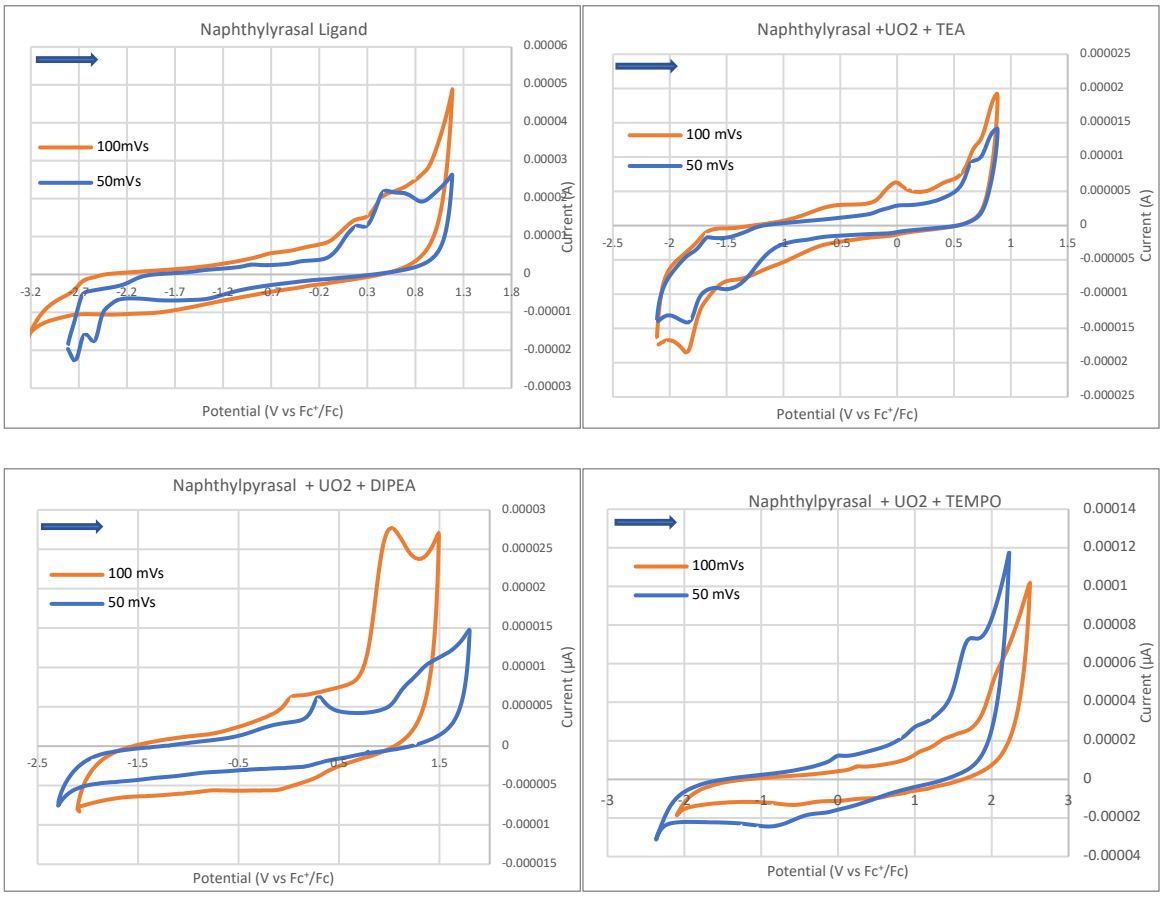

Figure 4.34. Cyclicvoltammagrams of Naphthylpyrasal ligand and alternate reaction (TEA, DIPEA, TEMPO) conditions in DCM 400 µM with $TBAPF_6$

When examining the reactions containing TEA, DIPEA, and TEMPO the semi reversible oxidation and reduction of the ligand are still observed. These features all seem to be scan rate dependent, as changes between the two different rates can be observed with some features becoming more well defined and others less defined. In the CV with TEA added (Figure 4.34, top right) at 100 mV s^{-1}, the first oxidation feature is at 0.01 V and the peak at 0.743 V - most likely due to merely the oxidations of the ligand as this feature persists in this region from the ligand data. The return peak at -1.4 V and -1.8 V are both within the range to be either reduction of the ligand or reduction of the uranyl that has been reported previously in the literature for similar compounds.[41,42]Additional definition of these reductive peaks is observed with a slower scan rate 50 mV s^{-1}.

In the diisopropylethylamine reaction CV (DIPEA, Figure 4.34, bottom left), while scanning at 100 mV s^{-1}, a large jump in current being passed on the first ligand oxidation at 1.06 V is observed. The first reductive feature of the ligand at 0.09 V is maintained; however, on the return sweep, no distinguishable features arise. Slowing the scan rate does appear to resolve the peak at 0.09 V, but the definition at the reduction peak at 1.06 V is diminished. Looking at the last CV, in the reaction with TEMPO present (Figure 4.34, bottom right), the 100 mV s^{-1} data shows no defined features at all; however, the 50 mV s^{-1} does reveal a little more. The feature at 0.01 V on the oxidative sweep is still present as well as the feature at 1.77 V due to ligand oxidation. On the return sweep, the formation of two unresolved features at 0.02V and -0.85 V are observed, likely the ligand reductions although this requires further resolution. It should be noted that over the scan rate of 200 mV s^{-1}, all of the samples resulted in cyclic voltammograms with severely rounded features until the reverse sweep and were unreadable. This is in contrast to most single

and double electron processes in small molecules that tend to resolve with quicker scan rates. Solubility of great concern here, and this will require additional electrochemical characterization possibly with a more coordinating solvent to further explore the nature of these compounds. This may require additional synthetic modifications of the ligand. In our current solvent system, interference may occur with slow diffusion of our complex across the electrode resulting in the broadening at higher scan rates. Another aspect requiring investigation is the effect of the ligand metal complex in air as uranium is easily oxidizable, potentially lower valent uranium species could be reached with maintaining an inert atmosphere.

Here recently, a third variation of this complex was prepared in a crystal suitable for diffraction of the Naphthylpyrasal-(UO_2^{2+}) complex with DIPEA that was (Figure 4.35). This crystal was grown out of 1,4-dioxane with slow diffusion of pentane and produces single crystals as orange plates. This crystal was also grown in the space group $P\ 2_{1/n}$. However, this structure was found to be very different that the previous two. Once again, the $U\text{-}N_{imine}$ average bond lengths of 2.552 Å and the $U\text{-}O_{phenol}$ average bond lengths of 2.287 Å are on par for uranyl coordination. Looking at the -yl bond lengths in this structure as compared to the previous two, these lengths are the longest at 1.786 Å and 1.718 Å. Similar to the N-oxide structure, a distortion from planarity in the O_{yl}—U—O_{yl} bond angle is observed. The angle of distortion is 175.06° (4.94°). Once again, we suspect that this is due to antibonding orbital interactions between the $O_{\text{-yl}}$ and the metal center.[35] Another notable feature of this complex is the coordination of a water molecule to fill the fifth coordination site. This water coordination is believed to occur due to the steric bulk of the DIPEA as opposed to that of the triethylamine. The $U\text{-}O_{water}$ bond length is 2.389 Å which is typical length for coordinating water in a $[UO_2]^{2+}$ complex. With the introduction of the less

sterically hindering substituent, the orientation of the naphthyl arms change drastically. In the two previous structures, the arms tilted up to for a bowl to facilitate with coordination of the of the metal center as well as to mitigate steric strain from the triethylamine substituent. The arms are allowed now to sit closer to parallel with the backbone, however, they do remain slightly twisted in an up and down configuration to accommodate the uranyl metal center.

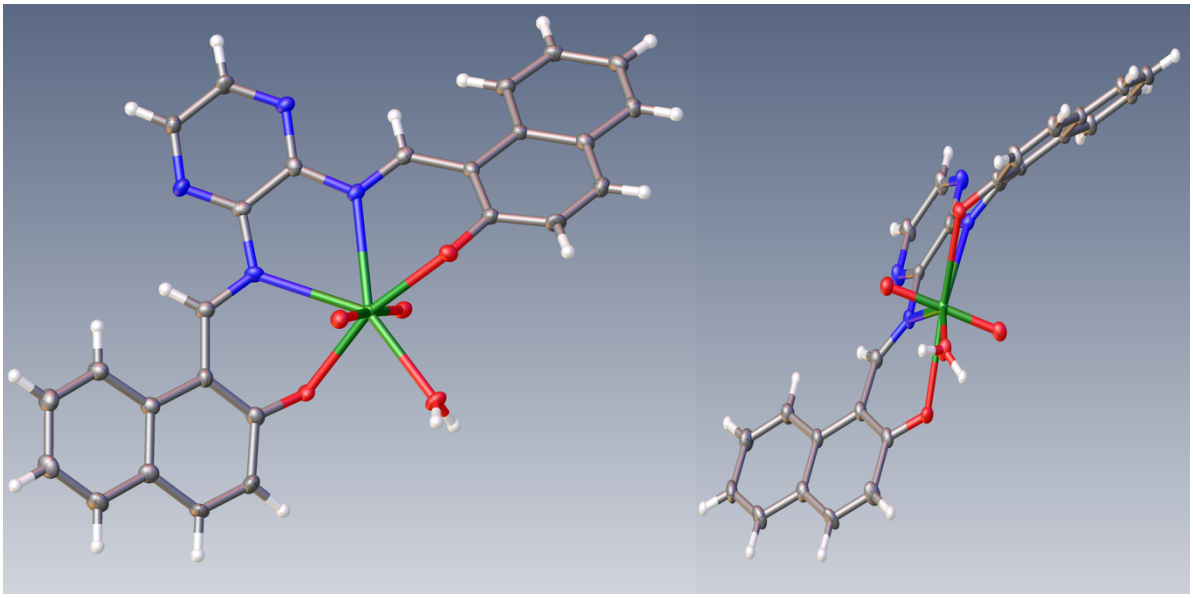

Figure 4.35. Naphthylpyrasal-UO_2 + DIPEA crystal structure grown from 1,4-Dioxane/Pentane. Atoms shown are labeled: H in white, O in red, N in blue, C in grey, U in green.

Conclusions

In conclusion, we have shown the ability to form a new N-oxide actinide complex though selection of crystallization conditions. We have also set forth a plausible hypothesis to the formation of these units in the solid state and characterized the products of these conditions. It has shown to both slightly lengthen both -yl oxygen bonds as well as distort the linearity of the uranyl moiety up to nearly 5°. Furthermore, this naphthylpyrasal ligand in comparison to naphthylsalophen and its uranyl complexes seems to show a slightly greater ability to gain access to a U (V) species under the correct conditions. This suggest that this complex should be

exceptional as a ligand to facilitate access to a U (V) structure. Further experimentation will need to be conducted under inert atmosphere to further corroborate these finding. Also, a more suitable solvent will need to be used to further refine the electrochemical characterization that does not further hinder solubility.

Synthesis

Caution! The uranium metal salt – $UO_2(OAc)_2 \cdot 2H_2O$ – used in this study contained depleted uranium. Standard precautions for handling radioactive materials or heavy metals such as uranyl nitrate and lead sulfate were followed.

Electrochemical measurements were carried out using a CH Instruments 660 E potentiostat in dichloromethane with tetrabutylammonium perchlorate ($TBAPF_6$) supporting electrolyte (0.1 M). Ligand and complex solutions (800 μM) were purged with N_2 for 45 minutes immediately prior to experiments. A three-electrode cell consisting of a glassy-carbon-disk working electrode, Pt-wire counter electrode, and Ag/AgCl/saturated KCl/H_2O reference electrode was used. Data were corrected to versus ferrocene based on averaged values for $E_{1/2}(Fc^+/Fc)$ collected using the same three-electrode cell before and after each set of experiments. All data reported was using an initial anodic sweep and return cathodic sweep.

Synthesis of Naphthylpyrasal 0.001 mol of 2,3-diaminopyrazine was dissolved in 20 mL DCM and 20 mL EtOH in a 100 mL round bottom flask. The addition of 0.002 mol of 2-hydroxy-1-naphthaldehyde and 2 molar equivalents of TFA were completed, and the reaction is then heated to reflux temperature for 16 hours. Once the reaction was completed, a bright orange solid was produced. This was filtered from the remaining solution and washed with EtOH. Yield: 42%; TOF MS (ESI+) m/z (M + H) Calc. 419.1508, Found:419.1493; 1H NMR (600 MHz, $CDCl_3$) δ 7.34 (d,5H), 7.56 (s, 2H), 7.69 (s, 2H), 7.83 (s, 2H), 8.28 (d, 5H), 10.22 (s, 2H).

Synthesis of Naphthylpyrasal-UO_2{TEA} In a 100 mL round bottom flask containing a stir bar, 0.0597 mmol of ligand was dissolved in THF followed by the addition of 2 molar equivalents of triethylamine to aid in deprotonation of the ligand. Next, 0.0597 mmol of uranyl acetate dissolved in MeOH was added to the mixture, and the reaction was heated to reflux temperature for 8 hours. Next, the reaction was taken to dryness under reduced pressure via rotary evaporation. The solid was then washed with EtOH followed by hexanes. The solid was allowed to dry in an oven under reduced pressure. Yield: 74%; TOF MS (ESI+) m/z (M + 2Na) Calc.: 1474.3992, Found: 1474.4580; 1H NMR (500 MHz, $CDCl_3$) δ

Synthesis of Naphthylpyrasal-UO_2{DIPEA} In a 100 mL round bottom flask containing a stir bar, 0.0597 mmol of ligand was dissolved in THF followed by 2 molar equivalents of diisopropylethylamine to aid in deprotonation of the ligand. Next 0.0597 mmol of uranyl acetate dissolved in MeOH was added and the reaction was heated to reflux temperature for 8 hours. Next, the reaction was taken to dryness under reduced pressure by means of a rotary evaporator. The solid was then washed with EtOH followed by hexanes. The solid was allowed to dry in a vacuum oven under reduced pressure. Yield: 66% ; TOF MS (ESI+) m/z (M + K) Calc.: 757.1578, Found 757.4818; ^{1}H NMR (500 MHz, DMF-d_7) δ 7.39 -7.46 (m, 4H), 7.69 (t, 2H, J = 7.5), 7.95 (d, 2H, J = 7.8), 8.35 (d, 2H, J = 9.1), 8.51 (d, 2H, J = 8.4), 8.67 (s, 2H), 11.12 (s, 2H).

Synthesis of Naphthylpyrasal-UO_2{TEMPO} In a 100 mL round bottom flask containing a stir bar, 0.0597 mmol of ligand was dissolved in THF followed 2 molar equivalents of TEMPO were added to the reaction. Next, 0.0597 mmol of uranyl acetate dissolved in MeOH was added, and the reaction was heated to reflux temperature for 8 hours. Next, the reaction was taken to dryness

under reduced pressure by means of rotary evaporation. The solid was then washed with EtOH followed by hexanes. The solid was allowed to dry in a vacuum oven under reduced pressure. Yield: 62%; ^{1}H NMR (500 MHz, DMF-d_7) δ 7.39 – 7.46 (m, 4H), 7.69 (t, 2H, J = 7.8), 7.95 (d, 2H, J = 8.5), 8.67 (s, 2H), 11.12 (s, 2H).

References

(1) Cowie, B. E.; Douair, I.; Maron, L.; Love, J. B.; Arnold, P. L. Selective Oxo Ligand Functionalisation and Substitution Reactivity in an Oxo/Catecholate-Bridged UIV/UIV Pacman Complex. *Chem. Sci.* **2020**, *11* (27), 7144–7157. https://doi.org/10.1039/D0SC02297G.

(2) Assefa, M. K.; Wu, G.; Hayton, T. W. Uranyl Oxo Silylation Promoted by Silsesquioxane Coordination. *J. Am. Chem. Soc.* **2020**, *142* (19), 8738–8747. https://doi.org/10.1021/jacs.0c00990.

(3) Belkhiri, L.; Arliguie, T.; Thuéry, P.; Fourmigué, M.; Boucekkine, A.; Ephritikhine, M. Investigation of the Dithiolene Ligand Conformation in Analogous U(IV)/U(V) Complexes: X-Ray Diffraction and Density Functional Theory Analysis of the U···(CC) Interaction. *Organometallics* **2006**, *25* (11), 2782–2795. https://doi.org/10.1021/om060083d.

(4) Arnold, P. L.; Stevens, C. J.; Bell, N. L.; Lord, R. M.; Goldberg, J. M.; Nichol, G. S.; Love, J. B. Multi-Electron Reduction of Sulfur and Carbon Disulfide Using Binuclear Uranium(Iii) Borohydride Complexes. *Chem. Sci.* **2017**, *8* (5), 3609–3617. https://doi.org/10.1039/C7SC00382J.

(5) Bell, N. L.; Shaw, B.; Arnold, P. L.; Love, J. B. Uranyl to Uranium(IV) Conversion through Manipulation of Axial and Equatorial Ligands. *J. Am. Chem. Soc.* **2018**, *140* (9), 3378–3384. https://doi.org/10.1021/jacs.7b13474.

(6) Tatebe, C. J.; Kiernicki, J. J.; Higgins, R. F.; Ward, R. J.; Natoli, S. N.; Langford, J. C.; Clark, C. L.; Zeller, M.; Wenthold, P.; Shores, M. P.; Walensky, J. R.; Bart, S. C. Investigation of the Electronic Structure of Aryl-Bridged Dinuclear U(III) and U(IV) Compounds. *Organometallics* **2019**, *38* (5), 1031–1040. https://doi.org/10.1021/acs.organomet.8b00794.

(7) Niklas, J. E.; Hardy, E. E.; Gorden, A. E. V. Solid-State Structural Elucidation and Electrochemical Analysis of Uranyl Naphthylsalophen. *Chem. Commun.* **2018**, *54* (83), 11693–11696. https://doi.org/10.1039/c8cc05242e.

(8) Niklas, J. E.; Hunter, K. M.; Gorden, A. E. V. Bonding Interactions in Uranyl α-Diimine Complexes: A Spectroscopic and Electrochemical Study of the Impacts of Ligand Electronics and Extended Conjugation. *Inorg. Chem.* **2019**, *58* (22), 15088–15100. https://doi.org/10.1021/acs.inorgchem.9b01695.

(9) Mayhugh, J. T.; Niklas, J. E.; Forbes, M. G.; Gorden, J. D.; Gorden, A. E. V. Pyrrophens: Pyrrole-Based Hexadentate Ligands Tailor-Made for Uranyl (UO_2^{2+}) Coordination and Molecular Recognition. *Inorg. Chem.* **2020**, *59* (14), 9560–9568. https://doi.org/10.1021/acs.inorgchem.0c00439.

(10) Gorden, A. E. V.; Xu, J.; Raymond, K. N.; Durbin, P. Rational Design of Sequestering Agents for Plutonium and Other Actinides. *Chem. Rev.* **2003**, *103* (11), 4207–4282. https://doi.org/10.1021/cr990114x.

(11) Gorden, A. E. V.; DeVore, M. A.; Maynard, B. A. Coordination Chemistry with F-Element Complexes for an Improved Understanding of Factors That Contribute to Extraction Selectivity. *Inorg. Chem.* **2013**, *52* (7), 3445–3458. https://doi.org/10.1021/ic300887p.

(12) Kraft, S. J.; Williams, U. J.; Daly, S. R.; J. Schelter, E.; Kozimor, S. A.; Boland, K. S.; Kikkawa, J. M.; Forrest, W. P.; Christensen, C. N.; Schwarz, D. E.; Fanwick, P. E.; Clark, D. L.; Conradson, S. D.; Bart, S. C. Synthesis, Characterization, and Multielectron Reduction Chemistry of Uranium Supported by Redox-Active α-Diimine Ligands. **2011**, *50* (20), 9838–9848. https://doi.org/10.1021/ic2002805.

(13) Kiernicki, J. J.; Cladis, D. P.; Fanwick, P. E.; Zeller, M.; Bart, S. C. Synthesis, Characterization, and Stoichiometric U–O Bond Scission in Uranyl Species Supported by Pyridine(Diimine) Ligand Radicals. *J. Am. Chem. Soc.* **2015**, *137* (34), 11115–11125. https://doi.org/10.1021/jacs.5b06217.

(14) Anderson, N. H.; Odoh, S. O.; Williams, U. J.; Lewis, A. J.; Wagner, G. L.; Lezama Pacheco, J.; Kozimor, S. A.; Gagliardi, L.; Schelter, E. J.; Bart, S. C. Investigation of the Electronic Ground States for a Reduced Pyridine(Diimine) Uranium Series: Evidence for a Ligand Tetraanion Stabilized by a Uranium Dimer. *J. Am. Chem. Soc.* **2015**, *137* (14), 4690–4700. https://doi.org/10.1021/ja511867a.

(15) Kiernicki, J. J.; Ferrier, M. G.; Lezama Pacheco, J. S.; La Pierre, H. S.; Stein, B. W.; Zeller, M.; Kozimor, S. A.; Bart, S. C. Examining the Effects of Ligand Variation on the Electronic Structure of Uranium Bis(Imido) Species. *J. Am. Chem. Soc.* **2016**, *138* (42), 13941–13951. https://doi.org/10.1021/jacs.6b06989.

(16) Garvey, R. G.; Ragsdale, R. O. The Coordination of Substituted Pyridine N-Oxides with Oxovanadium(IV) Cations. *Inorg. Chem.* **1965**, *4* (11), 1604–1608. https://doi.org/10.1021/ic50033a015.

(17) Herlocker, D. W.; Drago, R. S. Tetrahedral and Pseudo-Tetrahedral Complexes of Cobalt(II) with Trimethylamine N-Oxide. *Inorg. Chem.* **1968**, *7* (8), 1479–1484. https://doi.org/10.1021/ic50066a001.

(18) Hill, C. L.; Williamson, M. W. Electronic and Structural Properties of a Reactive Metalloporphyrin with N-Oxide Axial Ligands. Crystal and Molecular Structure of Bis(2,6-Lutidine N-Oxide)(Tetraphenylporphinato)Manganese(III) Perchlorate. *Inorg. Chem.* **1985**, *24* (19), 3024–3030. https://doi.org/10.1021/ic00213a031.

(19) Lu, K.-L.; Kumaresan, S.; Wen, Y.-S.; Hwu, J. R. Novel Osmium N-Oxide Complexes from the Reaction of Triosmium Clusters with 1-Hydroxybenzotriazole. *Organometallics* **1994**, *13* (8), 3170–3176. https://doi.org/10.1021/om00020a033.

(20) Sarma, R.; Karmakar, A.; Baruah, J. B. N-Oxides in Metal-Containing Multicomponent Molecular Complexes. *Inorg. Chem.* **2008**, *47* (3), 763–765. https://doi.org/10.1021/ic701639n.

(21) Ishida, N.; Ikemoto, W.; Narumi, M.; Murakami, M. Synthesis of Pyridine-N-Oxide–Borane Intramolecular Complexes by Palladium-Catalyzed Reaction of 2-Bromopyridine-N-Oxides with Alkynyltriarylborates. *Org. Lett.* **2011**, *13* (12), 3008–3011. https://doi.org/10.1021/ol2008439.

(22) Hnatejko, Z.; Kwiatek, D.; Dutkiewicz, G.; Kubicki, M.; Jastrząb, R.; Lis, S. Pyridine N-Oxide Complexes of Cu(II) Ions with Pseudohalides: Synthesis, Structural and Spectroscopic Characterization. *Polyhedron* **2014**, *81*, 728–734. https://doi.org/10.1016/j.poly.2014.07.041.

(23) Pointillart, F.; Guennic, B. L.; Maury, O.; Golhen, S.; Cador, O.; Ouahab, L. Lanthanide Dinuclear Complexes Involving Tetrathiafulvalene-3-Pyridine-N-Oxide Ligand: Semiconductor Radical Salt, Magnetic, and Photophysical Studies. *Inorg. Chem.* **2013**, *52* (3), 1398–1408. https://doi.org/10.1021/ic302095h.

(24) Polášek, M.; Kotek, J.; Hermann, P.; Císařová, I.; Binnemans, K.; Lukeš, I. Lanthanide(III) Complexes of Pyridine-N-Oxide Analogues of DOTA in Solution and in the Solid State. A New Kind of Isomerism in Complexes of DOTA-like Ligands. *Inorg. Chem.* **2009**, *48* (2), 466–475. https://doi.org/10.1021/ic801597z.

(25) Polášek, M.; Šedinová, M.; Kotek, J.; Vander Elst, L.; Muller, R. N.; Hermann, P.; Lukeš, I. Pyridine-N-Oxide Analogues of DOTA and Their Gadolinium(III) Complexes

Endowed with a Fast Water Exchange on the Square-Antiprismatic Isomer. *Inorg. Chem.* **2009**, *48* (2), 455–465. https://doi.org/10.1021/ic801596v.

(26) Pool, J. A.; Scott, B. L.; Kiplinger, J. L. A New Mode of Reactivity for Pyridine N-Oxide: C−H Activation with Uranium(IV) and Thorium(IV) Bis(Alkyl) Complexes. *J. Am. Chem. Soc.* **2005**, *127* (5), 1338–1339. https://doi.org/10.1021/ja044153o.

(27) Yahia, A.; Maron, L. Is Thorium a d Transition Metal or an Actinide? An Answer from a DFT Study of the Reaction between Pyridine N-Oxide and Cp2M(CH3)2 with M = Zr, Th, and U. *Organometallics* **2009**, *28* (3), 672–679. https://doi.org/10.1021/om800943a.

(28) Schmidt, A.-C.; Hermsen, M.; Rominger, F.; Dehn, R.; Teles, J. H.; Schäfer, A.; Trapp, O.; Schaub, T. Synthesis of Mono- and Dinuclear Vanadium Complexes and Their Reactivity toward Dehydroperoxidation of Alkyl Hydroperoxides. *Inorg. Chem.* **2017**. https://doi.org/10.1021/acs.inorgchem.6b02322.

(29) Jackson Lepage, C. R.; Mihichuk, L.; Lee, D. G. The Oxidation of Sulfides by Chromium(V). *Can. J. Chem.* **2003**, *81* (1), 75–80. https://doi.org/10.1139/v02-201.

(30) EATON, D. F. Nonlinear Optical Materials. *Science* **1991**, *253* (5017), 281. https://doi.org/10.1126/science.253.5017.281.

(31) Chettiyankandy, P.; Chowdhuri, S. Ion Solvation Scenario in an Aqueous Solution Mixture of Counteracting Osmolytes: Urea and Trimethylamine-N-Oxide (TMAO). *J. Mol. Liq.* **2019**, *293*, 111467. https://doi.org/10.1016/j.molliq.2019.111467.

(32) Cortes, P.; Atria, A. M.; Contreras, M.; Garland, M. T.; Peña, O.; Corsini, G. MAGNETIC PROPERTIES AND ANTIBACTERIAL ACTIVITY OF TETRANUCLEAR COPPER COMPLEXES BRIDGED BY OXO GROUP. *J. Teh Chil. Chem. Soc.* **2006**, *51* (3), 957–960. http://dx.doi.org/10.4067/S0717-97072006000300005.

(33) Wu, J.; Liu, Y.; Hu, H.-C.; Wen, J.; Zhu, X.; Ouyang, X. Acid-Assisted Noncovalent Interaction with Enhanced Electron Transportation on Active/Interfacial Layers for 16.43% Nonfullerene Organic Solar Cells. *J. Phys. Chem. C* **2021**. https://doi.org/10.1021/acs.jpcc.0c10014.

(34) Hong, S.; Gupta, A. K.; Tolman, W. B. Intermediates in Reactions of Copper(I) Complexes with N-Oxides: From the Formation of Stable Adducts to Oxo Transfer. *Inorg. Chem.* **2009**, *48* (14), 6323–6325. https://doi.org/10.1021/ic900435p.

(35) Tourneux, J.-C.; Berthet, J.-C.; Cantat, T.; Thuéry, P.; Mézailles, N.; Ephritikhine, M. Exploring the Uranyl Organometallic Chemistry: From Single to Double Uranium−Carbon Bonds. *J. Am. Chem. Soc.* **2011**, *133* (16), 6162–6165. https://doi.org/10.1021/ja201276h.

(36) Jiang, J.; Rao, L.; Bernardo, P. D.; Zanonato, P.; Bismondo, A. Complexation of Uranium(vi) with Acetate at Variable Temperatures. *J. Chem. Soc. Dalton Trans.* **2002**, No. 8, 1832–1838. https://doi.org/10.1039/B106642K.

(37) Panwar, V.; Bansal, A.; Ray, S. S.; Jain, S. L. Renewable Waste Rice Husk Grafted Oxo-Vanadium Catalyst for Oxidation of Tertiary Amines to N-Oxides. *RSC Adv.* **2016**, *6* (75), 71550–71556. https://doi.org/10.1039/C6RA13571D.

(38) Thangavelu, S. G.; Cahill, C. L. Uranyl-Promoted Peroxide Generation: Synthesis and Characterization of Three Uranyl Peroxo [(UO2)2(O2)] Complexes. *Inorg. Chem.* **2015**, *54* (9), 4208–4221. https://doi.org/10.1021/ic502767k.

(39) Jayasinghe, A. S.; Applegate, L. C.; Unruh, D. K.; Hutton, J.; Forbes, T. Z. Utilizing Autoxidation of Solvents To Promote the Formation of Uranyl Peroxide Materials. *Cryst. Growth Des.* **2019**, *19* (3), 1756–1766. https://doi.org/10.1021/acs.cgd.8b01735.

(40) Colladon, M.; Scarso, A.; Strukul, G. Mild Catalytic Oxidation of Secondary and Tertiary Amines to Nitrones and N-Oxides with H2O2 Mediated by Pt(Ii) Catalysts. *Green Chem.* **2008**, *10* (7), 793–798. https://doi.org/10.1039/B805404E.

(41) Isse, A. A.; Gennaro, A.; Vianello, E. Electrochemical Reduction of Schiff Base Ligands H2salen and H2salophen. *Electrochimica Acta* **1997**, *42* (13–14), 2065–2071. https://doi.org/10.1016/s0013-4686(97)85482-5.

(42) Sethi, S.; Panigrahi, R.; Paul, A. K.; Mallik, B. S.; Parhi, P.; Das, P. K.; Behera, N. Detailed Characterization of Dioxouranium(vi) Complexes with a Symmetrical Tetradentate N2O2-Benzil Bis(Isonicotinoyl Hydrazone) Ligand. *Dalton Trans.* **2020**, *49* (30), 10603–10612. https://doi.org/10.1039/d0dt02014a.

Chapter 5
Future Work and Preliminary Data

Conclusions

This work has covered three new types of ligands that take advantage of mixed donor systems and show the capability to coordinate f-block elements efficiently. These were found to produce unique photophysical phenomena in response to said coordination events. The salimidizine type, naphthylsalophen type, and naphthylpyrasal type ligands have been synthesized and characterized using UV-Vis and fluorescence spectroscopy, X-ray diffraction, and electrochemical techniques. Initially. these ligands were conceived to selectively coordinate and identify uranyl ions in solution but have been shown to coordinate lanthanides as well.

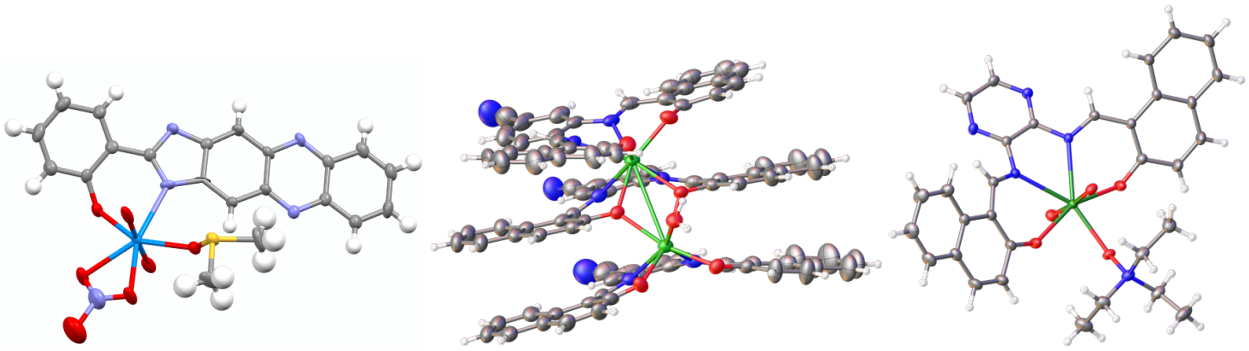

Figure 5.36.Crystal structures of Salimidizine-UO2 complex, [Er_2(L-CN)$_3$(H_2O)], Naphthylpyrasal-UO2-N-oxide complex

Salimidizine and its derivatives were shown to be exceptional fluorescence sensors in identifying uranyl ions in solution. This is due to the extended conjugation and mixed donor bidentate salen type binding pocket. Although we were unable to selectively coordinate uranyl, we were able to induce unique fluorescence responses from both copper (II) and uranyl respectively. This allowed for differentiation of each metal ion. Further characterization was completed via X-ray crystallography on the salimidizine and DTB-salimidizine free base ligands as well as the uranyl coordinated salimidizine complex which was used to shed light on the binding environment when complexed with the metal.

Cyanonaphthylsalophen was shown to facilitate two photon up-conversion in an efficient manner. When complexed with Nd (III), Er (III), and Yb (III) ions these complexes form 3:2 ligand to metal complexes or triple decker sandwich complexes. Though the use of the antenna effect for sensitization, and the correct Förster distance as well as properly positioned energy levels, this complex functions well as a single molecule up-converter. Studying these complexes with both solid and solution state fluorescence allowed for explanation into the capability of these complexes to participate in these up-conversion. These complexes display efficient one photon Nd (III) and Yb (III) centered emission and weak Er (III) centered emission. Mixed metal complexes containing Er (III), Yb (III), and Y (III) in specific percentages were also synthesized. These complexes were able to emit red and green centered emissions when stimulated with a low power 980 nm laser. This coupled with the X-ray diffraction data has allowed for further explanation into putting physical parameters of these Förster distances in this complex.

Naphthylpyrasal was shown to coordinate uranyl and form unusual actinide and N-oxide containing compounds. This ligand also shows promise for being able to possibly stabilize radicals that may be of interest in the preparation of lower valent uranium species. Examination of this ligand in solid state allowed observation of altering the coordination sphere of the uranyl ion by changing the crystallization solvents. Triethylamine coupled with the presence of peroxides in the crystallization solvents seem to be the source of the N-oxide formation since it has been shown to form these N-oxides with triethylamine and transition metals present.[1] Further investigation led to reactions being set up with DIPEA and TEMPO to see the effects of bulkier substituents would still form these N-oxide complexes. Characterization using X-ray crystallography led to structural identification of three separate and distinct naphthylpyrasal-UO_2 crystal structures. No other N-

oxide complexes were formed which leased to the assumption that DIPEA was too bulky to coordinate in the fifth site and. Also, in the crystallographic data, there was also no elongation of the -yl oxygens which would suggest that any reduction of the uranyl center was taking place, however, in two of the structures there was ~5° bends in the typically linear -yl bond which should be noted. Further investigation into the feasibility of stabilizing the lower valent uranium species will need to be attempted. Reactions will need to be attempted under air and water free conditions to examine the behavior in the presence of these lower oxidation states of uranium. Furthermore, attempts to synthesize and isolate a functionalized -yl oxygen containing uranium complex with the naphthylpyrasal ligand should be attempted. Finally examining the ability of the naphthylpyrasal-UO_2 to form peroxides should be examined. There will need to be reactions similar to what was laid out in Thangavelu et. al.[2] and Jayasunghe et. al.[3] to examine the complexes ability under various reaction conditions while following the formation of peroxides in solution.

Future work and Preliminary Findings

Modification of Naphthylsalophen Ligands

As covered in chapter 3, we have seen that the cyanonaphthylsalophen has shown the ability to efficiently facilitate two photon up-conversion processes. Moving forward we are examining ways of altering these ligands further in an attempt to tune the Förster distance between the metal centers. We have been able to synthesize eight new ligands that utilize placement of electron donating and withdrawing groups on the backbone portion of the ligand. These ligands are made similarly to that of the cyanonaphthylsalophen by taking advantage of the condensation reaction between the different diamino backbones and 2-hydroxyl-1-naphthylaldehydes.

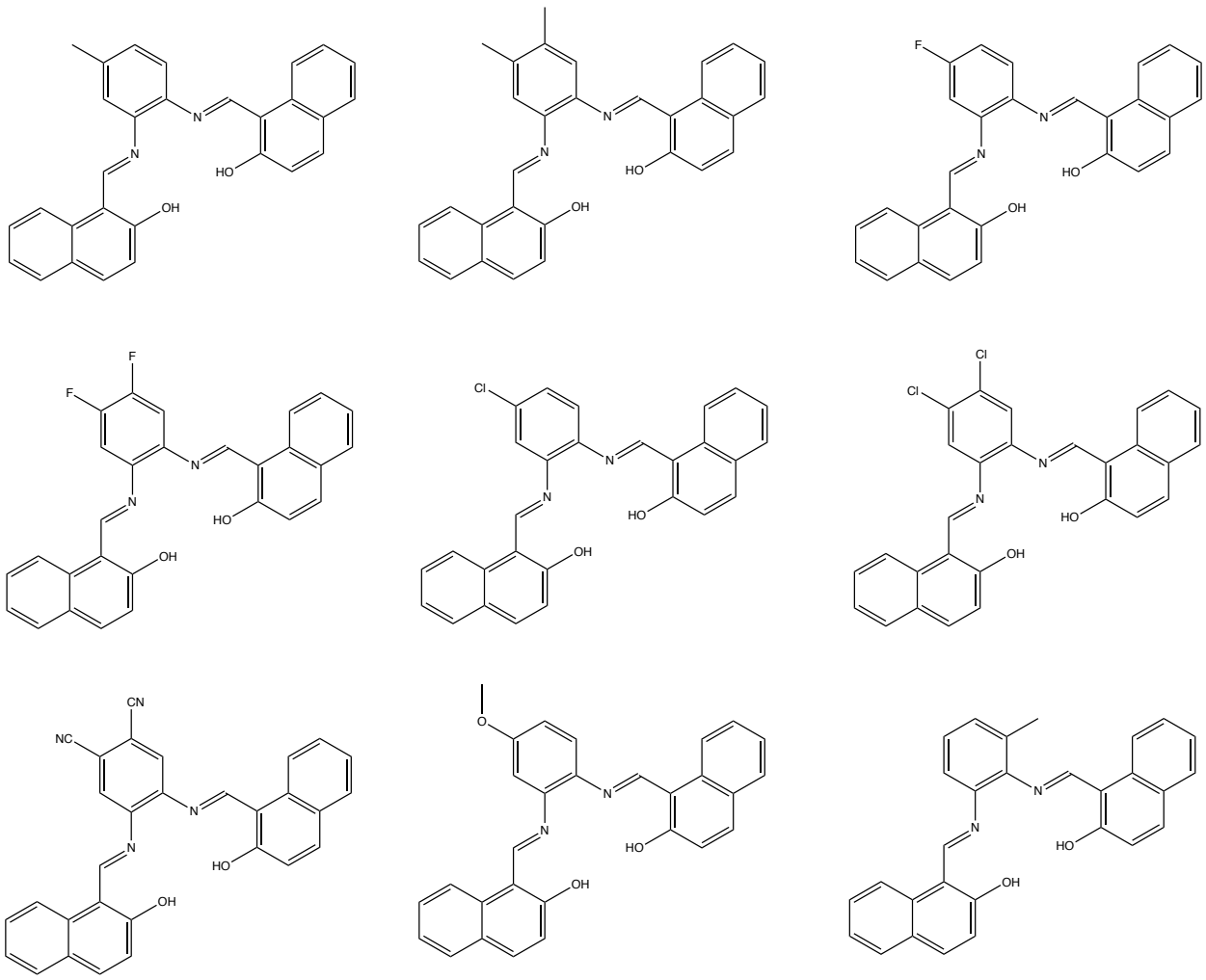

Figure 5.37. Functionalized naphthylsalophen ligands

Listed above in Figure 5.37 are 4-methylnaphthylsalophen, 3-methylnaphthylsalophen, dimethylnaphthylsalophen, fluoronaphthylsalophen, difluoronaphthylsalophen, chloronaphthylsalophen, dichloronaphthylsalophen, dicyanonaphthylsalophen, and methoxynaphthylsalophen. The next step with this project is to first synthesize several different Ln (III) ions to form these triple decker charge balance complexes with all the ligands listed above. Following these syntheses, it will be needed to characterize the solid-state fluorescence, solution state fluorescence, and to determine the potential for up conversion processes. It would also be of

interest us use calculations to determine singlet and triplet energy levels. This will allow for new data to predict metal ligand interactions that will result in the optimal energy level overlap for taking advantage of the antenna in the respective complexes. Such work will need to take into account the distance between the donor and acceptor as it will be crucial to examine all these ligands several Ln(III) ions to probe this potential means to tune this Förster distance/radius to increase the efficiency of up conversion processes.[4–6] Below (Table 5.3) is a list of compounds that have already been prepared and characterized by mass spec.

Methoxynaphthylsalophen	Methylnaphthylsalophen	Dimethylnaphthylsalophen	Cyanonaphthylsalophen	Dicyanonaphthylsalophen
Nd	Gd	Nd	Nd	Tb
Gd	Er	Tb	Gd	Er
Er	Yb	Er	Tb	Yb
Yb		Yb	Dy	
Lu			Tm	
			Lu	
Chloronaphthylsalophen	Dichloronaphthylsalophen	Fluoronaphthylsalophen	Difluoronaphthylsalophen	
Nd	Er	Nd	Nd	
Gd	Yb	Gd	Gd	
Er		Er	Er	
Yb		Yb	Yb	

Table 5.3. Synthesized Metal Complexes with Substituted Naphthylsalophen Ligands

There remains room for examining the ability of these ligands to coordinate uranyl ions. By altering the electronic properties of the ligand through substitution to the outer portion of the ligand, there is the potential to alter binding affinity and coordination environment of the metal ion in these complexes. The ability to alter the strength of the ligands donor atoms coordinated to the equatorial sites of uranyl plays a huge role in terms of being able to potentially reduce uranium metal center.[7] This can be significant in altering reactivity of the metal itself for reduction or

altering the ability to functionalize the -yl bonds. These aspects warrant further investigation into the effects of the substituted naphthylsalophens coordination of uranyl ions.

Further modification to this ligand has led us to synthesize a water-soluble version of these naphthylsalophens. Due to the current poor solubility of the cyano-naphthylsalophen, reactions must be run in harsh organic solvents such as THF and 1,4-dioxane. Taking into consideration the potential uses of these up converting complexes, we need be able to have higher solubility in aqueous media. The plan moving forward to overcome this obstacle is to make a water-soluble version of the naphthylsalophen ligand. Furthermore, the ability to have a water soluble adduct for aqueous uranium chemistry can be of use in various environmental, geological, and nuclear technologies.[8]

The first strategy for synthesizing this water soluble naphthylsalophen adduct is to sulfinate the 2-hydroxy-1-naphthaldehyde arms of the ligand. This method has been shown to increase a water solubility for metal coordination with similar systems.[9,10] Until we have isolated a pure product and to show proof of concept on an analogues ligand framework, reaction have been carried out with o-phenylenediamine due to the lower cost compared to the 3,4-diaminobenzonitrile. Once proof of concept is established, reactions will commence to synthesize the sulfonated cyanonaphthylsalophen. We have successfully synthesized the sulfonated hydroxy naphthaldehyde and are currently working on synthesizing the sulfonated naphthylsalophen ligand (Figure 5.37)

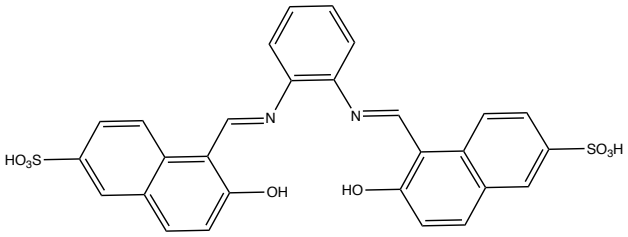

Figure 5.38. Sulfonated naphthylsalophen

Naphthylpyrasal project

The naphthylpyrasal ligand, previously seen in chapter 4, has the potential to help stabilize lower valent uranium species through its heterocyclic backbone.[11] First, there will need to be an adequate solvent found for better electrochemical analysis of these compounds. The ability to maintain solubility while also having the interaction of a coordination solvent could be beneficial not only in the investigation of its redox activity but also in the ability to help stabilize the lower valent uranium species. With that step accomplished, the remainder of this research will need to be conducted under inert atmosphere to help with preventing oxidation of the uranium metal center while allowed easier access to the lower valent uranium species. This can be accomplished by either running a reaction with U (III) complexes and taking advantage of reagents capable of 2 electron oxidation such as NO or N_2O.[12] There is also the avenue to reduce the uranium metal center through either reductive functionalization of the UO_2^{2+} or light mediated reduction.[13] The isolation and characterization of these compounds will help shed further light on routes of isolation of U (V) species, but also the fundamental interactions of *f*-block chemistry.

Synthesis

Caution! The uranium metal salt – $UO_2(OAc)_2 \cdot 2H_2O$ – used in this study contained depleted uranium. Standard precautions for handling radioactive materials or heavy metals such as uranyl nitrate and lead sulfate must be followed

Synthesis of Chloronaphthylsalophen. In a 100 mL round bottom containing a stir bar, 4-chloro-o-phenelyene diamine (0.0015 mol, 0.2139g) was dissolved in EtOH. Next, 230 μL (0.0030 mol) of TFA was added to the solution followed by 2-hydroxy-1-naphthaldehyde (0.0030 mol, 0.5165g). The reaction was heated to reflux temperature for 6 hr. Orange solid formed in the reaction to suggest the reaction was gone to completion. After the reaction was finished, the resulting orange solid was filtered and washed with more EtOH. Yield: 90%, TOF MS (ESI+) m/z (M + H) Calc.: 451.1213, Found:451.1211; 1H NMR (600 MHz, THF-d8) δ 7.09 (dd, 2H, J = 9.1, 6.4), 7.32 (m, 2H), 7.39 (dd, 1H, J = 8.5, 6.6), 7.49 (q, 2H, J = 7.74), 7.60 (d, 1H, J = 8.5), 7.71 (s, 1H), 7.76 (d, 2H, J =7.9), 7.87(dd, 2H, J = 9.1, 5.0), 8.36 (d, 1H, J = 8.4), 8.42 (d, 1H, J = 8.5), 9.70 (d, 2H, J = 9.78), 14.91 (s, 1H), 14.94 (s, 1H); 13C NMR (600 MHz, THF-d8) δ 120.29, 120.36, 120.56, 121.14, 121.21, 121.53, 123.91, 123.98, 127.34, 128.30, 128.35, 128.58, 132.77, 133.93, 134.00, 136.38, 136.64, 140.94, 143.10, 159.73, 160.11, 166.72, 167.11.

Synthesis of Dichloronaphthylsalophen. In a 100 mL round bottom containing a stir bar, 4,5-dichloro-o-phenelyene diamine (0.0015 mol, 0.2655g) was dissolved in EtOH. Next, 230 μL (0.0030 mol) of TFA was added to the solution followed by 2-hydroxy-1-naphthaldehyde (0.0030 mol, 0.5165g). The solution was heated to reflux temperature for 6 hr. An orange solid formed in the reaction suggesting that the reaction was completed. After the reaction was finished, the

resulting orange solid was filtered and washed with more EtOH. Yield: 86%, TOF MS (ESI+) m/z (M + H) Calc.: 485.0824, Found: 485.0842; 1H NMR (500 MHz, DMF-d7) δ 7.11 (d, 2H, J = 9.1), 7.40 – 7.45 (m, 2H), 7.59 (t, 2H, J = 8.0), 7.88 (d, 2H, J = 9.5), 8.03 – 8.07 (m, 2H), 8.24 (s, 2H), 8.67 (d, 2H, J = 8.5), 9.91 (s, 2H), 15.02 (s, 2H); 13C NMR (500 MHz, DMF-d7) δ 109.96, 115.87, 119.86, 120.84, 121.01, 121.60, 123.76, 123.93, 127.70, 128.10, 128.33, 129.19, 129.64, 133.44, 135.65, 137.07, 140.16.

Synthesis of Dicyanonaphthylsalophen. In a 100 mL round bottom containing stir bar, 4,5-diaminophthalanitrile (0.0017 mol, 0.100g) was dissolved in EtOH. Next, 265 μL (0.0034 mol) of TFA was added to the backbone followed by 2-hydroxy-1-naphthaldehyde (0.0034 mol, 0.5921g). The solution was heated to the reflux temperature for 6 hr. An orange solid formed in the reaction ~~to~~ suggesting that the reaction was completed. After the reaction was finished, the resulting orange solid was filtered and washed with more EtOH. Yield: 37%, TOF MS (ESI+) m/z (M + H) Calc.: 467.1508, Found: 467.1513; 1H NMR (XXX MHz, DMF-d7) δ 7.06 (s, 2H), 7.41 (s, 2H), 7.61 (t, 2H, J = 8.2), 7.82 - 7.93 (m, 2H), 8.51 (t, 2H, J = 8.2), 8.64 (s, 2H), 8.70 (s, 2H), 9.80 - 9.93 (m, 2H), 14.66 (s, 2H).

Synthesis of Methoxynaphthylsalophen. In a 100 mL round bottom containing a stir bar, 4-methoxy-o-phenelyene diamine (0.0015 mol, 0.2073g) was dissolved in EtOH. Next, 230 μL (0.0030 mol) of TFA was added to the backbone followed by 2-hydroxy-1-naphthaldehyde (0.0030 mol, 0.5165g). The solution was heated to the reflux temperature for 6 hr. An orange solid formed in the reaction suggesting that the reaction was completed. After the reaction was finished, the resulting orange solid was filtered and washed with more EtOH. Yield: 53%, TOF MS (ESI+)

m/z (M + Na) Calc.: 469.1528, Found: 469.1512; 1H NMR (600 MHz, THF d-8) δ 3.87 (s, 3H), 7.04 (d, 1H, J = 7.1), 7.15 (d, 2H, J = 9.0), 7.22 (s, 1H), 7.36 (m, 2H), 7.54 (t, 2H, J = 7.5), 7.63 (d, 1H, J = 8.6), 7.81 (d, 2H, J = 7.7), 7.91 (dd, 2H, J = 13.6), 15.15 (s, 1H), 15.22 (s, 1H); 13C NMR (600 MHz, THF d-8) δ 27.86, 32.29, 53.13, 103.08, 107.68, 107.83, 110.68, 117.82, 117.87, 118.36, 118.54, 119.03, 121.13, 121.30, 123.08, 125.55, 125.73, 125.81, 127.04, 127.07, 131.39, 131.56, 132.93, 133.82, 140.55, 155.43, 157.69, 163, 32, 165.05.

Synthesis of 4-methylnaphthylsalophen. In a 100 mL round bottom containing a stir bar, 4-methyl-o-phenelyene diamine (0.0015 mol, 0.2043g) was dissolved in EtOH. Next, 230 μL (0.0030 mol) of TFA was added to the backbone followed by 2-hydroxy-1-naphthaldehyde (0.0030 mol, 0.5165g). The solution was heated to reflux temperature for 6 hr. An orange solid formed in the reaction suggesting that the reaction was completed. After the reaction was finished, the resulting orange solid was filtered and washed with more EtOH. Yield: 93%, TOF MS (ESI+) m/z (M + Na) Calc.: 453.1579, Found: 453.1566; 1H NMR (600 MHz, $CDCl_3$) δ 2.43 (s, 3H), 7.14 (m, 4H), 7.28 (m, 3H), 7.46 (s, 2H), 7.68 (s, 2H), 7.75 (d, 2H, J = 7.6), 8.09 (s, 2H), 9.36 (d, 2H, J = 12.7), 15.11 (s, 2H); 13C NMR (600 MHz, $CDCl_3$) δ 20.20, 108.24, 117.65, 117.98, 118.39, 120.99, 121.28, 122.40, 122.46, 126.32, 126.35, 126.88, 126.95, 128.26, 132.09, 132.17, 135.27, 135.59, 135.87, 137.95, 145.32, 154.40, 167.77, 168.70.

Synthesis of 3-methylnaphthylsalophen. In a 100 mL round bottom charged with a stir bar, **2,**3-diaminotiluene (0.0014 mol, 0.1662g) was dissolved in EtOH. Next, 215 μL (0.0028 mol) of TFA was added to the backbone followed by 2-hydroxy-1-naphthaldehyde (0.0030 mol, 0.5165g). The

solution was heated to reflux temperature for 6 hr. An orange solid formed in the reaction suggesting that the reaction was completed. After the reaction was finished, the resulting orange solid was filtered and washed with more EtOH. Yield: 37%, TOF MS (ESI+) m/z (M + H) Calc.: 431.1760, Found:431.1750; 1H NMR (500 MHz, $CDCl_3$) δ 2.43 (s, 3H), 6.97 (d, 1H, J = 9.1), 7.17 (d, 1H, J = 9.2), 7.24-7.26 (m, 6H), 7.35 (t, 1H, J = 7.8), 7.53 (t, 1H, J = 8.3), 7.69-7.76 (m, 3H), 7.81-7.82 (m, 2H), 8.19 (d, 1H, J = 8.5), 9.36 (s, 1H), 9.55 (s, 1H), 14.86 (s, 1H), 15.18 (s,1H); 13c NMR (500 MHz, $CDCl_3$) δ 18.84, 108.93, 109.37, 117.34, 119.16, 119.26, 120.82, 121.14, 123.37, 123.59, 126.33, 127.49, 127.62, 127.87, 128.00, 129.02, 129.11, 129.35, 131.99, 132.89, 133.19, 135.82, 136.13, 139.45, 139.94, 157.74, 163.20, 166.08, 167.25.

Synthesis of Dimethylnaphthylsalophen. In a 100 mL round bottom containing a stir bar, 4-methoxy-o-phenelyene diamine (0.0015 mol, 0.2043g) was dissolved in EtOH. Next, 230 μL (0.0030 mol) of TFA was added to the backbone followed by 2-hydroxy-1-naphthaldehyde (0.0030 mol, 0.5165g). The solution was heated to reflux temperature for 6 hr. An orange solid formed in the reaction suggesting that the reaction was completed. After the reaction was finished, the resulting orange solid was filtered and washed with more EtOH. Yield: 93%, TOF MS (ESI+) m/z (M + Na) Calc.: 467.1735, Found: 467.1718; 1H NMR (600 MHz, $CDCl_3$) δ 2.33 (s, 6H), 7.12 (d, 4H, J = 11.0), 7.30 (m, 2H), 7.46 (m, 2H), 7.68 (d, 2H, J = 7.4), 7.75 (d, 2H, J = 9.0), 8.10 (d, 2H, J = 8.1), 9.34 (s, 2H), 15.18 (s, 2H); 13C NMR (600 MHz, $CDCl_3$) δ 18.63, 75.99, 108.18, 117.98, 118.79, 121.21, 122.35, 126.29, 126.84, 128.23, 132.15, 135.10, 135.25, 135.62, 153.95, 168.29.

Synthesis of Fluoronaphthylsalophen. In a 100 mL round bottom containing a stir bar, 4-fluoro-o-phenelyene diamine (0.0017 mol, 0.2169g) was dissolved in EtOH. Next, 265 μL (0.0030 mol) of TFA was added to the backbone followed by 2-hydroxy-1-naphthaldehyde (0.0034 mol, 0.5923g). The solution was heated to reflux temperature for 6 hr. An orange solid formed in the reaction suggesting that the reaction was completed. After the reaction was finished, the resulting orange solid was filtered and washed with more EtOH. Yield: 82%, TOF MS (ESI+) m/z (M + H) Calc.: 435.1509, Found: 435.1520; 1H NMR (600 MHz, DMF-d7) δ 7.10 (d, 1H, J = 9.1), 7.17 (d, 1H, J = 9.1), 7.35 (t, 1H, J = 7.5, 7.0), 7.44 (dd, 2H, J = 7.2, 5.6), 7.62 (t, 2H, J = 7.5), 7.89-8.04 (m, 8H), 8.68 (t, 2H, J = 9.0), 15.29 (s, 2H); 13C NMR (600 MHz, DMF-d7) δ 106.60, 106.77, 109.71, 109.82, 113.66, 113.81, 120.70, 120.83, 121.55, 121.76, 123.75, 123.87, 127.51, 127.64, 128.23, 126.36, 129.20, 133.40, 133.56, 136.45, 136.82, 137.29, 140.79, 158.29, 159.35, 161.06, 162.68, 166.85, 169.35.

Synthesis of Difluoronaphthylsalophen. In a 100 mL round bottom containing a stir bar, 4,5-difluoro-o-phenelyene diamine (0.0017 mol, 0.2479g) was dissolved in EtOH. Next, 265 μL (0.0034 mol) of TFA was added to the backbone followed by 2-hydroxy-1-naphthaldehyde (0.0034 mol, 0.5923g). The solution was heated to reflux temperature for 6 hr. An orange solid formed in the reaction suggesting that the reaction was completed. After the reaction was finished, the resulting orange solid was filtered and washed with more EtOH. Yield: 91%, TOF MS (ESI+) m/z (M + Na) Calc.: 475.1234, Found: 475.1203; 1H NMR (600 MHz, DMF-d7) δ 7.16 (d, 2H, J = 9.0), 7.44 (t, 2H, J = 7.3), 7.63 (t, 2H, J = 7.6), 7.92 (d, 2H, J = 7.8), 8.07 (t, 2H, J = 12.5, 9.0), 8.21 (t, 2H, J = 9.7), 8.71 (d, 2H, J =8.3), 15.12 (s, 2H); 13C NMR (600 MHz, DMF-d7) δ 108.88,

109.84, 120.82, 123.85, 127.64, 128.31, 129.20, 133.43, 136.86, 137.18, 148.05, 149.50, 159.69, 167.41.

Synthesis of Sulfonated naphthaldehyde. Following a modified procedure taking from the literature in a paper by Jiang et.al.,[14] in a 50 mL round-bottom flask charged with a magnetic stir bar was added 2-hydroxy-1-naphthaldehyde (2.5179 g; 14.623 mmol) before adding concentrated sulfuric acid (12.5 mL) dropwise over ice. The solution was allowed to warm to room temperature before heating to 40 °C and allowing to stir for 20hrs. The reaction mixture was then added to 40 mL ice water and a pale beige precipitate formed. The mixture was then reheated to 70 °C before filtering through glass wool to yield a red-orange solution to which was then added NaCl (8.0541 g) and cooling in an ice bath to precipitate a pink product. This product was then isolated by vacuum filtration and allowed to dry to yield a pink powder. The crude powder was then recrystallized out of minimal amounts of H_2O to afford 1.2587 g of hermosa pink product Yield: 31%, 1H NMR (500 MHz, D_2O) δ ^{1}H-NMR (D_2O, 500MHz): δ(ppm)= 6.93(d, 1H), 7.80(dd, 1H), 7.85(d, 1H), 8.05(s, 1H), 8.20(d, 1H), 10.32(s, 1H).

Gerneral **Procedure for Synthesis of a Naphthylsalophen Metal complex.** The substituted naphthylsalophen ligand (0.174 mmol) was dissolved in 100 mL of THF in a 250ml round bottom flask. The Ln^{III} acetate or chloride (Ln^{III} = Nd^{III}, Gd^{III}, Tb^{III}, Dy^{III}, Tm^{III}, Er^{III}, or Yb^{III}) (0.087 mmol) was dissolved in MeOH and added to the solution, followed by the addition of triethylamine (TEA) (200 μL, 1.43 mmol). The solution was refluxed for 6 hours. During this time, the color changed from light orange to either light yellow or dark orange. The excess solvent was removed

under reduced pressure yielding the solid sample. The solid was recrystallized from a mixture of THF and hexanes, then filtered and washed with ethanol.

- Methoxy-Naphthylsalophen
    - Nd: TOF MS (ESI+) m/z (M+H) Calc.: 1621.9540, Found: 1621.2760
        - Yield: 90%
    - Gd: TOF MS (ESI+) m/z (M+H) Calc.: 1649.2982, Found: 1649.2865
        - Yield: 58%
    - Er: TOF MS (ESI+) m/z (M+H) Calc.: 1668.3190, Found: 1668.3185
        - Yield: 46%
    - Yb: TOF MS (ESI+) m/z (M+H) Calc.: 1680.3199, Found: 1680.3301
        - Yield: 50%
    - Lu: TOF MS (ESI+) m/z (M+H) Calc.: 1683.3315, Found: 1683.3173
        - Yield: 68%
- Methyl-Naphthylsalophen
    - Gd: TOF MS (ESI+) m/z (M+H) Calc.: 1600.9810, Found: 1600.2943
        - Yield: 32%
    - Er: TOF MS (ESI+) m/z (M+H) Calc.: 1619.9910, Found: 1619.3230
        - Yield: 53%
    - Yb: TOF MS (ESI+) m/z (M+H) Calc.: 1632.5810, Found: 1632.3317
        - Yield: 25%
- Dimethyl-Naphthylsalophen
    - Nd: TOF MS (ESI+) m/z (M+H) Calc.: 1616.0380, Found: 1616.3013

        - Yield: 75%
    - Tb: TOF MS (ESI+) m/z (M+H) Calc.: 1645.3629, Found: 1645.3606
        - Yield: 55%
    - Er: TOF MS (ESI+) m/z (M+3H) Calc.: 1661.3884, Found: 1661.3706
        - Yield: 55%
    - Yb: TOF MS (ESI+) m/z (M+H) Calc.: 1674.3821, Found: 1674.3921
        - Yield: 40%
- Cyano-Naphthylsalophen
    - Nd: TOF MS (ESI+) m/z (M+H) Calc.: 1606.2195, Found: 1606.2124
        - Yield: 26%
    - Gd: TOF MS (ESI+) m/z (M+H) Calc.: 1634.2570, Found: 1634.2382
        - Yield: 65%
    - Tb: TOF MS (ESI+) m/z (M+H) Calc.: 1636.2547, Found: 1636.2499
        - Yield: 85%
    - Dy: TOF MS (ESI+) m/z (M+H) Calc.: 1644.2656, Found: 1644.2645
        - Yield: 62%
    - Tm: TOF MS (ESI+) m/z (M+H) Calc.: 1656.2725, Found: 1656.2760
        - Yield: 84%
    - Lu: TOF MS (ESI+) m/z (M+H) Calc.: 1669.2856, Found: 1669. 2668
        - Yield: 69%
- Dicyano-Naphthylsalophen
    - Tb: TOF MS (ESI+) m/z (M+Na) Calc.: 1733.2224, Found: 1733.2098
        - Yield: 25%

    - Er: TOF MS (ESI+) m/z (M+H) Calc.: 1728.2561, Found: 1728.2430
        - Yield: 60%
    - Yb: TOF MS (ESI+) m/z (M+H) Calc.: 1741.2575, Found: 1741.2430
        - Yield: 60%
- Chloro-Naphthylsalophen
    - Nd: TOF MS (ESI+) m/z (M+H) Calc.: 1635.2020, Found: 1635.1029
        - Yield: 81%
    - Gd: TOF MS (ESI+) m/z (M+H) Calc.: 1661.1496, Found: 1661.1411
        - Yield: 49%
    - Er: TOF MS (ESI+) m/z (M+Na) Calc.: 1703.1442, Found: 1703.1337
        - Yield: 75%
    - Yb: TOF MS (ESI+) m/z (M+H) Calc.: 1693.1747, Found: 1693.1654
        - Yield: 81%
- Dichloro-Naphthylsalophen
    - Er: TOF MS (ESI+) m/z (M+H) Calc.: 1807.5518, Found: 1807.0084
        - Yield: 70%
    - Yb: TOF MS (ESI+) m/z (M+2H) Calc.: 1661.1496, Found: 1661.1411
        - Yield: 78%
- Fluoro-Naphthylsalophen
    - Nd: TOF MS (ESI+) m/z (M+H) Calc.: 1585.8472, Found: 1585.1827
        - Yield: 79%
    - Gd: TOF MS (ESI+) m/z (M+2Na) Calc.: 1660.2129, Found: 1660.2197
        - Yield: 79%

- Er: TOF MS (ESI+) m/z (M+Na) Calc.: 1653.2332, Found: 1653.2142
  - Yield: 78%
- Yb: TOF MS (ESI+) m/z (M+H) Calc.: 1643.4712, Found: 1643.2521
  - Yield: 92%

- Difluoro-Naphthylsalophen
  - Nd: TOF MS (ESI+) m/z (M+H) Calc.: 1639.1851, Found: 1639.1802
    - Yield: 83%
  - Gd: TOF MS (ESI+) m/z (M+H) Calc.: 1667.2146, Found: 1667.2098
    - Yield: 75%
  - Er: TOF MS (ESI+) m/z (M+H) Calc.: 1686.2229, Found: 1686.2202
    - Yield: 72%
  - Yb: TOF MS (ESI+) m/z (M+H) Calc.: 1698.2422, Found: 1698.2428
    - Yield: 83%

References

(1) Panwar, V.; Bansal, A.; Ray, S. S.; Jain, S. L. Renewable Waste Rice Husk Grafted Oxo-Vanadium Catalyst for Oxidation of Tertiary Amines to N-Oxides. *RSC Adv.* **2016**, *6* (75), 71550–71556. https://doi.org/10.1039/C6RA13571D.

(2) Thangavelu, S. G.; Cahill, C. L. Uranyl-Promoted Peroxide Generation: Synthesis and Characterization of Three Uranyl Peroxo [(UO2)2(O2)] Complexes. *Inorg. Chem.* **2015**, *54* (9), 4208–4221. https://doi.org/10.1021/ic502767k.

(3) Jayasinghe, A. S.; Applegate, L. C.; Unruh, D. K.; Hutton, J.; Forbes, T. Z. Utilizing Autoxidation of Solvents To Promote the Formation of Uranyl Peroxide Materials. *Cryst. Growth Des.* **2019**, *19* (3), 1756–1766. https://doi.org/10.1021/acs.cgd.8b01735.

(4) *Luminescence of Lanthanide Ions in Coordination Compounds and Nanomaterials*, 1st ed.; de Bettencourt-Dias, A., Ed.; John Wiley & Sons Ltd.: United Kingdom, 2014.

(5) Melle, S.; Calderón, O. G.; Laurenti, M.; Mendez-Gonzalez, D.; Egatz-Gómez, A.; López-Cabarcos, E.; Cabrera-Granado, E.; Díaz, E.; Rubio-Retama, J. Förster Resonance Energy Transfer Distance Dependence from Upconverting Nanoparticles to Quantum Dots. *J. Phys. Chem. C* **2018**, *122* (32), 18751–18758. https://doi.org/10.1021/acs.jpcc.8b04908.

(6) Lin, S.-L.; Chen, H.-C.; Chang, C. A. Enhancing Förster Resonance Energy Transfer (FRET) Efficiency of Titania–Lanthanide Hybrid Upconversion Nanomaterials by Shortening the Donor–Acceptor Distance. *Nanomaterials* **2020**, *10* (10). https://doi.org/10.3390/nano10102035.

(7) Bell, N. L.; Shaw, B.; Arnold, P. L.; Love, J. B. Uranyl to Uranium(IV) Conversion through Manipulation of Axial and Equatorial Ligands. *J. Am. Chem. Soc.* **2018**, *140* (9), 3378–3384. https://doi.org/10.1021/jacs.7b13474.

(8) Faizova, R.; Scopelliti, R.; Chauvin, A.-S.; Mazzanti, M. Synthesis and Characterization of a Water Stable Uranyl(V) Complex. *J. Am. Chem. Soc.* **2018**, *140* (42), 13554–13557. https://doi.org/10.1021/jacs.8b07885.

(9) Bhattacharjee, S.; Anderson, J. A. Synthesis and Characterization of Novel Chiral Sulfonato–Salen–Manganese(Iii) Complex in a Zinc–Aluminium LDH Host. *Chem. Commun.* **2004**, No. 5, 554–555. https://doi.org/10.1039/B315325H.

(10) Reimann, M. J.; Salmon, D. R.; Horton, J. T.; Gier, E. C.; Jefferies, L. R. Water-Soluble Sulfonate Schiff-Base Ligands as Fluorescent Detectors for Metal Ions in Drinking Water and Biological Systems. *ACS Omega* **2019**, *4* (2), 2874–2882. https://doi.org/10.1021/acsomega.8b02750.

(11) Kiernicki, J. J.; Cladis, D. P.; Fanwick, P. E.; Zeller, M.; Bart, S. C. Synthesis, Characterization, and Stoichiometric U–O Bond Scission in Uranyl Species Supported by Pyridine(Diimine) Ligand Radicals. *J. Am. Chem. Soc.* **2015**, *137* (34), 11115–11125. https://doi.org/10.1021/jacs.5b06217.

(12) Hoerger, C. J.; La Pierre, H. S.; Maron, L.; Scheurer, A.; Heinemann, F. W.; Meyer, K. Reductive Disproportionation of Nitric Oxide Mediated by Low-Valent Uranium. *Chem. Commun.* **2016**, *52* (72), 10854–10857. https://doi.org/10.1039/C6CC06095A.

(13) Fortier, S.; Hayton, T. W. Oxo Ligand Functionalization in the Uranyl Ion (UO22+). *Inorg. React. Mech.* **2010**, *254* (3), 197–214. https://doi.org/10.1016/j.ccr.2009.06.003.

(14) Jiang, L.; Wang, L.; Guo, M.; Yin, G.; Wang, R.-Y. Fluorescence Turn-on of Easily Prepared Fluorescein Derivatives by Zinc Cation in Water and Living Cells. *Sens. Actuators B Chem.* **2011**, *156* (2), 825–831. https://doi.org/10.1016/j.snb.2011.02.048.

Appendix 1

B3LYP/cc-pVDZ(-PP) Cartesian coordinates (in Å) of the optimal geometries for the ground and pertinent excited electronic state of the investigated uranyl and copper complexes.

L_1Cu^{2+}(AcO)							
Ground State				**Excited State**			
C	5.942091	-2.399390	0.000228	C	5.993400	-2.400341	0.004794
C	5.552291	-1.075670	0.000218	C	5.571285	-1.113640	-0.305673
C	4.981401	-3.434910	0.000108	C	5.048269	-3.359241	0.371211
C	4.176431	-0.696130	0.000078	C	4.182433	-0.740403	-0.257984
C	3.199051	-1.751660	0.000018	C	3.207124	-1.763420	0.065838
C	3.641861	-3.102570	0.000008	C	3.666026	-3.022558	0.400444
H	7.006511	-2.647610	0.000338	H	7.054083	-2.654147	-0.028358
H	6.281631	-0.264240	0.000288	H	6.273034	-0.325655	-0.582315
H	2.912391	-3.916330	-0.000112	H	2.959957	-3.797059	0.706179
H	5.290600	-4.480900	0.000078	H	5.354621	-4.372482	0.633624
C	1.786801	-1.456360	0.000048	C	1.754273	-1.467339	0.043146
N	1.210981	-0.242540	0.000058	N	1.195145	-0.260658	0.104400
N	0.817981	-2.433790	0.000108	N	0.805169	-2.436356	-0.015819
C	-0.177549	-0.430700	0.000058	C	-0.204811	-0.446049	0.082724
C	-0.435629	-1.845650	0.000068	C	-0.460167	-1.833504	0.000964
C	-1.212049	0.476940	0.000038	C	-1.250102	0.475355	0.107105
C	-1.698709	-2.382040	0.000048	C	-1.739831	-2.365196	-0.059829
C	-2.794659	-1.468950	-0.000002	C	-2.828495	-1.455347	-0.035591
C	-2.545609	-0.031620	0.000008	C	-2.576830	-0.019181	0.047368
N	-3.564129	0.848260	-0.000022	N	-3.596715	0.876876	0.072147
N	-4.044619	-1.964670	-0.000022	N	-4.086180	-1.955392	-0.092660
C	-4.807909	0.347780	-0.000052	C	-4.846648	0.371343	0.016958
C	-5.052499	-1.079140	-0.000042	C	-5.094640	-1.055574	-0.067222
C	-5.925569	1.242910	-0.000082	C	-5.961642	1.258538	0.040795
C	-6.403969	-1.550450	-0.000082	C	-6.441373	-1.512788	-0.124032
C	-7.205719	0.751030	-0.000102	C	-7.255538	0.775580	-0.015712
C	-7.447029	-0.659590	-0.000102	C	-7.497232	-0.619766	-0.098870
H	-1.047789	1.553040	0.000068	H	-1.088344	1.549433	0.177057
H	-1.905199	-3.452730	0.000038	H	-1.950590	-3.433203	-0.125937
H	-5.711569	2.313180	-0.000082	H	-5.746205	2.327091	0.105229
H	-8.055719	1.437020	-0.000122	H	-8.099177	1.469794	0.003622
H	-8.476889	-1.023760	-0.000122	H	-8.524981	-0.988353	-0.142936
H	-6.560179	-2.630710	-0.000082	H	-6.599552	-2.591421	-0.187342
O	3.902781	0.576380	-0.000012	O	3.879294	0.484778	-0.486618
H	0.999741	-3.426850	-0.000102	H	0.982011	-3.421232	-0.155750

Cu	2.224141	1.435370	-0.000232	Cu	2.198700	1.412708	-0.069877
C	1.322201	5.205280	0.000818	C	1.525467	5.203537	0.224477
C	1.691961	3.750090	-0.000212	C	1.793888	3.734978	0.106009
H	2.219371	5.835850	-0.008362	H	2.346810	5.786474	-0.209025
H	0.714551	5.424670	0.892288	H	1.403926	5.460667	1.288314
H	0.697001	5.422160	-0.878942	H	0.575940	5.442106	-0.277165
O	2.900071	3.365030	-0.002272	O	2.895494	3.282595	-0.349185
O	0.781011	2.849270	0.001568	O	0.920847	2.874908	0.468705
$L_1Cu^{2+}(AcO)(W)$							
Ground State				**Excited State**			
C	-5.394811	-3.203752	-0.068122	C	-5.466654	-3.166207	-0.012159
C	-5.152433	-1.849497	-0.170893	C	-5.180929	-1.841719	-0.323732
C	-4.331481	-4.119269	0.102071	C	-4.430093	-4.022399	0.359549
C	-3.829005	-1.314540	-0.106381	C	-3.839660	-1.324653	-0.271992
C	-2.747669	-2.251165	0.038908	C	-2.768481	-2.242566	0.054244
C	-3.038950	-3.638365	0.150172	C	-3.091125	-3.543086	0.390801
H	-6.423166	-3.571453	-0.113597	H	-6.495340	-3.528767	-0.048860
H	-5.963501	-1.130662	-0.296657	H	-5.961486	-1.133440	-0.604926
H	-2.227040	-4.354224	0.302640	H	-2.307348	-4.238338	0.698672
H	-4.527656	-5.187874	0.198709	H	-4.630996	-5.061410	0.622987
C	-1.380335	-1.798092	0.045078	C	-1.355957	-1.792672	0.026802
N	-0.941144	-0.527953	0.084022	N	-0.927679	-0.534839	0.089868
N	-0.313492	-2.666577	0.002447	N	-0.313669	-2.659563	-0.044846
C	0.460862	-0.568792	0.052780	C	0.487227	-0.576905	0.056475
C	0.868944	-1.947926	-0.004689	C	0.883213	-1.930541	-0.031925
C	1.399890	0.438404	0.055662	C	1.437524	0.442557	0.071996
C	2.180290	-2.348305	-0.057989	C	2.209214	-2.331119	-0.099624
C	3.176336	-1.327382	-0.054589	C	3.202331	-1.318260	-0.074736
C	2.778900	0.074045	0.003779	C	2.808152	0.084110	0.010040
N	3.698678	1.056386	0.011153	N	3.731479	1.078357	0.035576
N	4.470378	-1.688558	-0.105281	N	4.503965	-1.689254	-0.133759
C	4.987699	0.690432	-0.040062	C	5.025962	0.701944	-0.023354
C	5.379874	-0.702016	-0.099370	C	5.416160	-0.692894	-0.109601
C	6.004914	1.697998	-0.035909	C	6.045543	1.697384	-0.000660
C	6.772462	-1.027868	-0.152051	C	6.802493	-1.012287	-0.168673
C	7.328916	1.344029	-0.087524	C	7.380878	1.346961	-0.059889
C	7.716185	-0.032345	-0.146142	C	7.762037	-0.017380	-0.144424
H	1.127657	1.490701	0.106090	H	1.175096	1.497054	0.132929
H	2.495106	-3.391294	-0.104420	H	2.524384	-3.372734	-0.171741
H	5.680541	2.739160	0.008830	H	5.723821	2.738794	0.064158
H	8.102126	2.115509	-0.084546	H	8.150438	2.122423	-0.042152
H	8.777988	-0.285584	-0.186678	H	8.821704	-0.279925	-0.190637
H	7.040742	-2.084933	-0.196360	H	7.068568	-2.069345	-0.233289
O	-3.691732	-0.026406	-0.192668	O	-3.658344	-0.076460	-0.500333

H	-0.393278	-3.666990	-0.110063	H	-0.391855	-3.655455	-0.196468
Cu	-2.142818	1.057305	0.075016	Cu	-2.105586	1.061632	-0.003671
O	-0.844718	2.304377	0.949531	O	-0.948918	2.256791	1.066788
H	-1.394228	3.237666	0.918241	H	-1.538126	3.134415	1.162847
H	-0.635106	2.096140	1.872422	H	-0.564883	1.970221	1.907516
C	-4.159367	4.754154	-0.730664	C	-4.171763	4.717098	-0.718750
C	-3.123312	3.813244	-0.153972	C	-3.191971	3.761891	-0.074879
H	-4.121690	4.712376	-1.829933	H	-3.894247	4.865359	-1.773998
H	-3.986703	5.780006	-0.382632	H	-4.171488	5.678926	-0.191790
H	-5.163318	4.416439	-0.429588	H	-5.179619	4.274777	-0.708525
O	-2.268557	4.266757	0.654102	O	-2.510830	4.140239	0.907456
O	-3.199386	2.594288	-0.540323	O	-3.133148	2.588389	-0.609060
$L_1UO_2^{2+}$(AcO)							
Ground State				**Excited State**			
C	4.544877	3.984935	-0.003402	C	-4.831834	3.890710	-0.088207
C	4.366077	2.699401	-0.493735	C	-4.611812	2.618782	0.421394
C	3.468760	4.696165	0.555993	C	-3.761341	4.603957	-0.631784
C	3.103003	2.067001	-0.441600	C	-3.302421	2.019187	0.395413
C	1.998909	2.795265	0.104019	C	-2.186489	2.798335	-0.110354
C	2.216805	4.101872	0.600268	C	-2.449890	4.041243	-0.641540
H	5.535449	4.443923	-0.047028	H	-5.832477	4.324780	-0.072254
H	5.193435	2.136326	-0.928188	H	-5.417439	2.016810	0.843437
H	1.391345	4.645178	1.067326	H	-1.640896	4.623184	-1.086934
H	3.616048	5.698416	0.960646	H	-3.913320	5.601115	-1.046555
C	0.654894	2.234403	0.112100	C	-0.794453	2.269093	-0.069695
N	0.304414	0.945980	0.036950	N	-0.421989	1.000398	-0.199861
N	-0.460293	3.036758	0.187336	N	0.280911	3.087248	0.070925
C	-1.092362	0.900455	0.037931	C	0.987510	0.985695	-0.145773
C	-1.596846	2.243890	0.134557	C	1.446456	2.307694	0.033336
C	-1.950062	-0.174137	-0.031706	C	1.881700	-0.081877	-0.228860
C	-2.935474	2.545036	0.155090	C	2.792375	2.631170	0.140293
C	-3.850120	1.452419	0.080535	C	3.729897	1.568317	0.063002
C	-3.352236	0.084642	-0.011520	C	3.267309	0.193835	-0.121451
N	-4.197706	-0.960099	-0.081025	N	4.138146	-0.842272	-0.202555
N	-5.168721	1.716894	0.098561	N	5.047219	1.865093	0.162059
C	-5.509720	-0.689297	-0.062421	C	5.450508	-0.537922	-0.102107
C	-6.003276	0.669802	0.028895	C	5.908992	0.825319	0.082920
C	-6.451081	-1.766142	-0.134288	C	6.417751	-1.580093	-0.178798
C	-7.417091	0.894030	0.044646	C	7.307334	1.068074	0.181654
C	-7.797516	-1.508316	-0.116324	C	7.769069	-1.304282	-0.078417
C	-8.285028	-0.165278	-0.025960	C	8.216991	0.028675	0.103006
H	-1.614538	-1.209510	-0.109692	H	1.578146	-1.120331	-0.381965
H	-3.331899	3.558505	0.222961	H	3.164429	3.646850	0.278591
H	-6.051482	-2.779395	-0.202669	H	6.045012	-2.596847	-0.318408

H	-8.512927	-2.331791	-0.171376	H	8.498016	-2.115997	-0.138671
H	-9.363124	0.009804	-0.013800	H	9.287503	0.233324	0.180775
H	-7.762290	1.927082	0.113975	H	7.625293	2.103398	0.320824
O	2.954695	0.847320	-0.927701	O	-3.156408	0.811140	0.790719
H	-0.440883	4.045960	0.131062	H	0.238569	4.076144	0.277041
U	1.956854	-0.966379	-0.129624	U	-1.825032	-1.039369	0.084815
O	2.534189	-0.521772	1.502393	O	-2.484705	-0.777294	-1.549689
O	1.304075	-1.402793	-1.734778	O	-1.216661	-1.222008	1.744978
C	2.333134	-5.146308	0.754614	C	-1.945651	-5.278686	-0.369022
C	2.218654	-3.674516	0.475241	C	-1.927209	-3.785838	-0.236825
H	1.936187	-5.695184	-0.115641	H	-1.377726	-5.706930	0.473464
H	1.729167	-5.415368	1.631488	H	-1.440534	-5.578353	-1.297663
H	3.384470	-5.429013	0.894611	H	-2.974843	-5.657078	-0.336599
O	1.128946	-3.055287	0.731992	O	-0.886614	-3.119239	-0.571768
O	3.194444	-3.035807	-0.044230	O	-2.935056	-3.153810	0.233115

$L_1UO_2^{2+}$(AcO)(W)

Ground State				**Excited State**			
C	4.156296	4.431063	-0.087906	C	4.288344	4.463747	-0.035373
C	4.086260	3.099635	-0.471907	C	4.207573	3.152249	-0.481563
C	3.010374	5.109403	0.363084	C	3.142400	5.089946	0.459952
C	2.866507	2.386829	-0.417123	C	2.966446	2.421222	-0.439149
C	1.692807	3.078732	0.018230	C	1.769028	3.109141	0.010737
C	1.799949	4.434150	0.407874	C	1.895854	4.397385	0.481930
H	5.115084	4.953321	-0.130948	H	5.239845	4.996838	-0.061869
H	4.968392	2.561484	-0.822053	H	5.077580	2.615871	-0.862295
H	0.919765	4.956021	0.792058	H	1.024101	4.914402	0.887276
H	3.071423	6.150119	0.684284	H	3.185803	6.116330	0.826226
C	0.392311	2.423208	0.026294	C	0.435769	2.444684	-0.024471
N	0.135417	1.111425	0.044246	N	0.178178	1.155312	0.159430
N	-0.777700	3.147664	0.008075	N	-0.705297	3.158807	-0.214844
C	-1.255404	0.966496	0.020957	C	-1.226969	1.013784	0.090696
C	-1.854118	2.274215	-0.006757	C	-1.797201	2.281935	-0.153942
C	-2.034893	-0.168833	0.029504	C	-2.029068	-0.120240	0.215188
C	-3.210355	2.481022	-0.040998	C	-3.163589	2.484363	-0.288299
C	-4.045406	1.324272	-0.040644	C	-4.008684	1.351302	-0.165953
C	-3.451594	-0.007461	-0.000665	C	-3.431868	0.034014	0.088019
N	-4.221688	-1.111455	0.009061	N	-4.213117	-1.068774	0.216409
N	-5.379177	1.495353	-0.073087	N	-5.346515	1.529635	-0.289068
C	-5.549260	-0.933693	-0.023887	C	-5.544587	-0.883082	0.093727
C	-6.137469	0.389536	-0.066293	C	-6.116235	0.425434	-0.162914
C	-6.412087	-2.076766	-0.017272	C	-6.420950	-1.999340	0.217995
C	-7.563293	0.513193	-0.100582	C	-7.529763	0.541297	-0.282015
C	-7.773113	-1.914832	-0.051046	C	-7.789731	-1.845977	0.096469

C	-8.354138	-0.607112	-0.093113	C	-8.347979	-0.566973	-0.155327
H	-1.622061	-1.178110	0.059964	H	-1.630432	-1.116882	0.409944
H	-3.676797	3.466244	-0.067348	H	-3.617538	3.457347	-0.479668
H	-5.941866	-3.061150	0.014060	H	-5.963915	-2.972138	0.410703
H	-8.428316	-2.788718	-0.046624	H	-8.447383	-2.713167	0.193939
H	-9.441665	-0.508544	-0.119722	H	-9.431308	-0.459108	-0.249413
H	-7.980540	1.521210	-0.132509	H	-7.933655	1.537202	-0.475679
O	2.820573	1.125206	-0.800455	O	2.951392	1.186561	-0.765308
H	-0.826748	4.148301	-0.126655	H	-0.745365	4.134867	-0.474652
U	1.898699	-0.724840	0.009307	U	1.794508	-0.762587	0.077209
O	2.350459	-0.232474	1.672913	O	2.401458	-0.312398	1.701358
O	1.326782	-1.264606	-1.596828	O	1.266758	-1.170907	-1.579046
O	0.501475	-2.491257	0.981619	O	0.615876	-2.451873	0.936463
H	1.036749	-3.349673	0.673275	H	1.362134	-3.666133	0.437151
H	0.474411	-2.540659	1.949705	H	0.471018	-2.538428	1.891773
C	4.302001	-4.657024	-0.449192	C	4.244165	-4.755596	-0.703216
C	3.123817	-3.814775	-0.024955	C	3.166491	-3.834219	-0.214290
H	4.570883	-4.396782	-1.485506	H	4.225571	-4.745781	-1.805948
H	4.059114	-5.724562	-0.385954	H	4.070045	-5.782420	-0.359156
H	5.172329	-4.420115	0.181145	H	5.225810	-4.386408	-0.379093
O	2.022373	-4.348820	0.229193	O	2.037423	-4.389624	0.096722
O	3.330387	-2.536996	0.056917	O	3.370030	-2.597969	-0.140833

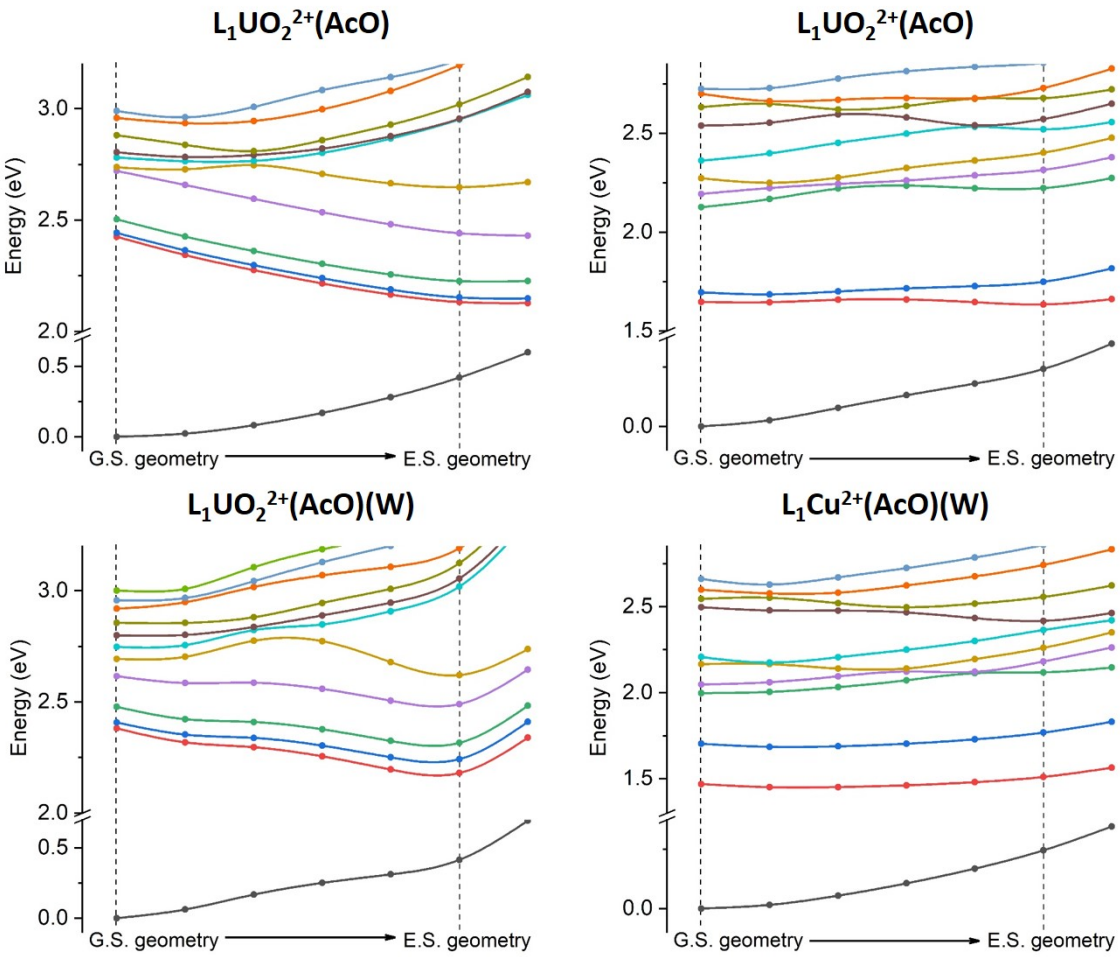

Figure Appendix 39. Potential energy profiles for the investigated copper and uranyl complexes.

Appendix 2

Crystallographic Tables

CIFs for the following structures can be obtained from the Cambridge Crystallographic Data Centre (CCDC) in addition to tables containing the following information: contain the following information: fractional atomic coordinates ($\times 10^4$) and equivalent isotropic displacement parameters ($å^2 \times 10^3$), anisotropic displacement parameters ($å^2 \times 10^3$), bond lengths, bond angles, torsion angles, and hydrogen atom coordinates ($å \times 10^4$) and isotropic displacement parameters ($å^2 \times 10^3$).

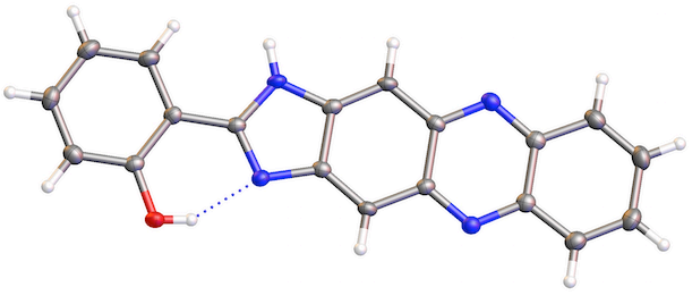

Table 1 Crystal data and structure refinement for Hiti070117_0m.

Identification code	Hiti070117_0m
Empirical formula	$C_{19}H_{12}N_4O$
Formula weight	312.33
Temperature/K	?
Crystal system	monoclinic
Space group	$P2_1/n$
a/Å	6.6597(6)
b/Å	30.064(3)
c/Å	7.2617(6)
α/°	90
β/°	108.293(2)
γ/°	90
Volume/Å^3	1380.5(2)
Z	4
ρ_{calc}g/cm^3	1.5027
μ/mm^{-1}	0.098
F(000)	648.3
Crystal size/mm^3	0.2 × 0.15 × 0.05
Radiation	Mo Kα (λ = 0.71073)
2Θ range for data collection/°	5.42 to 54.96
Index ranges	$-8 \le h \le 8$, $-39 \le k \le 39$, $-9 \le l \le 9$
Reflections collected	13927
Independent reflections	3173 [R_{int} = 0.0386, R_{sigma} = 0.0348]
Data/restraints/parameters	3173/0/218
Goodness-of-fit on F^2	1.067
Final R indexes [I>=2σ (I)]	R_1 = 0.0582, wR_2 = 0.1239
Final R indexes [all data]	R_1 = 0.0784, wR_2 = 0.1332
Largest diff. peak/hole / e Å^{-3}	0.41/-0.33

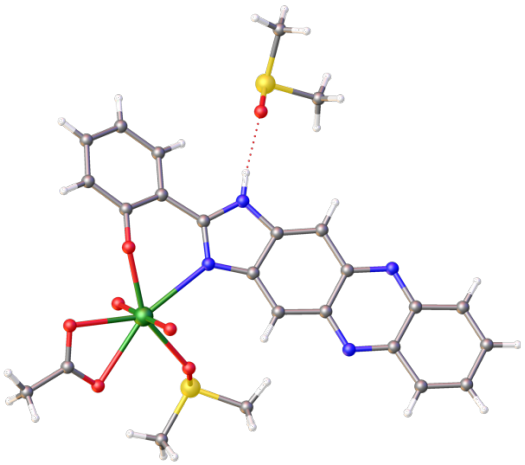

Table 1 Crystal data and structure refinement for bam115bJN091119.

Identification code	bam115bJN091119
Empirical formula	$C_{25}H_{26}N_4O_7S_2U$
Formula weight	796.65
Temperature/K	273.(2)
Crystal system	monoclinic
Space group	$P2_1/n$
a/Å	8.585(5)
b/Å	20.419(11)
c/Å	16.091(9)
α/°	90
β/°	101.633(8)
γ/°	90
Volume/Å^3	2763.(3)
Z	4
ρ_{calc}g/cm^3	1.915
μ/mm^{-1}	6.077
F(000)	1536.0
Crystal size/mm^3	0.100 × 0.100 × 0.100
Radiation	Mo Kα (λ = 0.71073)
2Θ range for data collection/°	3.26 to 53.14
Index ranges	$-10 \leq h \leq 10$, $-25 \leq k \leq 25$, $-20 \leq l \leq 20$
Reflections collected	33110
Independent reflections	5707 [R_{int} = 0.0639, R_{sigma} = 0.0441]
Data/restraints/parameters	5707/11/357
Goodness-of-fit on F^2	1.069
Final R indexes [I>=2σ (I)]	R_1 = 0.0450, wR_2 = 0.1157
Final R indexes [all data]	R_1 = 0.0602, wR_2 = 0.1281
Largest diff. peak/hole / e Å^{-3}	3.75/-1.15

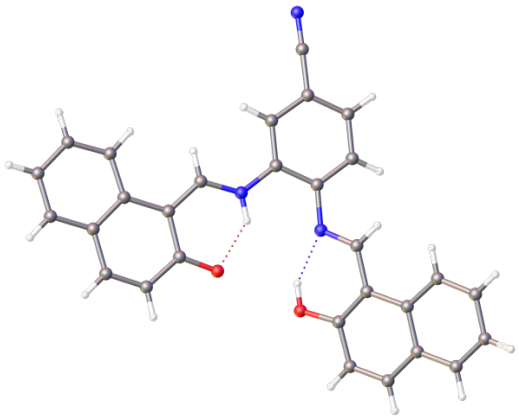

Table 1. Crystal data and structure refinement for Ethan102519Final.

Identification code	Ethan102519Final
Empirical formula	$C_{29}H_{19}N_3O_2$
Formula weight	441.47
Temperature/K	100.(2)
Crystal system	monoclinic
Space group	$P2_1/c$
a/Å	10.8315(7)
b/Å	7.1085(4)
c/Å	27.6783(18)
α/°	90
β/°	90.302(4)
γ/°	90
Volume/Å^3	2131.1(2)
Z	4
ρ_{calc}g/cm^3	1.376
μ/mm^{-1}	0.703
F(000)	920.0
Crystal size/mm^3	0.153 × 0.035 × 0.008
Radiation	Cu Kα (λ = 1.54178)
2Θ range for data collection/°	6.38 to 144.22
Index ranges	$-13 \leq h \leq 13$, $-8 \leq k \leq 7$, $-34 \leq l \leq 34$
Reflections collected	31468
Independent reflections	4186 [R_{int} = 0.0932, R_{sigma} = 0.0570]
Data/restraints/parameters	4186/0/308
Goodness-of-fit on F^2	1.051
Final R indexes [I>=2σ (I)]	R_1 = 0.0609, wR_2 = 0.1570
Final R indexes [all data]	R_1 = 0.0949, wR_2 = 0.1780
Largest diff. peak/hole / e Å^{-3}	0.48/-0.24

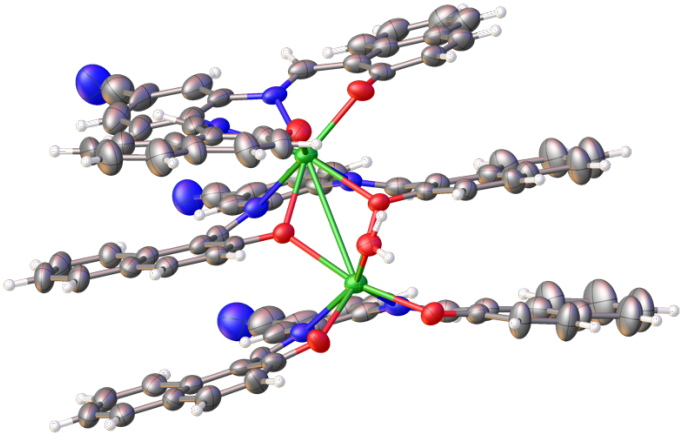

Table 1 Crystal data and structure refinement for Ethan102519bFinal.

Identification code	Ethan102519bFinal
Empirical formula	$C_{87}H_{55}Er_2N_9O_8$
Formula weight	1688.92
Temperature/K	100.(2)
Crystal system	triclinic
Space group	P-1
a/Å	10.3689(8)
b/Å	18.7929(18)
c/Å	18.9759(17)
α/°	107.514(6)
β/°	95.038(5)
γ/°	104.652(5)
Volume/Å^3	3357.3(5)
Z	2
ρ_{calc}g/cm^3	1.671
μ/mm^{-1}	5.078
F(000)	1680.0
Crystal size/mm^3	0.136 × 0.080 × 0.010
Radiation	Cu Kα (λ = 1.54178)
2Θ range for data collection/°	4.96 to 130.64
Index ranges	-12 ≤ h ≤ 12, -22 ≤ k ≤ 22, -22 ≤ l ≤ 22
Reflections collected	129841
Independent reflections	11507 [R_{int} = 0.0926, R_{sigma} = 0.0409]
Data/restraints/parameters	11507/3/955
Goodness-of-fit on F^2	1.051
Final R indexes [I>=2σ (I)]	R_1 = 0.0521, wR_2 = 0.1357
Final R indexes [all data]	R_1 = 0.0743, wR_2 = 0.1499
Largest diff. peak/hole / e Å^{-3}	2.12/-1.50

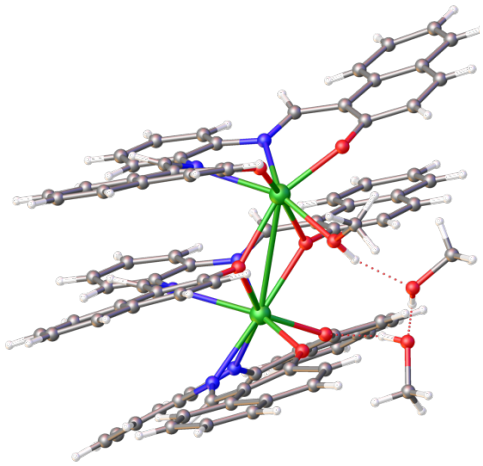

Table 1 Crystal data and structure refinement for Ethan051820Final.

dentification code	Ethan051820Final
Empirical formula	$C_{87}H_{66}Er_2N_6O_9$
Formula weight	1673.97
Temperature/K	110.(2)
Crystal system	triclinic
Space group	P-1
a/Å	10.2859(3)
b/Å	17.5752(4)
c/Å	18.8837(5)
α/°	82.6280(10)
β/°	86.2010(10)
γ/°	82.4910(10)
Volume/Å^3	3352.23(15)
Z	2
ρ_{calc}g/cm^3	1.658
μ/mm^{-1}	2.557
F(000)	1676.0
Crystal size/mm^3	0.210 × 0.170 × 0.100
Radiation	Mo Kα (λ = 0.71073)
2Θ range for data collection/°	4.38 to 61.12
Index ranges	-14 ≤ h ≤ 14, -25 ≤ k ≤ 24, -27 ≤ l ≤ 27
Reflections collected	248191
Independent reflections	20541 [R_{int} = 0.0232, R_{sigma} = 0.0119]
Data/restraints/parameters	20541/3/945
Goodness-of-fit on F^2	1.045
Final R indexes [I>=2σ (I)]	R_1 = 0.0169, wR_2 = 0.0434
Final R indexes [all data]	R_1 = 0.0178, wR_2 = 0.0439
Largest diff. peak/hole / e Å^{-3}	1.20/-1.02

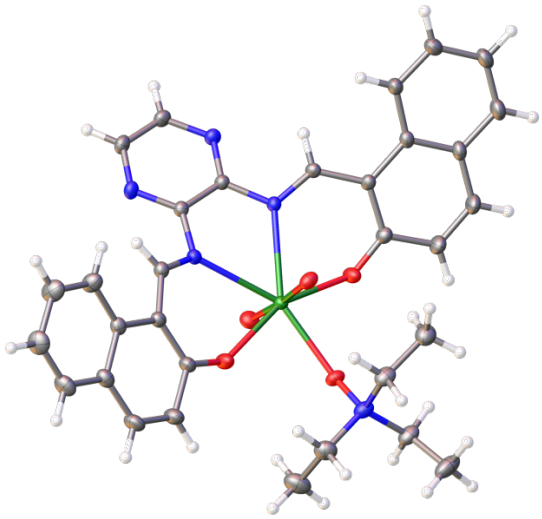

Table 1 Crystal data and structure refinement for Ethan051620Final.

Identification code	Ethan051620Final
Empirical formula	$C_{32}H_{31}N_5O_5U$
Formula weight	803.65
Temperature/K	110.(2)
Crystal system	monoclinic
Space group	$P2_1/c$
a/Å	8.2479(4)
b/Å	15.3041(7)
c/Å	22.7377(11)
α/°	90
β/°	93.167(2)
γ/°	90
Volume/Å^3	2865.7(2)
Z	4
ρ_{calc}g/cm^3	1.863
μ/mm^{-1}	5.716
F(000)	1560.0
Crystal size/mm^3	0.320 × 0.150 × 0.010
Radiation	Mo Kα (λ = 0.71073)
2Θ range for data collection/°	4.46 to 72.84
Index ranges	$-13 \le h \le 13$, $-25 \le k \le 25$, $-37 \le l \le 37$
Reflections collected	114715
Independent reflections	13974 [R_{int} = 0.0494, R_{sigma} = 0.0284]
Data/restraints/parameters	13974/0/391
Goodness-of-fit on F^2	1.017
Final R indexes [I>=2σ (I)]	R_1 = 0.0295, wR_2 = 0.0784
Final R indexes [all data]	R_1 = 0.0399, wR_2 = 0.0835
Largest diff. peak/hole / e Å^{-3}	4.05/-2.53

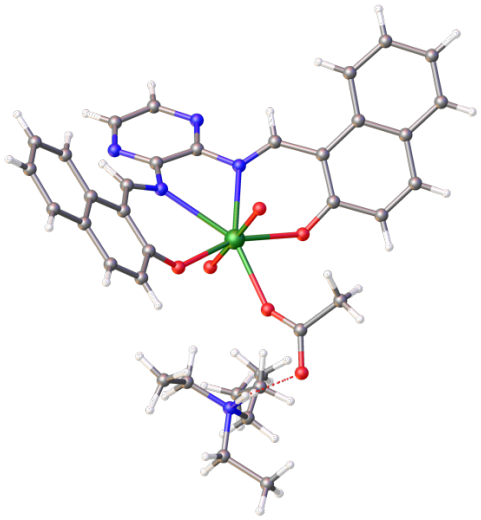

Table 1 Crystal data and structure refinement for Ethan121110Final.

Identification code	Ethan121110Final
Empirical formula	$C_{34}H_{35}N_5O_6U$
Formula weight	847.70
Temperature/K	120.(2)
Crystal system	monoclinic
Space group	$P2_1/c$
a/Å	19.1996(6)
b/Å	9.7082(3)
c/Å	19.0766(5)
α/°	90
β/°	116.209(2)
γ/°	90
Volume/Å^3	3190.18(17)
Z	4
ρ_{calc}g/cm^3	1.765
μ/mm^{-1}	14.766
F(000)	1656.0
Crystal size/mm^3	0.060 × 0.050 × 0.005
Radiation	Cu Kα (λ = 1.54178)
2Θ range for data collection/°	5.12 to 136.48
Index ranges	$-23 \le h \le 23$, $-11 \le k \le 11$, $-22 \le l \le 22$
Reflections collected	61888
Independent reflections	5822 [R_{int} = 0.1696, R_{sigma} = 0.0736]
Data/restraints/parameters	5822/470/440
Goodness-of-fit on F^2	1.091
Final R indexes [I>=2σ (I)]	R_1 = 0.0577, wR_2 = 0.1397
Final R indexes [all data]	R_1 = 0.0852, wR_2 = 0.1526
Largest diff. peak/hole / e Å^{-3}	1.90/-2.40

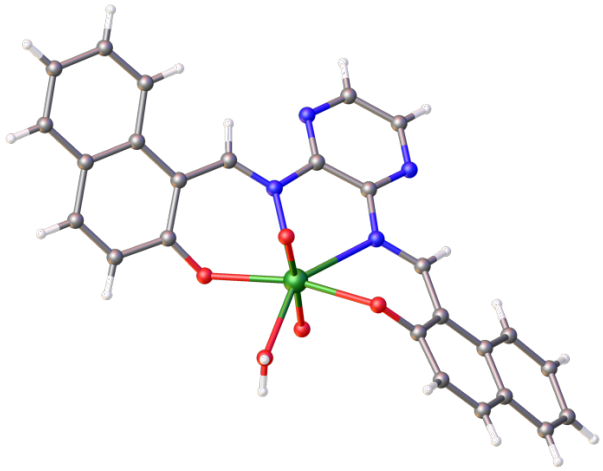

Table 1 Crystal data and structure refinement for AGor21_03.

Identification code	AGor21_03
Empirical formula	$C_{26}H_{18}N_4O_5U$
Formula weight	704.47
Temperature/K	99.9(3)
Crystal system	monoclinic
Space group	$P2_1/n$
a/Å	7.25260(10)
b/Å	23.0277(2)
c/Å	13.52000(10)
α/°	90
β/°	101.9970(10)
γ/°	90
Volume/Å^3	2208.67(4)
Z	4
ρ_{calc}g/cm^3	2.119
μ/mm^{-1}	21.110
F(000)	1336.0
Crystal size/mm^3	0.073 × 0.028 × 0.022
Radiation	Cu Kα (λ = 1.54184)
2Θ range for data collection/°	7.678 to 154.982
Index ranges	$-9 \leq h \leq 9$, $-27 \leq k \leq 28$, $-17 \leq l \leq 13$
Reflections collected	24486
Independent reflections	4615 [R_{int} = 0.0444, R_{sigma} = 0.0298]
Data/restraints/parameters	4615/1/329
Goodness-of-fit on F^2	1.080
Final R indexes [I>=2σ (I)]	R_1 = 0.0245, wR_2 = 0.0617
Final R indexes [all data]	R_1 = 0.0266, wR_2 = 0.0628
Largest diff. peak/hole / e Å^{-3}	1.25/-1.18